SUB-DIFFUSIVE AND SUB-ADVECTIVE VISCOUS FLUID FLOWS IN DEBRIS AND POROUS MEDIA

DISSERTATION
SUBMITTED FOR THE
PARTIAL FULFILLMENT OF THE REQUIREMENT FOR
THE MASTER OF PHILOSOPHY (M. Phil.) DEGREE
IN MATHEMATICS

BY

KHIM BAHADUR KHATTRI

DEPARTMENT OF NATURAL SCIENCES
SCHOOL OF SCIENCE
KATHMANDU UNIVERSITY, DHULIKHEL, KAVRE, NEPAL
MARCH, 2014

Certificate by the Supervisors

The dissertation entitled **Sub-diffusive and Sub-advective Viscous Fluid Flows in Debris and Porous Media** presented by Khim Bahadur Khattri under our supervision is hereby submitted for the partial fulfillment of the Master of Philosophy (M. Phil.) degree in Mathematics to the Department of Natural Sciences, School of Science, Kathmandu University, Dhulikhel, Kavre, Nepal.

Dr. Shiva P. Pudasaini
(Supervisor)
Professor, Kathmandu University
School of Science, Department of Natural Sciences
Dhulikhel, Kavre, Nepal

and

University of Bonn
Faculty of Mathematical and Natural Sciences
Department of Geodynamics and Geophysics
Meckenheimer Allee 176, D-53115 Bonn, Germany.
Date:

Dr. Dil B. Gurung
(Co-Supervisor)
Associate Professor, Kathmandu University
School of Science, Department of Natural Sciences
Dhulikhel, Kavre, Nepal.
Date:

Certificate of Approval

This dissertation entitled **Sub-diffusive and Sub-advective Viscous Fluid Flows in Debris and Porous Media** is submitted for the partial fulfillment of the Master of Philosophy (M. Phil.) degree in Mathematics to the Department of Natural Sciences, School of Science, Kathmandu University, in February 2014, by Khim Bahadur Khattri.

Approved by

Dr. Shiva P. Pudasaini
(Supervisor)
Professor, Kathmandu University, School of Science
Department of Natural Sciences, Dhulikhel, Kavre, Nepal and
University of Bonn, Faculty of Mathematical and Natural Sciences
Department of Geodynamics and Geophysics
Meckenheimer Allee 176, D-53115 Bonn, Germany.
Date:

Dr. Dil B. Gurung
(Co-Supervisor)
Associate Professor, Kathmandu University, School of Science,
Department of Natural Sciences, Dhulikhel, Kavre, Nepal.
Date:

Dr. Jyoti Upadhaya
Head of Department, Department of Natural Sciences
Professor, Kathmandu University, School of Science, Dhulikhel, Kavre, Nepal.
Date:

Dr. Santosh Man Maskey
(External Examiner)
Emeritus Professor of Mathematics, Tribhuvan University, Kathmandu, Nepal
Date:

Acknowledgements

Firstly, I would like to thank my thesis Supervisor Prof. Dr. Shiva P. Pudasaini and Co-supervisor and Coordinator of M. Phil. programme in Mathematics Associate Prof. Dr. Dil B. Gurung for continuous help, support and valuable guidance throughout this work. I will ever remain grateful to Prof. Pudasaini for his valuable lectures and precious time to guide for a high-quality research.

I would like to express my sincere gratitude to the external examiner Dr. Santosh Man Maskey for his valuable time, kind support and the suggestions. Many thanks to all M. Phil. scholars of Kathmandu University of my batch, especially to Mr. Jeevan Kafle, Mr. Parameshwari Kattel and Mr. Puskar Raj Pokhrel. Their reciprocal supports, not only during the exciting and productive but also the demanding phases, have been very important. I hope to enjoy such exchange of ideas and supports in the days to come.

Finally, I would like to thank all my family members and for their infinite love and continuous encouragement and supports.

Khim B. Khattri
Kathmandu University Registration Number: $012662 - 11$

Student's Declaration

I, Khim Bahadur Khattri, hereby declare that the research work entitled **Sub-diffusive and Sub-advective Viscous Fluid Flows in Debris and Porous Media** submitted here for the partial fulfillment of the Master of Philosophy (M.Phil.) degree in Mathematics to the Department of Natural Sciences, School of Science, Dhulikhel, Kavre, Kathmandu University in March 2014 is a genuine work which I carried out under the guidance of my supervisors and has not been published or submitted elsewhere for the requirement of any degree. Any literature, data or work done by others cited within this dissertation has been given due acknowledgement and are listed in the Bibliography.

Khim B. Khattri
Batch: 2011
Kathmandu University Registration number: $012662 - 11$

Abstract

In geophysical and industrial mass flows, both the solid and fluid phases may be involved. Following the general two-phase debris flow model by Pudasaini (2012) [77], and neglecting the solid deformation, inertial forces, and lateral variation of fluid velocity results in a novel sub-diffusive and sub-advective (SD-SA) equation (Pudasaini, 2014) [78] for fluid flows through general porous landscape and debris materials. The sub-diffusion and sub-advection model describes the fluid flows through inclined porous landscape and debris material with systematically derived nonlinear (quadratic) diffusion and advection fluxes. It appears that, in general, it is not possible to find the exact analytical solutions to the full sub-diffusion and sub-advection model. Pudasaini (2014) [78] constructed some exact solutions and numerical solutions to the sub-diffusion and sub-advection model.

Here, further advancement is made by constructing some additional exact solutions to the model equation for the sub-diffusion and sub-advection fluid flows in porous landscape and debris materials. However, some new exact solutions for the reduced SD-SA process is presented. To further construct analytical solutions for the SD-SA model, some special mathematical techniques, including, reduction to classical advection-diffusion equation, separation of variables and linearization are employed. Some advanced exact solutions are constructed by using Bring ultra-radical and hyper-geometric functions. In doing so, we also generate the Abel and Lineard equations in canonical form. The full SD-SA equations are integrated numerically by applying the high-resolution shock capturing TVD-NOC schemes. Exact and numerical solutions are compared for the sub-diffusive fluid flow, which shows that the numerical solutions match almost exactly with the exact solutions, thus, demonstrating the very high accuracy and performance of the numerical method and the computational code.

It is revealed that the sub-diffusion and sub-advection processes are fundamentally different as compared to the classical diffusion-advection process where the entire fluid pocket advects in the main flow direction, which at the same time also diffuses with spreading Gaussian profile. In contrast to the classical advection-diffusion of fluid where the tail of the initial substance distribution also advects in the downslope direction, for the fluid flow through porous media, the tail remains in its original position. Unlike the front of the classical diffusion-advection solution where the front is diffused, the front of the sub-diffusive and sub-advective fluid flow in porous media successively forms a downslope propagating strong bore, the diffusion is strongly constrained by a compact support. New insights into the proposed sub-diffusion and sub-advection equation, its exact and numerical solutions, underlying physics and applicabilities are discussed in detail. The results may help in constructing early warning and mitigation strategies in potentially catastrophic failures of landslides, reservoir dams and embankments in geo-disaster-prone areas such as the Himalayas, Alps and the Andes.

List of Symbols

$\mathcal{A}$	mobility number.
B	Beta function.
$\mathcal{B}$	normalization factor.
B_R	Bring radical.
C	coefficient of sub-advection.
b	basal surface of flow.
C_{DG}	generalized drag coefficient.
$\mathcal{C}$	virtual mass coefficient.
$\mathcal{F}$	fluid-like contribution in generalized drag, C_{DG}.
$\mathcal{G}$	solid-like contribution in generalized drag, C_{DG}.
g	gravity constant.
g^x, g^z	components of gravitational acceleration.
H	fluid table, $H = \alpha_f h$.
h	debris flow height, $h = h_s + h_f$.
h_f	fluid contribution to flow height, $h_f = \alpha_f h$.
h_s	solid contribution to flow height, $h_s = \alpha_s h$.
$\mathbf{I}$	unit matrix.
J	exponent for linear or quadratic drag.
K_0	constant of integration.
K_D	consistency index.
K_{HB}	Herchel- Bulkley consistency index.
K_1	constant, $K_1 = \xi^2/8D$.
K_2	constant, $K_2 = 2\mathcal{M}^{1/2}/(4\pi D)^{1/4}$.
K, K_x	earth pressure coefficients.
L	typical extent of debris flow.
m_0	constant.
m_f	fluid momentum flux, $m_f = \alpha_f h u_f$.
m_s	solid momentum flux, $m_s = \alpha_s h u_s$.
$\mathcal{M}$	mass per unit area, $\mathcal{M} = M/A$.
N	normal load.

N_R	Reynolds number, $N_R = \sqrt{gL}\rho_f H/\alpha_f \eta_f$.
$N_{R_\mathcal{A}}$	quasi-Reynolds number/mobility number.
$\mathcal{P}$	parameter combining solid-like and fluid-like drag contributions.
p_{b_f}	effective fluid pressure at base.
p_{b_s}	effective solid pressure at base.
Re_p	particle Reynolds number, $Re_p = \rho_f d\mathcal{U}_T/\eta_f$.
S	source terms.
S_f	source terms for the fluid-phase.
S_s	source terms for the solid-phase.
t, T, τ	time.
u_f	velocity for fluid.
u_s	velocity for solid.
$\mathcal{U}_s$	particle sedementation velocity.
$\mathcal{U}_T$	terminal velocity of a particle.
x	spatial coordinate along down-slope direction.
α_f	volume fraction for fluid.
α_s	volume fraction for solid.
β_f, β_s	lateral hydraulic pressure parameters.
γ	density ratio, $\gamma = \rho_f/\rho_s$.
δ	basal friction angle.
η_f	fluid viscosity.
ε	aspect ratio, $\varepsilon = H/L$.
μ	basal friction coefficient, $\mu = \tan\delta$.
ξ	vertical distribution of α_s.
ρ	debris bulk density.
ρ_f, ρ_s	fluid, solid phase density.
ϕ	internal friction angle.
χ	vertical shearing of fluid velocity.
ζ	slope angle.
Θ	step function.
∇	gradient operator.
$\otimes$	tensor product.

Publications

A. Published Papers

1. Kafle, J., Kattel, P., Pokhrel, P. R., Khattri, K. B., Gurung, D. B., Pudasaini, S. P., 2013: Dynamic Interaction Between a Two-Phase Submarine Landslide and a Fluid Reservoir. *Int. J. Lsld. Env.* 1(1), 35-36.

2. Kattel, P., Kafle, J., Khattri, K. B., Pokhrel, P. R., Gurung, D. B., Pudasaini, S. P., 2013: Dynamic's of Three-Dimensional, Two-Phase Landslides and Debris Flows. *Int. J. Lsld. Env.* 1(1), 39-40.

3. Khattri, K. B., Pokhrel, P. R., Kafle, J., Kattel, P., Gurung, D. B., Pudasaini, S. P., 2013: Some New Insights into the Fluid Flows in Debris Material and Porous Landscape. *Int. J. Lsld. Env.* 1(1), 43-44.

4. Pokhrel, P. R., Khattri, K. B., Kattel, P., Kafle, J., Gurung, D. B., Pudasaini, S. P., 2013: Enhanced Descriptions of Real Two-Phase Landslides and Debris Flows. *Int. J. Lsld. Env.* 1(1), 75-76.

B. Submitted Papers

1. Kafle, J., Kattel, P., Pokhrel, P. R., Khattri, K. B., Gurung, D. B., Pudasaini, S. P., 2013: Dynamic Interaction Between a Two-Phase Submarine Landslide and a Reservoir.

2. Kattel, P., Kafle, J., Khattri, K. B., Pokhrel, P. R., Gurung, D. B., Pudasaini, S. P., 2013: Dynamic Simulation of Three-dimensional, Two-phase Landslides and Debris Flows.

3. Khattri, K. B., Pokhrel, P. R., Kafle, J., Kattel, P., Gurung, D. B., Pudasaini, S. P., 2013: Fluid Flows in Porous Landscape and Debris Material: Some New Insights.

4. Pokhrel, P. R., Khattri, K. B., Kattel, P., Kafle, J., Gurung, D. B., Pudasaini, S. P., 2013: Real Two-Phase Landslides and Debris Flows: Enhanced Simulations.

Presentations

1. Khattri, K. B., 2013: *New mathematical models and simulations of sub-diffusive and sub-advective viscous fluid flows in debris and porous media.*
   In: The DAAD Partnership Activities Workshop Organized by Department of Natural Sciences, School of Science, Kathmandu University on "Numerical Methods for Ordinary and Partial Differential equation", September 2-13, 2013, Kathmandu University Dhulikhel, Nepal.

2. Kafle, J., Kattel, P., Pokhrel, P. R., Khattri, K. B., Gurung, D. B., Pudasaini, S. P., 2013: *Dynamic interaction between a two phase submarine landslide and a fluid reservoir.*
   In: The 11th International Symposium on Mitigation of Geo-disasters in Asia (MGDA-11), 22-28 October, 2013, Kathmandu and Pokhara, Nepal.

3. Kattel, P., Kafle, J., Khattri, K. B., Pokhrel, P. R., Gurung, D. B., Pudasaini, S. P., 2013: *Dynamics of three-dimensional, two phase landslides and debris flows.*
   In: The 11th International Symposium on Mitigation of Geo-disasters in Asia (MGDA-11), 22-28 October, 2013, Kathmandu and Pokhara, Nepal.

4. Khattri, K. B., Pokhrel, P. R., Kafle, J., Kattel, P., Gurung, D. B., Pudasaini, S. P., 2013: *Some new insights into the fluid flows in debris material and porous landscape.*
   In: The 11th International Symposium on Mitigation of Geo-disasters in Asia (MGDA-11), 22-28 October, 2013, Kathmandu and Pokhara, Nepal.

5. Pokhrel, P. R., Khattri, K. B., Kattel, P., Kafle, J., Gurung, D. B., Pudasaini, S. P., 2013: *Enhanced descriptions of real two phase landslides and debris flows.*
   In: The 11th International Symposium on Mitigation of Geo-disasters in Asia (MGDA-11), 22-28 October, 2013, Kathmandu and Pokhara, Nepal.

6. Kafle, J., Kattel, P., Pokhrel, P. R., Khattri, K. B., Gurung, D. B., Pudasaini, S. P., 2014: *A two-phase, 3D subaerial debris flow impinging a reservoir: Dynamics of induced tsunami and submarine debris flows.*
   In: The 5th National Conference of Mathematics (NCM-2014), Nepal Mathematical Society, January 28-30, 2014, Surkhet, Nepal.

7. Kattel, P., Kafle, J., Pokhrel, P. R., Khattri, K. B., Gurung, D. B., Pudasaini, S. P., 2014: *Physical-mathematical modeling and high-resolution simulations of a real two-phase, three dimensional debris flow dynamics.*
   In: The 5th National Conference of Mathematics (NCM-2014), Nepal Mathematical Society, January 28-30, 2014, Surkhet, Nepal.

8. Khattri, K. B., Pokhrel, P. R., Kafle, J., Kattel, P., Gurung, D. B., Pudasaini, S. P., 2014: *Some exact and numerical solutions for fluid flows in debris and porous media with sub-diffusive and sub-advective Model.*
   In: The 5th National Conference of Mathematics (NCM-2014), Nepal Mathematical Society, January 28-30, 2014, Surkhet, Nepal.

9. Pokhrel, P. R., Khattri, K. B., Kattel, P., Kafle J., Gurung, D. B., Pudasaini, S. P., 2014: *General phase-eigenvalues for two-phase mass flows and their implications in enhanced simulations.*
   In: The 5th National Conference of Mathematics (NCM-2014), Nepal Mathematical Society, January 28-30, 2014, Surkhet, Nepal.

List of Figures

Contents

Chapter 1

Fluid Flows in Porous Landscape and Debris Materials

1.1 General Aspects of Fluid Flows in Porous Media

A porous medium is a substance that contains pores or, void spaces between solid or granular materials through which passes the fluid (air or, liquid). Sand, soil, gravel, rocks and debris materials, and natural landscapes are some examples of porous media in geophysical context. In the context of fluid flow, porous medium can be defined as a solid matrix through which small interconnected cavities occupying a remarkable fraction of its volume are distributed. These cavities are of two types: Large ones are called *pores* and *throats*. These allow the bulk flow of fluid. Small ones, comparable to the size of the molecules, which do not have an impact on the bulk flow of fluid though they may participate in other transportation phenomena like diffusion [8, 93]. The complexities of the microscopic pore structure are usually avoided by resorting to macroscopic physical properties to describe and characterize the porous medium [9, 64, 93]. The macroscopic properties are strongly related to the underlying microscopic structure. The best known examples of these properties are the *porosity* and the *permeability*. Porosity describes the relative fractional volume of the void space to the total volume, while permeability quantifies the capacity of the medium to transmit fluid by the exchange of concentration [8, 64, 93].

From the geophysical prospective, the fluid flows through porous and debris media are important aspects as it is coupled with the stability of the slope, the subsurface hydrology, and the transportation of the chemical substances in the porous landscape. Other examples are the consolidation and seepage of the fluid during the deposition processes of an avalanche, debris flow and landslide [8, 78]. There are several geo-physical and

industrial applications of fluid flows through porous media. This includes the flow of liquid or gas through the solid matrix like soil, clay, gravel and sand, or through sponge and foam. Proper understanding of fluid flows in debris material and porous landscape, and in general through porous media, is an important aspect in industrial applications, geotechnical engineering, subsurface hydrology and natural hazard related phenomena [6, 7, 59, 64, 78, 101, 104].

Fluid flow through porous media is a subject of common interest and has emerged as a separate field of study. Better and reliable understanding of the slope stability analysis, landslide initiation, debris flow and avalanche dynamics and their deposition morphologies, seepage of fluid through porous matrix, and consolidation requires more accurate and advanced knowledge of fluid flows in porous materials [9, 78]. In these scenarios, advective and diffusive fluid flows through porous media plays an important role to properly characterize the subsurface hydrology, and in general hydrogeology.

By constructing some new models and their exact solutions, recently Pudasaini (2014) [78] has revealed that sub-diffusion and sub-advection equations are needed to properly describe the fluid flows through porous landscape and debris materials. The sub-diffusive and sub-advective fluid flow in porous media is fundamentally different than the diffusive and advective fluid flow or diffusion of heat, tracer particles and pollutant in fluid. It is revealed that in the sub-diffusive process, the fluid diffuses slowly in time, and thus to maintain the mass balance, the flow (substance) is less spread in the lateral direction [60, 78]. There is a large difference between the *sub-diffusive solution* and solution with *classical diffusion model*.

In a sub-diffusive flows, the diffusion and dispersion is much slow and much less spread as compared to the same with the classical diffusion model. Pudasaini (2014) [78] proposes that in a sub-diffusive process, the flow of fluid through the porous media and debris material should be modelled with the non-linear (quadratic) flux diffusion equation rather than the classical linear diffusion equation. This is called the generalized porous medium flow phenomenon. In a sub-diffusive process, the lateral fluid spreading is constrained. And thus such a process is completely different from the classical diffusion-advection process, where the entire fluid pocket advects in the main flow direction, which at the same time also diffuses with spreading Gaussian profile. In contrast to the classical advection-diffusion of fluid where the tail of the initial substance distribution also advects in the downslope direction, for the fluid flow through porous media, the tail remains in its original position. Unlike the front of the classical diffusion-advection solution where the front is diffused, the front of the sub-diffusive and sub-advective fluid flow in porous media

successively forms a downslope propagating strong bore [78].

Pudasaini (2014) [78] developed a sub-diffusion and sub-advection model, and constructed some exact solutions and numerical solutions to the model. Based on this model [78], here, further advancement is made by constructing some additional exact solutions for the sub-diffusion and sub-advection fluid flows in porous landscape and debris materials. The new exact solutions are compared with the high resolution numerical solutions of the full sub-diffusion and sub-advection equations, and other numerical solutions available in literature (e.g., Lutsko and Boon, (2007) [59]). The new exact solutions capture basic features of the full model equations as revealed in the numerical simulations.

1.2 A Brief Historical Background

Einstein (1905) [27] proposed diffusion equations that follow from the mean field in terms of probabilities that the particle performs elementary displacement at each time step. The solution to the Fokker-Planck equation for diffusion processes appeared to be in the Gaussian shape. In the 1930's, a non-linear diffusion equation was proposed on a purely phenomenological basis, in particular, to describe the diffusion process in porous media, called the Porous Media Equation [64] which is fundamentally different from the classical linear diffusion equation. Here, linearity refers to the linearity associated with the underlying fluxes (diffusion and advection fluxes). This generalized diffusion process, when generalized with diffusive term, has a q-Gaussian solution [49, 59, 60, 78]. Until the 1990's, more fundamental basis was proposed for the generalized Porous Media Equation; using various statistical mechanics approaches [1, 3, 12, 14, 21, 58, 100]. Abe and Thurner [1] attempted to generalize the classical derivation of Einstein by introducing the concept of escort probabilities into the master equation for a random walk. Aside from the ad hoc nature of the generalization, this resulted in the porous media equation plus an additional term which may cause some problem in long-time behaviour of the model.

There have been several attempts to describe the relationship between the porous media equation and a continuous time random walk. Curado and Nobre [21] have shown that the porous media equation emerges from a continuous time random walk in which the transition rates, that are constants in the classical random walk, depend on some power of the distribution. Borland [14] and Anteneodo and Tsallis [3] have discussed the fact that the porous media equation corresponds to a Langevin equation with multiplicative noise but, given the equivalence of the Fokker-Planck and Langevian descriptions, that is an another way of writing the same result. Lutsko and Boon [59] have shown that an

assumption of non linear response in an ordinary fluid leads to the porous media equation.

1.2.1 Porous Media Equation

Classically, the flow of an ideal gas (or, liquid) through a homogeneous porous medium is described by the Porous Medium Equation [6, 7, 64]. The equation is derived by using the continuity equation for the flow of ideal gas through the porous medium, the Darcy law relating fluid pressure gradient to the mean velocity, and by assuming a state equation for ideal gas in which pressure is an explicit exponent (≥ 1) function of the gas density [8, 64, 78]. This leads to the porous media equation that is similar in form to the classical diffusion equation except in the porous medium equation the diffusive flux is non-linear with exponent equal to or greater than 2 [92, 101], which is ultimately responsible for the slow diffusion process. Exact solutions exist for the porous medium equation, e.g., the Barenblatt solution [6, 7, 12] in similarity (to source) form. Classical diffusion equation can be extended to include the advection of the fluid in porous medium by adding linear advection term. However, by developing a new sub-advection and sub-diffusion model equation, Pudasaini (2014) [78] showed that a number of important physical processes, such as the flow of a fluid through porous landscape and debris materials are governed by the nonlinear advection and diffusion processes.

1.2.2 Advances in Porous Media Flow Modeling

Recently, Pudasaini (2014) [78] proposed a new sub-diffusion and sub-advection model to describe the fluid flows through inclined porous landscape and debris material with systematically derived non-linear (quadratic) diffusion and advection fluxes. The new equation derived is based on the two-phase mass flow model (Pudasaini, 2012) [77], which is then solved analytically and numerically with high resolution numerical methods. Analytical and exact solutions to simplified cases of nonlinear two-phase mass flow model equations are necessary to calibrate numerical simulations of flow depth and velocity profiles in the porous landscape and debris material [77]. Of particular importance is the fluid flow through the immobile solid skeleton in the debris material and porous landscape. The reduced and problem-specific solutions provide important insights into the full behavior of the complex two-phase system [78], mainly the flow of fluid through the porous media. Broadly speaking, these results can further be applied to the problems related to hydrogeology, environmental pollution remediation, and fluid flows through bone and skin in biomedical engineering [61]. The new model equations and the solutions are discussed in detail in [78] by focusing their physical significance, advancements over classical models,

and the applicabilities of the model and solutions in porous and debris materials.

Here, further advancement is made by constructing some additional exact solutions to the sub-diffusion and sub-advection equations (Pudasaini, 2014) [78]. Three fundamental processes are involved in the construction of the exact solutions. These exact solutions are constructed by transforming the model equation, in the form, to the classical diffusion-advection equation, considering the separation of the variables techniques, and also linearizing the non-linear model equation around a fixed point. All the exact solutions reveal important insights into the underlying physics of fluid flows in the porous landscape and the debris materials. These exact solutions, thus, may play important role in advanced and accurate descriptions of fluid flows in general porous media.

1.3 Importance of the Problem

With some physically justified assumptions relevant to some practical problems, the generalized two-phase mass flow model equation [77] is reduced to simple sub-advection and sub-diffusion equation for the flow of viscous fluid through the porous media (Pudasaini, 2014) [78]. One would always like to solve the full or reduced model equation analytically with all principal parameters and boundary and initial values as general as possible. Such a solution, if one is able to compute it analytically and explicitly, is superior to all other possible solutions. Such special exact analytical solutions are important, because

- they can in many cases predict phenomena that are observable in nature; example includes the initiation of landslides,
- they may help in comparing results with corresponding results obtained from other existing models, and
- they are crucial to test the efficiency and applicability of numerical solution techniques.

The exact solutions of the employed model equations (also see, Pudasaini, 2014 [78]) may reveal many essential physics of fluid flow in porous media, and thus, may find ample applications in modeling and simulation in environmental and industrial fluid flows through general porous media. These analytical solutions provide important insight in to the full behavior of the system. Analytical solutions provide important insights into the physical feature of such processes.

Chapter 2

The Sub-Diffusion and Sub-Advection Model

In this chapter, different rheological models are presented that are often in use in modeling the mass flows, including rheological models for bulk deformations and the deformation of the solid and the fluid phases in a real two-phase debris motion. The general two-phase mass flow model by Pudasaini (2012) [77] are presented along with important aspects of the model equations. Based on the generalized two-phase mass flow model (Pudasaini, 2012, Pudasaini and Miller, 2012a,b) [77, 81, 82] and following Pudasaini (2014)[78] A novel dynamical model equation for sub-diffusive and sub-advective flow of viscous fluid in porous and debris materials is derived under the assumption that solid deformation and motion is negligible as compared to the fluid. Then, the properties and the significance of the new sub-diffusion and sub-advection model are discussed in detail from the physical and application point of view.

2.1 Rheology Related to Two-Phase Debris Flows

[1]Before presenting the two phase mass flow model by Pudasaini (2012) [77] for the motion of the mixture of solid particles and the fluid, a short description on the basic flow rheologies associated with the deformation of the solid and the fluid phases are presented. Material response to a stress is known as rheology, and a relationship between stress and strain is called a constitutive model [75]. In a continuum mechanics description, a material is considered to be a continuum rather than a set of discrete constituents [39]. A moving

[1]This section closely follows the Lecture Notes: *Dynamics of Geophysical Mass Movements, Vol. I, and Vol. II, 2007*, by Shiva P. Pudasaini, Department of Geodynamics and Geophysics, University of Bonn, Germany [75].

continuum material can be described by the balance laws [25, 26, 39, 67, 77, 80]

$$\nabla.\mathbf{u} = 0, \tag{2.1}$$

$$\rho\left\{\frac{\partial \mathbf{u}}{\partial t} + \nabla(\mathbf{u}\otimes\mathbf{u})\right\} = -\nabla.\mathbf{p} + \rho\mathbf{g}, \tag{2.2}$$

where ∇ is gradient operator, $\mathbf{u}$ is the velocity, $\partial/\partial t$ indicates differentiation with respect to time, $\otimes$ is the tensor product, $\mathbf{p}$ is the pressure tensor (the negative Cauchy stress tensor) and $\mathbf{g}$ is the gravitational acceleration. The balance equations (2.1) and (2.2), along with appropriate constitutive equations and suitable initial and boundary conditions, result in a system of partial differential equations modelling the geophysical mass flows [39, 80]. However, note that, depending on the effectively single-phase, or a two-phase mass flows, we would need two separate mass and momentum balance equations for the solid and the fluid phases, respectively [39, 67, 77].

A. Elasticity: Different materials may behave differently when the same stress is applied. Ideally, materials can be modelled as a simple elastic, plastic, or viscous material. An *elastic* material shows a conservative property in which part of the mechanical energy is used to produce deformation which is stored within the material and the material comes back to its original configuration when the stress is removed [75, 80]. Under usual conditions and under relatively low loads, solid materials usually behave as an elastic material, e.g., a beam.

B. Plasticity: In general, a solid body behaves as an elastic material (i.e., the material regains its original shape when the applied stress is released) under some threshold value of stress, called the *yield stress.* However, beyond that threshold value, the material exhibits non-recoverable deformation even if the stress is released. Such a deformation is called *plastic* deformation and the material is said to be in a plastic state. During a plastic deformation, energy dissipation and stress do not depend on rate of deformation [35, 75, 93]. Thus, plasticity is a property of a material to undergo non-recoverable change of shape in response to an applied force. Clay, mild steel and granular materials are some examples of plastic materials [35].

C. Viscosity: *Viscosity* is the tendency of a liquid to resist flow due to its internal friction. During a viscous deformation, mechanical energy is dissipated into heat [93]. A viscous deformation is non-recoverable. For viscous material, the stress is proportional to the strain rate [75]. A viscous material is described by [4, 80, 99]

$$\tau = K_D(\partial u/\partial y)^n, \tag{2.3}$$

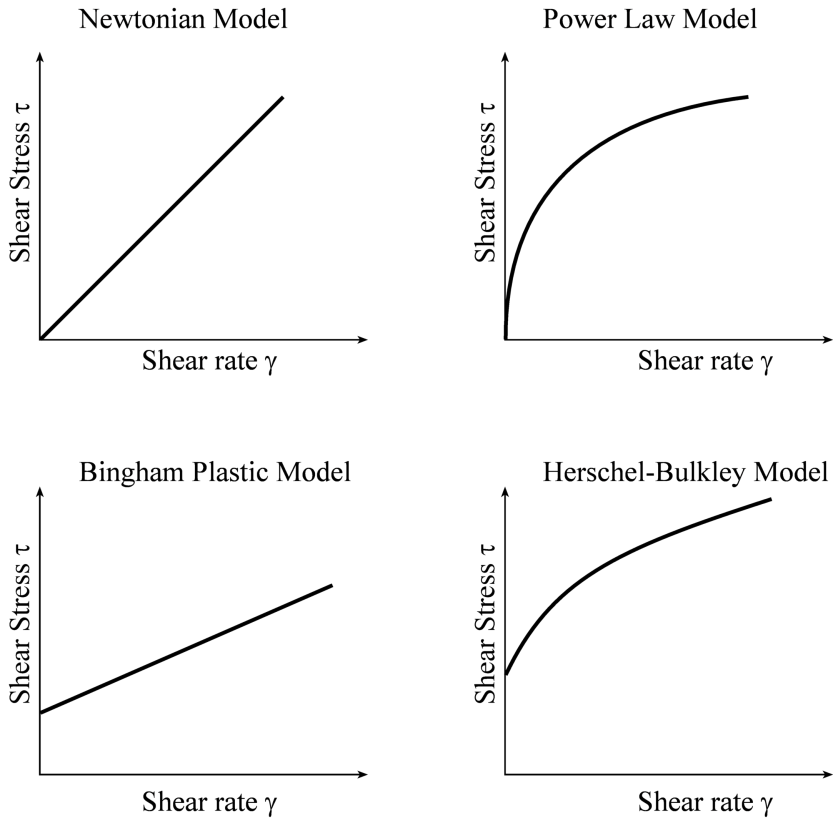

Figure 2.1: Different rheological models showing the relationship between the shear stress τ verses shear-rate γ. This figure has been reproduced from the Lecture Notes by Pudasaini [75].

where, τ is the applied stress, $\partial u/\partial y$ is the strain-rate, K_D is the consistency index, n is an exponent. The flow which satisfy (2.3) with linear exponent ($n = 1$) is called the Newton's law of viscosity, for which $K_D = \eta$ is the fluid viscosity. Water, glycerine, ethanol, air, benzene, are some examples of Newtonian fluids [75]. The flow which is not Newtonian is called non-Newtonian, examples include, non-linear, or power laws, with $n > 1$, or $n < 1$. Fluids like blood, paints and polymer of high molecular weight show non-Newtonian behaviour [62, 80, 93]. So, the viscous material exhibit time dependent behaviour. Less viscous materials deform relatively faster and easily than more viscous materials [35]. So, the viscosity is related to the fluid behaviour, whereas the elasticity is associated with the solid deformation.

D. Viscoelastic: In reality, materials can be much more complex than the ideal elastic, plastic, or viscous materials. So, the behaviour of a real material is better described by a combinations of elastic, plastic, and viscous materials [10, 75]. However, it also depends on how we combine and arrange different material components in order to produce a more

complex and composite material. One of such many combinations is called Viscoelasticity. *Viscoelasticity* is a time-dependent property in which a material under the given stress produces both an elastic and a viscous response. A viscoelastic material shows viscous flow behaviour under an applied stress, but a portion of mechanical energy is conserved and is recovered after the stress is relaxed. Viscoelastic materials have the ability to creep, recover, undergo stress relaxation and absorb energy like in the cohesive dry snow avalanche, wood, metal, polymer, etc. [10, 35, 75].

When the elastic (solid, E, which corresponds to the Young's modulus, or the modulus of elasticity, i.e., the Hook's law) and viscous (fluid, η, which corresponds to the Newtonian viscosity) elements are arranged in series, we obtain a composite *Maxwell* viscoelastic material. For a Maxwell viscoelasticy, the total strain-rate is given by [35, 75]:

$$\frac{d\varepsilon}{dt} = \frac{1}{E}\frac{d\sigma}{dt} + \frac{\sigma}{\eta}, \tag{2.4}$$

where σ is the stress, E is the elastic constant (solid property), η is the dynamic viscosity (fluid property), ε is the strain [35].

E. Bingham Plastic: *Viscoplasticity* is another hybrid material property in which a material acts like a solid until a critical stress value, called the *yield stress*, but flows like a viscous fluid beyond this yield stress, τ_y [26, 35, 77]. The velocity gradient for a viscoplastic material is described by [62]:

$$\frac{\partial u}{\partial y} = \begin{cases} 0, & \text{if} \quad \tau < \tau_y, \\ \dfrac{\tau - \tau_y}{\eta}, & \text{if} \quad \tau \geq \tau_y, \end{cases} \tag{2.5}$$

where, x is the coordinate in the flow (down-slope direction), u is the (fluid) velocity in the flow, or x-direction, and y is the direction perpendicular to the channel (slope). So, (2.5) means that the material is rigid for shear stress τ less than a threshold value τ_y, but it deforms as if it was a Newtonian viscous material once the yield strength is reached ($\tau \geq \tau_y$). The material described by (2.5) is called *Bingham plastic* material, which can also be written as

$$\tau = \tau_y + \eta\frac{\partial u}{\partial y}. \tag{2.6}$$

For highly concentrated sediment water mixture, the Bingham model can be used with $\tau_y = \tau_{yc} + N\tan\phi$, where τ_{yc} is cohesive yield stress, N is the normal stress, ϕ is friction angle between the solid particles [42, 77]. Viscoplastic materials are used in modeling mud and debris flows [76].

F. Herschel-Bulkley: In many situations, the flow can be better modelled by three

parameter *Herschel-Bulkley* rheology, see in Fig. 2.1, which is the extension of the Bingham plasticity, and extends the linear viscous to include the non-linear viscous deformation. The stress-strain non-linear relationship is given by (see, Fig. 2.1) [10, 76, 91, 93]:

$$\tau = \tau_y + K_{HB} \left(\frac{\partial u}{\partial y} \right)^n, \tag{2.7}$$

where K_{HB} and n, are, respectively the Herschel-Bulkley consistency index, and non-linearity parameters that are to be determined by experiments [20]. Depending on the value of the exponent n, i.e., $n > 1$, or $n < 1$, the flow can be shear-thickening or dilatant fluid (e.g., some types of honey, 40% raw corn starch solution), or shear-thinning or pseudoplastic (e.g., apple sauce, banana puree) above some yield point [10, 11, 62, 77]. The Herschel-Bulkley model can be used to describe composite materials, such as, concrete, mud, and toothpaste [76]. The Herschel-Bulkley model reduces to the power-law, when the yield-stress is zero, to the Bingham plastic model when the flow behavior exponent is unity, and to the Newton's law for viscous fluids when both the yield-stress is zero and the flow behavior exponent is unity, i.e., $K_{HB} = \eta$ [11, 93].

G. Pressure- and Rate-Dependent Coulomb-Viscoplasticity: Recently, Domnik and Pudasaini (2012) [25], and Domnik et al. (2013) [26] have proposed more advanced viscoplastic models to better describe the full dynamics of the rapid flows of granular materials down the channels impinging on rigid walls or, transiting into the deposition. Their models are called the pressure and rate-dependent Coulomb-viscoplastic rheological models [25, 26]. In contrasts to the Herschel-Bulkley, or Bingham plasticity, the models presented by Domnik and Pudasaini (2012) [25] and Domnik et al. (2013) [26] do not include any fit parameters, and these models are thus fully described by the phenomenological parameters of the materials. By presenting several flow simulations, from the material collapse and silo outlet to the final depositions, they have demonstrated the applicability of their new rheological models with very high computational performances while coupling between the full-dimensional and reduced dimensional models in a novel multi-scaling modelling and simulation strategy [25, 26]. Their novel model describes several important and unique behaviour observed in geophysical mass flows, such as avalanches and debris flows, including the solid-fluid and fluid-solid transitions, during the mass collapse, or release, flow obstacle interactions and deposition processes.

For incompressible dry granular flows, Domnik and Pudasaini (2012) [25] and Domnik et al. (2013) [26] began with the fluid mechanical mass and momentum balance equations

$$\nabla . \mathbf{u} = 0, \tag{2.8}$$

$$\frac{d\mathbf{u}}{dt} = \nabla . \boldsymbol{\sigma} + \mathbf{g}, \tag{2.9}$$

where, $\boldsymbol{\sigma}$ is the Cauchy stress tensor normalized by the bulk density ρ, and the gravitational components for channel flows are given by $\mathbf{g}(\zeta) = (g\sin\zeta, -g\cos\zeta)^T$, with gravity constant g, ζ is the channel inclination angle, and d/dt is the material derivative. The motion and the settlement are described by constitutive laws [2, 5, 31, 43]

$$\boldsymbol{\sigma} = -p\mathbf{I} + 2\nu\mathbf{D} + 2\tau_y\frac{\mathbf{D}}{||\mathbf{D}||}, \tag{2.10}$$

which is the normalized stress tensor for a viscoplastic material (fluid), where p is the normalized pressure. The symmetric part of the velocity gradient $\mathbf{D} = \frac{1}{2}[(\nabla\mathbf{u}) + (\nabla\mathbf{u})^T]$ is the strain-rate tensor, ν is the kinematic viscosity, and τ_y is the yield stress. The norm of the strain-rate tensor is defined by $||\mathbf{D}|| = \sqrt{2\mathrm{tr}(\mathbf{D}^2)}$. In terms of an effective viscosity:

$$\nu_{\text{eff}} = \nu + \frac{\tau_y}{||\mathbf{D}||}, \tag{2.11}$$

equation (2.10) can be written as $\boldsymbol{\sigma} = -p\mathbf{I} + 2\nu_{\text{eff}}\mathbf{D}$. However, $\nu_{\text{eff}} \to \infty$ as $||\mathbf{D}|| \to 0$. To overcome this problem in computation, Domnik et al. (2013) [26] introduced the exponential factor m_y as

$$\nu_{\text{eff}} = \nu + \frac{\tau_y}{||\mathbf{D}||}\left(1 - e^{-m_y||\mathbf{D}||}\right). \tag{2.12}$$

The material behaves as a Newtonian fluid for $\tau_y = 0$.

As explained above, a Bingham material is described by a constant yield stress. However, in granular flows, this may not be enough to describe a complex dynamical pressure-dependent yield property of the material. To capture such typical flow behaviour of a geophysical mass flows, Domnik et al. (2013) [26] proposed a pressure dependent yield stress

$$\tau_y = \tau_p p, \tag{2.13}$$

for describing the frictional nature of the granular material in a better way. This forms a Drucker-Prager yield criterion [74] with no cohesion

$$\sqrt{II_{\sigma D}} \geq \tau_p p, \tag{2.14}$$

where, $II_{\sigma D}$ is the second invariant of the deviatoric stress tensor [74]. The relation (2.14) simply tells us that material undergoes plastic yielding when deviatoric stress is greater than the yield stress. In two dimensional space, the Drucker-Prager yield surface is equivalent to Mohr-Coulomb yield surface with $\tau_p = \sin\phi$ where, ϕ is the internal friction angle, usually ϕ is on the order of 30°. With several complex flow simulations, from silo outlet to the flow obstacle interactions, and depositions with solid-fluid and fluid-solid transitions,

Domnik et al. (2013) [26] demonstrated that the pressure-dependent yield stress is a very good rheological model. They have shown that, the classical Bingham plastic model cannot appropriately describe the depositional behaviour of the granular material which can very well be described and simulated by the rate- and pressure-dependent Coulomb-viscoplastic model. Furthermore, cohesion can easily be included in the model (2.10) by $\tau_y = \tau_c + \tau_p p$, where, τ_c is tensile stress. However, for dry granular materials, usually, $\tau_c = 0$ [80].

H. Quadratic Model: O'Brien and Julien (1985) [66] proposed a quadratic rheological model to apply in sediment transport and hyper-concentrated flows:

$$\tau = \tau_y + \eta \left(\frac{\partial u}{\partial y} \right) + K_D \left(\frac{\partial u}{\partial y} \right)^2, \tag{2.15}$$

where, the first term includes the cohesive and Mohr-Coulomb yield strength (so, the solid property), the second term takes into account the viscous (fluid) effects, and the last term corresponds to the turbulent (inertial shear stress) and dispersive stresses [66, 75, 80].

I. Bagnold Grain Inertia: Owing to the complexity of the system, it is less probable to describe debris flows by any constitutive equations. However, in many cases, debris flow events can well be described by Bagnold-type dilatant fluid [4, 99] with $\tau = K_D(\partial u/\partial y)^n$, where K_D is a consistency index [76]. If the shear and normal stresses in the mixture (suspension) vary quadratically ($n = 2$) with the shear-rate, the motion is said to satisfy Bagnold's grain-inertia flow. If this relation is linear ($n = 1$), then, the flow is said to satisfy Bagnold's macroviscous flow [76]. These flow laws were derived by Bagnold in 1954 after performing some novel experiments in an annular coaxial cylinder rheometer [80], where he evaluated the effects of grain interaction in the suspension. These types of relationships have also been confirmed by many subsequent shear-cell experiments for both wet and dry mixtures [18] and computer simulations [63, 90]. However, note that, Hunt et al. (2002) [38] suggested that there can be some inconsistencies and shortcomings in Bagnold's experiments and data analysis [76]. Bagnold's rheology can be rewritten and put in the form of a Newtonian fluid $\tau = \eta_a(\partial u/\partial y)$ in which the corrected (apparent) viscosity $\eta_a = K_D(\partial u/\partial y)^{n-1}$ turns to be a function of the shear-rate. For $n = 1$, this corresponds to Newtonian viscous fluid with $K_D = \eta$ [76]. However, for $n = 2 > 1$ (shear thickening) the apparent viscosity increases with increasing shear-rate and one obtains the Bagnold's dilatant fluid. Similarly, for $n < 1$ the apparent viscosity decreases with increasing shear-rate and one obtains the shear thinning fluid [32, 76].

J. Mohr-Coulomb Plasticity: Savage and Hutter (1989) [88] proposed Mohr-Coulomb plastic yield criterion for rapid granular flows. This model has been successively and

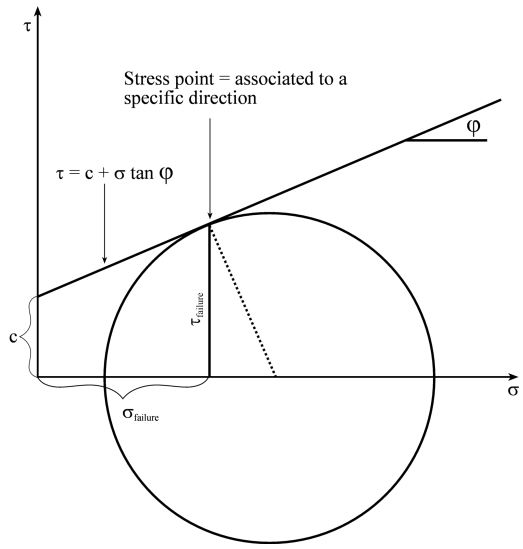

Figure 2.2: Coulomb envelop ($\tau = c+\sigma \tan\phi$), Mohr-circle, and the Mohr-Coulomb failure as the Mohr circle hits the Coulomb strength envelope in the $\sigma - \tau$ plane. This figure has been reproduced from the lecture notes by Pudasaini (2007) [75].

largely used for the deformation of the effectively single-phase materials, like avalanches and granular flows. This model assumes that the material fails plastically when the Mohr-circle of two-dimensional state of stress (in $\sigma - \tau$ plane) hits the Coulomb failure envelope given by

$$\tau = c + N \tan\phi, \tag{2.16}$$

where τ, c, N and ϕ, respectively, are the shear strength, cohesion, normal load, and the internal friction angle of the material. The failure situations for the active and passive states are explained in detail, e.g., in Pudasaini and Hutter (2007) [88] and Savage and Hutter (1989) [88]. However, a simple Mohr-Coulomb failure condition is presented in Fig. 2.2. Similarly, how to determine the internal (ϕ) and basal (δ) friction angles for given granular materials and sliding surfaces have been explained in detail and collectively in Pudasaini and Hutter (2007) [80] with values for different granular materials. The friction angles are low when grains and the basal surfaces, on which they flow, are smooth, and high when the grains and the basal surface are coarse. In general, ϕ is found in the range $15^\circ - 45^\circ$, higher values corresponds to gravel, whereas lower values may correspond to very smooth particles, such as glass beads. More complex granular flow models have also been proposed by Pouliquen and Forterre (2002) [73] , Jop et al. (2006) [43], Pudasaini (2011) [76], Domnik et al. (2013) [26].

K. Mohr-Coulomb Plasticity and Newtonian Viscous Law: The Mohr-Coulomb failure criterion have also been extensively used to describe the debris flow motions. Iver-

son (1997) [40], Iverson and Denlinger (2001) [41], and later, Pitman and Le (2005) [67], and Pudasaini et al. (2005) [83] utilized Mohr-Coulomb plasticity for the solid and Newtonian viscous law for the fluid component of the debris mixture.

L. Mohr-Coulomb Plasticity and Non-Newtonian Viscous Law: The fluid viscosity and the viscous stress may substantially depend on the amount of the solid particles in the mixture. To take this aspect into account, Pudasaini (2012) [77] proposed a non-Newtonian fluid rheology, in which the fluid viscous stress is enhanced by the solid-volume-fraction-gradient, and the solid phase is modelled by applying the Mohr-Coulomb plastic failure criterion.

2.2 The Physical-Mathematical Model for Two-Phase Mass Flows

Here, the general two-phase mass flow model proposed by Pudasaini (2012) is presented to describe the complete dynamics of a real two-phase debris flow as a mixture of the solid particles and the interstitial fluid from initiation to the final deposition [77]. The model is developed within the framework of the continuum mechanics. The two phases are characterized by distinct material properties: the fluid phase is characterized by its true density ρ_f, viscosity η_f, and isotropic stress distribution, whereas the solid phase is characterized by its material density ρ_s, internal and basal friction angles, ϕ and δ respectively, and an anisotropic stress distribution, K (lateral earth pressure coefficient). These characterizations and the presence of relative motion between these phases lead to two different mass and momentum balance equations for the solid and the fluid phases, respectively. Let u_s, u_f and $\alpha_s, \alpha_f\,(=1-\alpha_s)$ denote the velocities, and volume fractions for the solid and the fluid constituents, denoted by the suffices s and f, respectively. The general two-phase debris flow model by Pudasaini (2012) reduced to one-dimensional channel flows are described by the following set of non-linear partial differential equations [77, 81, 82]:

$$\frac{\partial}{\partial t}(\alpha_s h) + \frac{\partial}{\partial x}\left(\alpha_s h u_s\right) = 0, \tag{2.17}$$

$$\frac{\partial}{\partial t}(\alpha_f h) + \frac{\partial}{\partial x}\left(\alpha_f h u_f\right) = 0, \tag{2.18}$$

$$\frac{\partial}{\partial t}\left[\alpha_s h\left(u_s - \gamma\mathcal{C}(u_f - u_s)\right)\right] + \frac{\partial}{\partial x}\left[\alpha_s h\left(u_s^2 - \gamma\mathcal{C}(u_f^2 - u_s^2) + \frac{\beta_s h}{2}\right)\right] = hS_s, \tag{2.19}$$

$$\frac{\partial}{\partial t}\left[\alpha_f h\left(u_f + \frac{\alpha_s}{\alpha_f}\mathcal{C}(u_f - u_s)\right)\right] + \frac{\partial}{\partial x}\left[\alpha_f h\left(u_f^2 + \frac{\alpha_s}{\alpha_f}\mathcal{C}(u_f^2 - u_s^2) + \frac{\beta_f h}{2}\right)\right] = hS_f. \tag{2.20}$$

Equations (2.17) and (2.18) are the depth-averaged mass balance equations for the solid and fluid phases. Equations (2.19) and (2.20) are the depth-averaged momentum balance equations for the solid and the fluid components, respectively.

The force/source terms in the momentum equation for the solid-phase (2.19) is

$$S_s = \alpha_s \left[g^x - \frac{u_s}{|u_s|} \tan\delta p_{b_s} - \varepsilon p_{b_s} \frac{\partial b}{\partial x} \right] - \varepsilon \alpha_s \gamma p_{b_f} \left[\frac{\partial h}{\partial x} + \frac{\partial b}{\partial x} \right] + C_{DG}(u_f - u_s)|u_f - u_s|^{J-1}. \quad (2.21)$$

Similarly, the force/source term for the fluid-phase (2.20) is

$$S_f = \alpha_f \left[g^x - \varepsilon \left[\frac{1}{2} p_{b_f} \frac{h}{\alpha_f} \frac{\partial \alpha_s}{\partial x} + p_{b_f} \frac{\partial b}{\partial x} - \frac{1}{\alpha_f N_R} \left\{ 2 \frac{\partial^2 u_f}{\partial x^2} - \frac{\chi u_f}{\varepsilon^2 h^2} \right\} + \frac{1}{\alpha_f N_{R_\mathcal{A}}} \right.\right.$$
$$\left.\left. \left\{ 2 \frac{\partial}{\partial x} \left(\frac{\partial \alpha_s}{\partial x} (u_f - u_s) \right) \right\} - \frac{\xi \alpha_s (u_f - u_s)}{\varepsilon^2 \alpha_f N_{R_\mathcal{A}} h^2} \right] \right] - \frac{1}{\gamma} C_{DG}(u_f - u_s)|u_f - u_s|^{J-1}. \quad (2.22)$$

In equations (2.21) and (2.22), $J = 1$ or, 2 correspond the linear and quadratic drags, respectively, and the other parameters are

$$\beta_s = \varepsilon K p_{b_s}, \quad \beta_f = \varepsilon p_{b_f}, \quad p_{b_f} = -g^z, \quad p_{b_s} = (1-\gamma) p_{b_f},$$
$$C_{DG} = \frac{\alpha_s \alpha_f (1-\gamma)}{[\varepsilon \mathcal{U}_T \{\mathcal{P}\mathcal{F}(Re_p) + (1-\mathcal{P})\mathcal{G}(Re_p)\}]^J}, \quad \mathcal{F} = \frac{\gamma}{180} \left(\frac{\alpha_f}{\alpha_s} \right)^3 Re_p,$$
$$\mathcal{G} = \alpha_f^{M(Re_p)-1}, \quad \gamma = \frac{\rho_f}{\rho_s}, \quad Re_p = \frac{\rho_f d \mathcal{U}_T}{\eta_f},$$
$$N_R = \frac{\sqrt{gL} H \rho_f}{\alpha_f \eta_f}, \; N_{R_\mathcal{A}} = \frac{\sqrt{gL} H \rho_f}{\mathcal{A} \eta_f}, \; \alpha_f = 1 - \alpha_s, \; \mathcal{A} = \mathcal{A}(\alpha_f). \quad (2.23)$$

In the above equations, t is the time, h is the flow depth, α_s, α_f and ρ_s, ρ_f denote the volume fractions and densities of the solid and the fluid, respectively. p_{b_f} and p_{b_s} are associated with the effective fluid and solid pressures at the base, x and z are coordinates along the flow directions, and g^x and g^z are the components of gravitational acceleration along the x and z directions, respectively. The sketch of the coordinate system and the geometry of the sliding debris on an inclined plane is shown in Fig. 2.3. L and H are the typical length and depth of the flow, $\varepsilon = H/L$ is the aspect ratio (called the shallowness parameter [33, 88]), and $\mu = \tan\delta$ is the basal friction coefficient. The earth pressure coefficient, K is a function of δ, and ϕ, basal and internal friction angles of the solid particles, C_{DG} is the generalized drag coefficient. $\mathcal{U}_T$ is the terminal velocity of a particle [67, 87] and $\mathcal{P} \in [0, 1]$ is a parameter which combines the solid-like ($\mathcal{G}$) and fluid-like ($\mathcal{F}$)

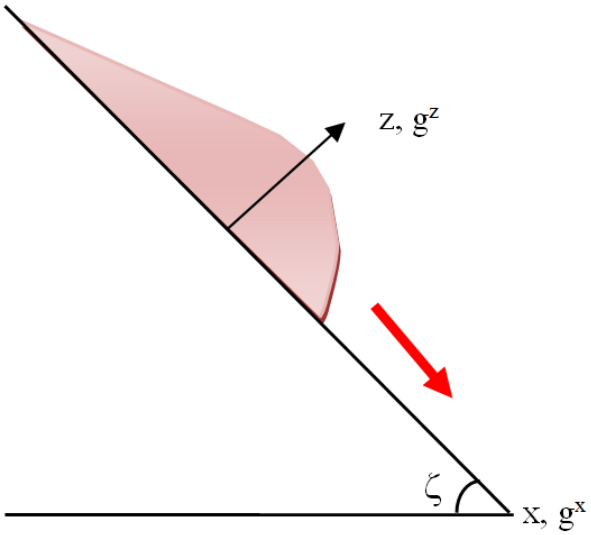

Figure 2.3: Sketch of the coordinate system and the geometry of the sliding debris on an inclined plane, or an inclined porous landscape.

drag contributions to flow resistance. γ is the density ratio, $\mathcal{C}$ is the virtual mass coefficient (solid particles induced kinetic energy of fluid phase) which is seen in all inertial terms in equations (2.19)-(2.20), η_f is the fluid viscosity, M is a function of the particle Reynolds number (Re_p) [67, 87], χ includes vertical shearing of fluid velocity, and ξ takes into account the different distributions of α_s. $\mathcal{A} = \mathcal{A}(\alpha_f)$ is the mobility of the fluid at the interface, and N_R and $N_{R_\mathcal{A}}$ are Reynolds numbers associated with the classical Newtonian, and enhanced non-Newtonian fluid viscous stresses, respectively (Pudasaini, 2012) [77]. Slope topography is represented by $b = b(x)$.

As for single-phase (Savage and Hutter, 1989 [88]) or, mixture flows (Iverson, 1997 [40]; Pudasaini et al., 2005 [83]) or two-phase flows (Fernandez-Nieto et al., 2008 [29]; Pitman and Le, 2005 [67]), it is assumed that solid-fluid mixture, and the solid- and fluid-phase constituents separately satisfy the kinematic free-surface and bottom boundary conditions [77]. The top surface is traction-free, and Coulomb sliding (for solid) and no-slip (for fluid) conditions are satisfied at the flow base [40, 41, 80, 83]. Although there seems to be lots of parameters in the list (2.23), all the parameters are well defined and well constrained from laboratory, or field data of debris flows. Furthermore, most of the parameters are derived from a very few basic parameters. For the assumptions made in the derivation of the model equations (2.17)-(2.20), and the justifications of those assumptions, we refer to Pudasaini (2012) [77].

In (2.17)-(2.20), there are four equations, two mass balance, and two momentum balance equations for the solid and the fluid, respectively, and four unknowns, mainly,

α_s, u_s, u_f, h. So, these equations can be integrated numerically. Given the material parameters listed in (2.23) and the basal topography, $b = b(x)$, equations (2.17)-(2.20) allow the debris flow depth h, volume fraction of the fluid α_f (or solid α_s), and the depth-averaged velocity components for solid, u_s and for fluid, u_f parallel to the basal surface, to be computed as functions of space and time, once appropriate initial and (numerical) boundary conditions are prescribed.

2.3 Some Important Aspects of the Model equations

In equations (2.19)-(2.20), left hand sides are inertial terms which include the lateral pressures (associated with β_s and β_f) and the virtual mass coefficient $\mathcal{C}$. The source in the solid momentum (2.21) has different contributions [77]: the first square bracket is associated with gravity, the Coulomb friction and the slope gradient; the second square bracket is associated with the buoyancy force; and the last term is associated with the generalized drag contribution (C_{DG}).

The source term for the fluid-momentum equation (2.22) also have multiple contributions to force [77]. The first three terms in (2.22) emerge from the gravity load applied to the fluid phase (first term), the fluid pressure at the bed (second term) and the topographic slope (third term). The fourth group of terms associated with N_R emerges from the viscous force contribution of the fluid phase. The fifth group of terms associated with $N_{R_\mathcal{A}}$ occurs because, viscous shear stress is enhanced by the solid-volume-fraction gradient. These are non-Newtonian viscous contributions [81, 82]. When gradients of the solid volume fraction, and/or the relative motions between the solid and fluid phases are not negligible, these terms play important role. The generalized drag C_{DG} associated with uniform flow are described by the last terms, it plays important role in two-phase debris flow dynamics. The generalized drag is modeled by a linear combination of the fluid like drag $\mathcal{F}$ and solid like drag $\mathcal{G}$ by the interpolation parameter $\mathcal{P}$.

In typical situations, the terms associated with N_R may be neglected, e.g., when N_R is sufficiently larger than the velocity diffusion contributions. Even when terms with N_R are negligible, terms associated with $N_{R_\mathcal{A}}$ may still be important, because they depend on the complex structure of the terms associated with $N_{R_\mathcal{A}}$. In fact, it depends on the second gradients of the solid volume fraction, and the first gradients of the relative motions between the phases. In many flow situations, these gradients can be large enough to control the effect of the factor $1/N_{R_\mathcal{A}}$ [77]. For example, when a natural-dam failure or landslide-induced debris flow begins, mixing between solid and fluid phases starts. In

this situation, the diffusion coefficient associated with $N_{R_\mathcal{A}}$can become very large. The non-dimensional number $N_{R_\mathcal{A}}$ is termed as the mobility number [77]. The term associated with β_s in (2.19) accounts for the buoyancy-reduced lateral pressure [81]. The solid load is reduced by the buoyancy force by the factor $(1-\gamma)$ as seen in p_{b_s}, Coulomb friction and in the drag term, C_{DG} [81].

These new contributions are mechanically important as they clearly enhance the flow mobility. Because, in the debris mixture, the solid load is not only accounted by its volume fraction α_s as it appears in the solid loads; Coulomb force, topographic gradients and the longitudinal pressure gradients; but the contributions of all these terms (except for the gravity load) in momentum equations must also be consistent and accompanied with buoyancy or the buoyancy reduced normal load. This is so, because, buoyancy has to play its role to reduce the normal load of the solid component in the mixture. Another essential point to note is the definition of the term N_R, which is here defined in terms of the fluid density, ρ_f which in Iverson and Denlinger (2001) [41] and Pudasaini et al. (2005) [83] model was defined in terms of the debris bulk density ρ [77].

As mentioned in Pudasaini (2012) [77] the model presented in (2.17)-(2.20) unifies the three pioneering theories in geophysical mass flows, the dry granular avalanche model of Savage and Hutter (1989) [88], the debris-flow model of Iverson (1997) [40] and Iverson and Denlinger (2001) [41], and the two-fluid debris-flow model of Pitman and Le (2005) [67], and the results in a new generalized two-phase debris-flow model. As special cases of the new general debris flow model, one recovers these relatively simple models for debris flows and avalanches. For the detailed discussions on the similarities and differences between the reduced model and the relatively simple classical models, we refer to Pudasaini (2012) [77]. But, here we outline some important aspects in brief.

- When both types of viscous terms (N_R and $N_{R_\mathcal{A}}$) are neglected, diffusion of the solid volume fraction is not considered explicitly, virtual mass force is not present ($\mathcal{C}=0$), the flow of fluid through solid-like or grain-rich debris flows is neglected ($\mathcal{P}=0$), and only the linear drag force is utilized, the model equations (2.17)-(2.20) are similar to Pitman and Le (2005) [67].

- Assume that the difference between the solid and fluid velocity is negligible, i.e., $u_s = u_f = u$, then, effect of solid and fluid volume fractions disappear 8 equations (2.17)-(2.22), reduced to simple and effectively single phase bulk debris flows [40, 41, 83].

- Setting $\alpha_s = 1$ and $\gamma = 0$ in equations (2.17)-(2.20) (implying that fluid phase is absent), one obtains the reduced model for dry granular flows or avalanches [33, 79,

80, 88].

- If we assume, $u_s \ll u_f$, non-inertial down-slope fluid flow, neglect the lateral variation of u_f, N_R and $N_{R_\mathcal{A}} \to \infty$, the above equations reduces to the generalized porous media equation [78]. We will derive such model equation below.

2.4 Generalized Porous Media Equation

First, the two-phase mixture model equations (2.17)-(2.23) are considered. In order to develop a model for the fluid flow through the debris and porous media, assume that the solid deformation and motion is negligible as compared to the fluid [78]. So, $u_s \ll u_f$, where u_s and u_f are solid- and the fluid-phase velocities in the debris mixture. Here, the analysis mainly focuses on the down slope flow. Furthermore, we assume a gentle slope and that the flow is non-inertial. Then, by neglecting the $y-$(lateral) variation of u_f, the model equations (2.18) and (2.20) with source term (2.22), reduces to the simple mass and momentum balance for the fluid-phase only in the down-slope (x) direction [78]:

$$\frac{\partial}{\partial t}(\alpha_f h) + \frac{\partial}{\partial x}(\alpha_f h u_f) = 0, \tag{2.24}$$

$$\frac{2}{N_R}\frac{\partial^2 u_f}{\partial x^2} - \left(\frac{2}{N_{R_\mathcal{A}}}\frac{\partial \alpha_s}{\partial x}\right)\frac{\partial u_f}{\partial x} - \left(\frac{1}{\gamma}C_{DG}u_f^{J-1} + \frac{2}{N_{R_\mathcal{A}}}\frac{\partial^2 \alpha_s}{\partial x^2}\right)u_f + \alpha_f\left(\sin\zeta - \cos\zeta\frac{\partial h}{\partial x}\right) = 0. \tag{2.25}$$

As mentioned above, C_{DG} is the generalized drag, $J = 1$ or, 2 must be chosen according to linear, or quadratic drag, N_R and $N_{R_\mathcal{A}}$ correspond to the viscous and enhanced non-Newtonian viscous stresses, γ is the density ratio between fluid and solid, h is the debris (or porous) material height, ζ is the slope angle, α_s, α_f are the solid and fluid volume fractions, respectively. So, α_f can be realized as the porosity.

In what follows, dynamical model equation for sub-diffusive and sub-advective flow of viscous fluid in porous and debris materials [77] is derived . In equation (2.25), if we set N_R, $N_{R_\mathcal{A}} \to \infty$, this leads to:

$$u_f^J = \frac{\gamma}{C_{DG}}\cos\zeta\alpha_f\left(\tan\zeta - \frac{\partial h}{\partial x}\right), \tag{2.26}$$

which is the generalized Darcy expression for the fluid velocity [24, 77]. For simplicity, we assume the linear drag, $J = 1$. Now, we consider the down-slope mass balance equation for fluid (2.24). Substituting u_f from (2.26), equation (2.24) takes the form

$$\frac{\partial}{\partial t}(\alpha_f h) - \frac{\partial}{\partial x}\left[\frac{\gamma\cos\zeta}{C_{DG}}\alpha_f(\alpha_f h)\frac{\partial h}{\partial x}\right] + \frac{\partial}{\partial x}\left[\frac{\gamma\sin\zeta}{C_{DG}}\alpha_f(\alpha_f h)\right] = 0. \tag{2.27}$$

As h is assumed to be known as the total porous material depth for fluid flow through a porous medium, $\gamma \sin\zeta / C_{DG} h$ can be considered as a parameter, So, we can write (2.27) as

$$\frac{\partial}{\partial t}(\alpha_f h) - \frac{\partial}{\partial x}\left[\frac{\gamma\cos\zeta}{C_{DG}}\alpha_f(\alpha_f h)\frac{\partial h}{\partial x}\right] + \frac{\partial}{\partial x}\left[\frac{\gamma\sin\zeta}{C_{DG}h}(\alpha_f h)^2\right] = 0,$$

or,

$$\frac{\partial}{\partial t}(\alpha_f h) - \frac{\partial}{\partial x}\left[(\alpha_f h)\left(\frac{\gamma\cos\zeta}{C_{DG}}\frac{\partial(\alpha_f h)}{\partial x} - h\frac{\gamma\cos\zeta}{C_{DG}}\frac{\partial \alpha_f}{\partial x}\right)\right] + \frac{\partial}{\partial x}\left[\frac{\gamma\sin\zeta}{C_{DG}h}(\alpha_f h)^2\right] = 0. \quad (2.28)$$

We may assume that $\partial\alpha_f/\partial x$ is small in case of diffusion process. We know that $\gamma < 1$, $\cos\zeta < 1$, and $1/C_{DG} < 1$ for fluid passing through the solid matrix. This implies that $\frac{\gamma\cos\zeta}{C_{DG}}\alpha_f(\alpha_f h)\frac{\partial h}{\partial x} \ll 1$, and thus can be neglected. So, the terms within the first square bracket in (2.28) can be simplified and approximated as (Pudasaini, 2014) [78]:

$$(\alpha_f h)\left[\frac{\gamma\cos\zeta}{C_{DG}}\frac{\partial(\alpha_f h)}{\partial x} - h\frac{\gamma\cos\zeta}{C_{DG}}\frac{\partial\alpha_f}{\partial x}\right] \approx (\alpha_f h)\left[\frac{\gamma\cos\zeta}{C_{DG}}\frac{\partial(\alpha_f h)}{\partial x}\right]. \quad (2.29)$$

Therefore, using (2.29), equation(2.28) can be written as

$$\frac{\partial}{\partial t}(\alpha_f h) - \frac{\partial}{\partial x}\left[(\alpha_f h)\left(\frac{\gamma\cos\zeta}{C_{DG}}\frac{\partial(\alpha_f h)}{\partial x}\right)\right] + \frac{\partial}{\partial x}\left[\frac{\gamma\sin\zeta}{C_{DG}h}(\alpha_f h)^2\right] = 0,$$

or,

$$\frac{\partial}{\partial t}(\alpha_f h) - \frac{\partial}{\partial x}\left[\left(\frac{\gamma\cos\zeta}{2C_{DG}}\frac{\partial(\alpha_f h)^2}{\partial x}\right)\right] + \frac{\partial}{\partial x}\left[\frac{\gamma\sin\zeta}{C_{DG}h}(\alpha_f h)^2\right] = 0.$$

Thus,

$$\frac{\partial}{\partial t}(\alpha_f h) - \left(\frac{\gamma\cos\zeta}{2C_{DG}}\right)\frac{\partial^2}{\partial x^2}(\alpha_f h)^2 + \left(\frac{\gamma\sin\zeta}{C_{DG}h}\right)\frac{\partial}{\partial x}(\alpha_f h)^2 = 0. \quad (2.30)$$

Here, $\alpha_f h = H$ is the fluid table (level of fluid) in the porous media. With this notation, equation (2.30) can be written as (Pudasaini, 2014) [78]:

$$\frac{\partial H}{\partial t} + C\frac{\partial H^\alpha}{\partial x} - D\frac{\partial^2 H^\alpha}{\partial x^2} = 0, \quad (2.31)$$

where $\alpha = 2$, and $D = \gamma\cos\zeta/(2C_{DG})$ and $C = \gamma\sin\zeta/(C_{DG}h)$ are the *sub-diffusion* and *sub-advection coefficients* (or simply called diffusion and advection coefficients). Here, for simplicity, variation of C in x is assumed to be negligible.

Alternatively, the above equation (2.31) can also be derived by using the conditions that

$\alpha_f^2 \ll 1$, $\gamma < 1$, $\sin\zeta < 1$, $1/C_{DG} < 1$, which follows from the assumption that the total debris depth is constant or does not vary so much with x (Pudasaini, 2014) [78]. This is justified as follows. Since the fluid volume fraction α_f is smaller than 1, $\alpha_f^2 \ll 1$. In natural condition, the true fluid and the solid densities are in the order of 1,100 kgm^{-3} and 2,700 kgm^{-3}, the density ratio $\gamma = \rho_f/\rho_s$ is smaller than unity. Similarly, since the landscape is assumed to be gently inclined, the inclination angle ζ is small, on the order of $15^\circ - 20^\circ$. So, $\sin\zeta < 1$. Furthermore, as explained in Pudasaini (2012)[77] for the fluid passing through the porous matrix, usually the drag coefficient is larger than unity. Hence, $1/C_{DG} < 1$. With this, the last term in (2.28) can be written as

$$\frac{\partial}{\partial x}\left[\frac{\gamma\sin\zeta}{C_{DG}h}(\alpha_f h)^2\right] = \left(\frac{\gamma\sin\zeta}{C_{DG}h}\right)\frac{\partial}{\partial x}(\alpha_f h)^2 - \alpha_f^2\left(\frac{\gamma\sin\zeta}{C_{DG}}\right)\frac{\partial h}{\partial x} \approx \left(\frac{\gamma\sin\zeta}{C_{DG}h}\right)\frac{\partial}{\partial x}(\alpha_f h)^2.$$

Equation (2.31) is called the *generalized porous media equation* [6, 7, 15, 28, 54, 55, 64, 101, 102, 104]. But, in the present model equation, D and C are explicitly expressed in terms of the density ratio, slope angle, and the generalized drag which already contains several physical parameters [77].

2.5 Sub-diffusion and Sub-advection Model

Equation (2.31) is called the *sub-diffusive and sub-advective model* (Pudasaini, 2014) [78]. As H evolves, (2.31) describes *a sub-diffusive and sub-advective flow* of fluid through porous and debris material. In hydrodynamic limit, this model is similar to Lutsko and Boon (2007) [59] for $\alpha = 2$. Importantly, here, the fluid is advecting due to the slope-induced gravity force and that, the advection coefficient is inversely related to the total debris depth. Also note that, the diffusion and advection coefficients are proportional to the density ratio and the slope angle, and inversely proportional to the drag coefficient.

From physical point of view, there are several important aspects of the new model equation (2.31). First, the great advantage is taken to have $\partial h/\partial x$ in u_f (with known power), and $\partial(\alpha_f h)/\partial t$ in mass balance over the classical porous media equation [6, 7, 15, 28, 54, 55, 64, 101, 102, 104]. Because, with this, no extra closure is needed to obtain a relationship (e.g., between u_f and the pressure gradient, $\partial h/\partial x$), which was needed in the derivation of the porous media equation; a relationship between pressure and density [78]. Second, the flux exponent $\alpha = 2$ corresponds to the fluid flow through porous and debris material as derived from the two-phase mass flow model (Pudasaini, 2012) [77]. In general, in the classical porous media equation (which corresponds to equation (2.31) with

$C = 0$) usually, α is not known, but can be used as a fit parameter (Pudasaini, 2014) [78]. However, in the derivation of equation (2.31), $\alpha = 2$ emerges explicitly and systematically from the underlying model. Explicit form of (2.31) with $\alpha = 2$ does not exist in literature, and has recently been derived by Pudasaini (2014)[78]. This is an important observation and presents a new insight in understanding the basic nature of the flow of fluid in the porous and debris material and natural landscape and lateral embankments.

Chapter 3

High Resolution Shock-Capturing Methods in One Spatial Dimension

3.1 Numerical Methods for Mass Flows

[1] The main aim is to solve the sub-diffusion and sub-advection equation (2.31). As this model seems to be simple, in principle, one could try to solve it analytically. However, as one can see in Chapter 5 that, most probably, it is not possible to solve this model with analytical methods. So, we need to appropriately integrate (2.31) numerically. Numerical simulation provides us with basic insights into the model equation and allows for the comparison between the reduced analytical solution and the numerical solution of the full model equation (2.31).

Numerical methods to solve the dynamical mass flow equations have their history developed from simple to complex. First, it started with plane (chute) flows [34, 88, 89] and then later sidewise confinement was relaxed, [33, 51, 98, 105] thereby treating the mass flow as two-dimensional flow [80]. Avalanche and debris flows down generally curved and twisted channels have also been solved numerically (Pudasaini et al., 2005a,b) [84, 85]. In case of geophysical mass flows, one has to consider large deformations and rapid motions. So, classical numerical schemes were unable to capture the associated shock phenomena. To address the sudden changes in the flow variables, e.g., velocity and flow height, modern numerical methods were developed and applied [80]. More on this can also be found in Tai (2000) and Tai et al., (2002) [97, 98].

Savage and Hutter [88] utilized the finite difference schemes, namely Lagrangean- and Eulerian-type, to solve the equations of motion describing the finite mass granular avalanche

[1] This chapter closely follows Chapter 7 of the *Avalanche Dynamics* book by Pudasaini and Hutter (2007) [80].

flow down a rough incline, spatially in one-dimension [80]. Lagrangean scheme was found to be simple, efficient and adequate to predict the observable behavior of the flow [80]. Eulerian approach, in which a fixed spatial grid that extends upstream and downstream of the moving pile was used, yield finite velocities upstream and downstream of the pile even at those parts of the bed, where there is no material and depth is zero. This resulted in sudden changes in the velocities corresponding to the front and rear of the pile, thereby destroying the stability in numerical integrate. Artificial viscosity was introduced to diffuse the instability but the velocities in the regions outside of that occupied by the pile began to affect the results in the region of the pile itself [80]. To overcome such difficulties a Lagrangean scheme was in use which used a material not that follows the motion of the avalanche. The approach in which the computational grid was advected with the moving material itself turned out to be more simple, more efficient and more reliable. However, it failed to capture the singularities [80].

Greve and Hutter [34] also used Lagrangean scheme for numerical computation of the avalanche height, velocity distribution, the front the rear and in-between position of the maximum avalanche height for different numerical and material parameter values for a motion of a granular avalanche in a convex and concave chute [80]. Traditionally, first-order upwind, and second-order Lax-Wendroff and Upwind Beam-Warming methods were in use. In traditional second-order central differencing methods, there arouse oscillations in the numerical solution for physical problems with large gradients of flow variables.

Shock formation is an essential mechanism in geophysical mass flows on an inclined surface merging in to a horizontal run out zone encountering an obstacle when the velocity becomes subcritical from supercritical state [80, 103]. So, we need to apply conservative high resolution numerical techniques that are capable to resolve the steep gradients and moving fronts [98].

In the present work, a high-resolution approach, namely the non-oscillatory central (NOC) schemes introduced by Nessyahu and Tadmor [65] is used, in which different cell reconstruction techniques- the Total Variation Diminishing (TVD) limiters (LeVque, 1990) [56] and an essentially non-oscillatory (ENO) cell reconstruction scheme Harten [37] are respectively applied. For the detailed discussion on the development of some high-resolution numerical methods that capture shock phenomena that is seen in different geophysical mass flows, we refer Nessayahu and Tadmor (1990), Tai (2000), Tai et al. (2002), Pudasaini and Hutter (2007) [65, 80, 97, 98]. Here, the description begins with the classical first and second order finite difference numerical schemes, and then, moves to the presentation of the modern high resolution shock capturing, TVD-NOC methods that have

been successfully applied to the simulations of the granular avalanches and debris flows in the past [80].

3.2 First-Order Schemes

For simplicity, the x-t plane of space and time will be discretised by choosing an uniform and stationary mesh width $\triangle x$ and a time step $\triangle t$. The discrete mesh points will be denoted by $(x_j,\, t^n)$ and are defined as [80]:

$$x_j = j\Delta x, \quad j = 0,\, 1,\, 2, \ldots; \quad t^n = n\Delta t, \quad n = 0,\, 1,\, 2, \ldots, \tag{3.1}$$

where the mesh cell x_j is bounded by the boundaries $x_{j-1/2}$, $x_{j+1/2}$ and $x_{j+1/2} = x_j + \Delta x/2$.

First, we consider the homogeneous, linear, advective scalar hyperbolic conservation law [80]:

$$\frac{\partial w}{\partial t} + a\frac{\partial w}{\partial x} = 0, \tag{3.2}$$

where a (the characteristic wave speed) is a positive constant. The second term $a\partial w/\partial x$ represents a flux derivative $\partial f/\partial x = a\partial w/\partial x$, with the physical flux $f = aw$, where w is a conservative variable. $\partial f/\partial w = a$ is the wave speed, that emerges from $\partial f/\partial x = (\partial f/\partial w)(\partial w/\partial x)$. Equation (3.2) is discretised by integrating it over the space-time domain $[x_{j-1/2},\, x_{j+1/2}] \times [t^n,\, t^{n+1}]$:

$$\int_{x_{j-1/2}}^{x_{j+1/2}} w(x,\, t^{n+1})\, dx = \int_{x_{j-1/2}}^{x_{j+1/2}} w(x,\, t^n)\, dx - \int_{t^n}^{t^{n+1}} \left\{ f(x_{j+1/2},\, t) - f(x_{j-1/2},\, t) \right\} dt. \tag{3.3}$$

The mean values of w and f are defined as [80]:

$$U_j^n = \frac{1}{\Delta x} \int_{x_{j-1/2}}^{x_{j+1/2}} w(x,\, t^n)\, dx, \qquad \mathcal{F}(U;\, j+1/2) = \frac{1}{\Delta t} \int_{t^n}^{t^{n+1}} f(x_{j+1/2},\, t)\, dt. \tag{3.4}$$

Now, (3.3) reduces to the following discretisation in general form:

$$U_j^{n+1} = U_j^n - \frac{\Delta t}{\Delta x} \left\{ \mathcal{F}(U;\, j+1/2) - \mathcal{F}(U;\, j-1/2) \right\}, \tag{3.5}$$

where $\mathcal{F}(U;\, j \pm 1/2)$ denote the numerical flux functions which are functions of the cell averages of the neighbouring cells on the cell boundaries at $x_{j+1/2}$ and $x_{j-1/2}$, respectively [80]. If the cell averages in the numerical flux functions are taken at the time level t^n, one obtains an explicit numerical scheme. This allows the determination of U^{n+1} explicitly, whereas using cell averages at time level t^{n+1} results in an implicit method. Explicit methods are largely used for time-dependent hyperbolic equations [80, 97, 98].

Upwind-Method: From the initial data, $w_0(x) = w(x, t = 0)$, the data U^0 for the approximate solution is defined as

$$U_j^0 = w_j^0(x). \tag{3.6}$$

To construct the approximation U^{n+1} from U^n, a time-marching procedure is used, in a several-levels method [80]. In many cases the derivatives in (3.2) may simply be replaced by appropriate finite difference approximations, e.g., utilizing the low order upwind flux [80, 97, 98].

$$\mathcal{F}^{UW}(U; j + 1/2) = aU_j^n, \quad \mathcal{F}^{UW}(U; j - 1/2) = aU_{j-1}^n. \tag{3.7}$$

For these numerical flux functions (3.5) results in the (low) first-order upwind method [80, 97, 98].

$$U_j^{n+1} = U_j^n - \nu(U_j^n - U_{j-1}^n), \tag{3.8}$$

where,

$$\nu = a\Delta t/\Delta x. \tag{3.9}$$

Upwind differencing was used in many of the high-resolution schemes for the approximation of the one-dimensional system of conservation laws. This method, although only of first order accuracy, does not result in any spurious oscillation near a discontinuity [80].

3.3 Second-Order Schemes

I. The Lax-Wendroff Method: Most of the second order methods solving the linear system (3.2) are directly based on finite difference approximations with the exception of the Lax-Wendroff method. This method uses Taylor series expansion of the conservative variable with the numerical fluxes [37, 80]:

$$\mathcal{F}(U; j + 1/2) = a\, U_{j+1/2}^{n+1/2}, \qquad \mathcal{F}(U; j - 1/2) = a\, U_{j-1/2}^{n+1/2}. \tag{3.10}$$

Using Taylor series expansion in time, neglecting the higher order terms, and using the conservation law (3.2) gives

$$w_{j+1/2}^{n+1/2} = w_j^n + \frac{\Delta x}{2} \left(\partial w/\partial x\right)_j^n - \frac{a\Delta t}{2} \left(\partial w/\partial x\right)_j^n . \tag{3.11}$$

By virtue of (3.11) and using central differences, the value of $U_{j+1/2}^{n+1/2}$ for the numerical flux (3.10) is approximated by

$$U_{j+1/2}^{n+1/2} = \frac{1}{2} \left(U_{j+1}^n + U_j^n\right) - \frac{\nu}{2} \left(U_{j+1}^n - U_j^n\right). \tag{3.12}$$

Substituting (3.10) and (3.12) into (3.5) yields the Lax-Wendroff scheme in central difference form,

$$U_j^{n+1} = U_j^n - \frac{\nu}{2}\left(U_{j+1}^n - U_{j-1}^n\right) + \frac{\nu^2}{2}\left(U_{j+1}^n - 2U_j^n + U_{j-1}^n\right). \tag{3.13}$$

The Taylor series expansion (3.13) at x_j indicates that the Lax-Wendroff method is of second order accuracy in space. Thus, from (3.10) and (3.12) the numerical flux in (3.13) can be realized as the high order Lax-Wendroff flux,

$$\mathcal{F}^{LW}(U; j+1/2) = \frac{a}{2}(U_{j+1}^n + U_j^n) - \frac{a\nu}{2}(U_{j+1}^n - U_j^n). \tag{3.14}$$

II. Upwind Beam-Warming Method: The Upwind Beam-Warming Method is just a one-sided version of the Lax-Wendroff method along with a second order approximation, where

$$U_j^{n+1} = U_j^n - \nu\left(U_j^n - U_{j-1}^n\right) - \frac{\nu}{2}(1-\nu)\left(U_j^n - 2U_{j-1}^n + U_{j-2}^n\right). \tag{3.15}$$

The numerical fluxes $U_{j+1/2}^{n+1/2}$ are given by an upwind method, i.e.,

$$U_{j+1/2}^{n+1/2} = U_j^n + \frac{1}{2}\left(U_j^n - U_{j-1}^n\right) - \frac{\nu}{2}\left(U_j^n - U_{j-1}^n\right). \tag{3.16}$$

3.4 Higher-Resolution Shock-Capturing Numerical Methods

3.4.1 Total Variation Diminishing Method

First-order finite difference methods are usually stable and monotonous. However, they are also strongly numerically diffusive, that causes the solution to become smeared out. Although, second-order or higher-order techniques are less dissipative, they are susceptible to non-linear, numerical instabilities that cause non-physical oscillations [80]. The high-resolution methods goes mid-way between the traditional first-order and higher-order difference schemes. Their central idea is:

- to avoid the introduction of under- and over-shoots (numerical oscillation).
- to maintain the numerical diffusion as small as possible, that is often achieved by different cell reconstruction techniques.

It is well known that in computing discontinuous solutions, the first order (e.g., upwind) method gives substantially smeared solutions, while the second order method (e.g., Lax-Wendroff or Beam-Warming) produces spurious oscillations (LeVeque, 1990) [56]. In order to develop a method that is of higher order and at the same time non-oscillatory

and capable of capturing shocks, it is relevent to define a powerful concept, called the Total Variation Diminishing (TVD) method [80].

The total variation (TV) of the mean value U^n is defined as

$$TV(U^n) = \sum_{j=0}^{N-1} |U_{j+1}^n - U_j^n|. \tag{3.17}$$

If values of U_{j+1}^n and U_j^n differ strongly from one another, any oscillation in the computed result increases the total variation. The *Total Variation Diminishing* condition:

$$TV(U^{n+1}) \leq TV(U^n), \tag{3.18}$$

for all grid functions U^n, provides a method that gives a solution without spurious oscillations near the discontinuities. Any numerical scheme which fulfils condition (3.18) will be a Total Variation Diminishing (TVD) method. Therefore, any TVD method is automatically monotonicity preserving. This means, in particular, that oscillations of the physical quantities like, velocity, or height jumps and other sharp gradients, can not arise near an isolated propagating discontinuity [56, 80].

General Criterion for a TVD Method: Consider a general two-sided numerical scheme

$$U_j^{n+1} = U_j^n - C_{j-1/2}\left(U_j^n - U_{j-1}^n\right) + D_{j+1/2}\left(U_{j+1}^n - U_j^n\right), \tag{3.19}$$

where, $C_{j-1/2}$ and $D_{j+1/2}$ dependent on data. The scheme (3.19) is a TVD method if the conditions

$$0 \leq C_{j-1/2}, \quad 0 \leq D_{j+1/2}, \quad 0 \leq C_{j-1/2} + D_{j+1/2} \leq 1, \quad \text{for all } j \tag{3.20}$$

are fulfilled [37, 80]. In particular, the low order upwind scheme (3.8) is a TVD method under the Courant-Friedrichs-Levy (CFL) condition $|a\Delta t/\Delta x| < 1$, [19, 80]. More on the higher-order TVD schemes can be found in Pudasaini and Hutter(2007) [80], Tai(2000) [97], Tai et al. (2001) [98] and Wang et al. [103].

3.4.2 Second Order TVD Schemes

Here, we present some numerical methods that are second order accurate for smooth solutions and yet provide well resolved, non-oscillatory discontinuities. The flux- and slope-limiters play major roles in second order TVD schemes [26, 53, 80, 97, 98].

Flux-Limiter Methods

For a better resolution of the solutions of hyperbolic conservation equations, a high-order flux $\mathcal{F}_H$ (e.g., some central difference methods) in the smooth regions and a low-order flux $\mathcal{F}_L$ (e.g., some monotone methods) are coupled in the vicinity of discontinuities. The coupling F reduces to $\mathcal{F}_H$ for the smooth, and to $\mathcal{F}_L$ for the discontinuous part of the solution. Here, a (low) first-order upwind scheme is coupled with the (high) second-order Lax-Wendroff scheme by introducing a flux limiter [53, 80].

Since the Lax-Wendroff scheme (3.13) can be cast in the form

$$U_j^{n+1} = U_j^n - \nu \left(U_j^n - U_{j-1}^n\right) - \frac{\nu}{2}(1-\nu)\left(U_{j+1}^n - 2U_j^n + U_{j-1}^n\right), \tag{3.21}$$

the high order Lax- Wendroff flux, $\mathcal{F}_H$, can be written as the sum of the low order upwind flux, $\mathcal{F}_L$ and a Lax-Wendroff correction $(\mathcal{F}_H - \mathcal{F}_L)$:

$$\mathcal{F}_H = \mathcal{F}_L + (\mathcal{F}_H - \mathcal{F}_L). \tag{3.22}$$

Here, $\mathcal{F}_L$ is the first order upwind scheme (3.8) and thus results in very diffusive solutions, whereas the correction term, $(\mathcal{F}_H - \mathcal{F}_L)$, is an anti-diffusive flux that captures discontinuities [96].

By virtue of (3.22), a method that includes the TVD property at discontinuities and holds second order accuracy on smooth solutions is defined by introducing a flux-limiter $\phi_j = \phi(U; j)$ [80]:

$$F = \mathcal{F}_L + \phi_j (\mathcal{F}_H - \mathcal{F}_L). \tag{3.23}$$

So, the value of ϕ_j is exclusively determined by the smoothness of the data. A flux limiter can be defined as

$$\phi_j = \phi(\theta_j), \qquad \theta_j = \frac{U_j^n - U_{j-1}^n}{U_{j+1}^n - U_j^n}, \tag{3.24}$$

where θ_j can be seen as a measure of the smoothness of the solution.

Hybridisation Between Upwind and Lax-Wendroff Methods

It is necessary to construct a condition on the flux-limiter ϕ_j so that a hybrid approach between the upwind and Lax-Wendroff methods satisfies the TVD requirement (3.20). The combination of first-order upwind and second-order Lax-Wendroff methods with the flux-limiter can be written as [53, 80, 96]:

$$F(U; j+1/2) = aU_j^n + \tfrac{1}{2}a(1-\nu)(U_{j+1}^n - U_j^n)\phi_j. \tag{3.25}$$

Using (3.25) in (3.5) gives

$$U_j^{n+1} = U_j^n - C_{j-1}\left(U_j^n - U_{j-1}^n\right) + D_j\left(U_{j+1}^n - U_j^n\right), \tag{3.26}$$

where

$$C_{j-1} = \nu - \frac{\nu}{2}(1-\nu)\phi_{j-1}, \quad D_j = -\frac{\nu}{2}(1-\nu)\phi_j. \tag{3.27}$$

However, since $D_j < 0$ for $\phi_j > 0$, (3.26) is not a TVD method. Equation (3.26) can be written as [80]:

$$U_j^{n+1} = U_j^n - C'_{j-1}(U_j^n - U_{j-1}^n) + D'_j(U_{j+1}^n - U_j^n), \tag{3.28}$$

with

$$C'_{j-1} = \nu + \frac{\nu}{2}(1-\nu)\left\{\frac{(U_{j+1}^n - U_j^n)\phi_j - (U_j^n - U_{j-1}^n)\phi_{j-1}}{U_j^n - U_{j-1}^n}\right\}, \; D'_j = 0. \tag{3.29}$$

Now, (3.29) satisfies the TVD condition (3.20), if

$$0 \le C'_j \le 1, \quad \text{for all} \quad j, \tag{3.30}$$

if the following holds true together with the CFL condition $|\nu| \le 1$:

$$\left|\frac{\phi(\theta_j)}{\theta_j} - \phi(\theta_{j-1})\right| \le 2, \qquad \text{for all} \quad \theta_j,\, \theta_{j-1}. \tag{3.31}$$

The requirement (3.31) is satisfied only if the following holds

$$0 \le \frac{\phi(\theta_j)}{\theta_j} \le 2, \quad \text{and} \quad 0 \le \phi(\theta_j) \le 2, \quad \text{for all} \quad \theta_j. \tag{3.32}$$

Some Flux Limiters: Several second-order TVD flux limiters have been constructed, including the following [80, 96]:

$$^{\text{Minmod}}\phi(\theta) = \max(0,\, \min(1,\, \theta)), \tag{3.33}$$

$$^{\text{Superbee}}\phi(\theta) = \max(0,\, \min(1,\, 2\theta),\, \min(\theta,\, 2)), \tag{3.34}$$

$$^{\text{Woodward}}\phi(\theta) = \max\left(0,\, \min(2,\, 2\theta,\, 0.5(1+\theta))\right). \tag{3.35}$$

3.4.3 Slope Limiters and Cell Reconstructions

The slope limiters are effective tools to develop appropriate piecewise linear cell reconstructions so that the numerical schemes hold the TVD property. Slope-limiter is very much similar to the flux-limiter. Here, slope limiters and cell reconstructions are considered for the Lax-Wendroff scheme. For $a > 0$, and $a < 0$, the upwind and Lax-Wendroff fluxes can be written as [53, 80]:

$$\mathcal{F}^{UW}(U; j+1/2) = \frac{1}{2}a(U_{j+1}^n + U_j^n) - \frac{1}{2}|a|(U_{j+1}^n - U_j^n), \tag{3.36}$$

$$\mathcal{F}^{LW}(U; j+1/2) = \frac{1}{2}a(U_{j+1}^n + U_j^n) - \frac{1}{2}a\nu(U_{j+1}^n - U_j^n). \tag{3.37}$$

The TVD flux for the Lax-Wendroff method is given by

$$F(U; j+1/2) = \mathcal{F}^{UW}(U; j+1/2) + \tfrac{1}{2}\phi_{j'} a(\mathrm{sgn}(\nu) - \nu)(U^n_{j+1} - U^n_j), \tag{3.38}$$

where, the flux limiter $\phi_{j'}$ is defined as

$$\phi_{j'} = \phi(\theta_{j'}), \quad \text{with} \quad \theta_{j'} = \frac{U^n_{j_a+1} - U^n_{j_a}}{U^n_{j+1} - U^n_j}, \qquad j_a = j - \mathrm{sgn}(a). \tag{3.39}$$

For $a > 0$ and $a < 0$ the TVD flux (3.38) can be written explicitly as [80]:

$$F(U; j+1/2) = a\left\{ U^n_j + \frac{\Delta x}{2}\frac{(U^n_{j+1} - U^n_j)}{\Delta x}\phi_j - \frac{\nu \Delta x}{2}\frac{(U^n_{j+1} - U^n_j)}{\Delta x}\phi_j \right\}, \tag{3.40}$$

$$F(U; j+1/2) = a\left\{ U^n_{j+1} - \frac{\Delta x}{2}\frac{(U^n_{j+1} - U^n_j)}{\Delta x}\phi_{j'} - \frac{\nu \Delta x}{2}\frac{(U^n_{j+1} - U^n_j)}{\Delta x}\phi_{j'} \right\}. \tag{3.41}$$

The possible oscillations in the Lax-Wendroff scheme can be caused by a poor choice of slopes between two grid values. This may lead to a piecewise linear reconstruction $\tilde{u}^n(x, t_n)$ with much larger total variation than in the given data U^n. This problem is eliminated by appropriately defining a slope-limiter.

For this, a reconstruction of the cell values by a piecewise linear function [80] is considered:

$$\tilde{u}^n(x, t_n) = U^n_j + \sigma_j (x - x_j), \quad \text{on the cell} \quad [x_{j-1/2}, x_{j+1/2}], \tag{3.42}$$

where, the slope σ_j depends on the data. So, for any choice of the slope σ_j, the mean value of the cell average $\tilde{u}^n(x, t_n)$ is equal to the data. Importantly, appropriate choice of slope σ_j significantly affects numerical results.

The slope limiter can be defined as [80]:

$$F(U; j+1/2) = a\, U^n_{j_1} + \frac{1}{2}|a|\sigma_{j_1}\Delta x - \frac{a}{2}\nu\sigma_{j_1}\Delta x, \tag{3.43}$$

with $j_1 = j$, if $a > 0$, and $j_1 = j + 1$, if $a < 0$, respectively. Therefore, with the definition (3.43), it can be seen that a piecewise linear reconstruction (3.42) is determined by the slope limiter. The slope-limiter plays an important role in determining the order of the resolution and the entire results of the methods.

3.4.4 TVD Lax-Friedrichs Method

A better cell reconstruction is necessary to obtain a spatially high-order differencing scheme. By applying the TVD limiters, the linear piecewise reconstruction is obtained.

The slope limiters avoid unwanted oscillations and provide second order accurate reconstructions for smooth solutions (except near the critical points) over the cell. So, the development of high-order resolution schemes without spurious oscillation is possible, but with the ability to capture a possible discontinuity [53, 80]. Simplicity is the main advantage of this method. Riemann problems need not to be solved.

In what follows, TVD methods are developed for the Lax-Friedrichs scheme [65, 80] which is defined by

$$U_j^{n+1} = U_j^n - \frac{\Delta t}{2\Delta x}\left\{ f_{j+1}^n - f_{j-1}^n - \frac{\Delta x}{\Delta t}\left(U_{j+1}^n - 2U_j^n + U_{j-1}^n\right)\right\}, \tag{3.44}$$

where $f_j^n = f(U_j^n)$. Here, the associated numerical fluxes are realized as:

$$\begin{aligned} \mathcal{F}_{j+1/2}^{LF} &= \tfrac{1}{2}\left\{ f_{j+1} + f_j - \tfrac{\Delta x}{\Delta t}\left(U_{j+1}^n - U_j^n\right)\right\}, \\ \mathcal{F}_{j-1/2}^{LF} &= \tfrac{1}{2}\left\{ f_j + f_{j-1} - \tfrac{\Delta x}{\Delta t}\left(U_j^n - U_{j-1}^n\right)\right\}. \end{aligned} \tag{3.45}$$

This method contains a dissipation term of the form

$$\phi_{j+1/2}^{LF} = \frac{\Delta x}{\Delta t}\left(U_{j+1}^n - U_j^n\right) = \frac{\Delta x}{\Delta t}\triangle U_{j+1/2}^n. \tag{3.46}$$

In this method, by replacing U_{j+1} and U_j by the second order accurate $U_{j+1/2}^R$ and $U_{j+1/2}^L$

$$U_{j+1/2}^L = U_j^n + \frac{1}{2}U_j', \quad U_{j+1/2}^R = U_{j+1}^n - \frac{1}{2}U_{j+1}', \tag{3.47}$$

$$\sigma_j = \left(\frac{U_{j+1}^n - U_j^n}{\Delta x}\right)\phi_j, \tag{3.48}$$

so that (3.38) (see, Fig. 3.1) improves the first-order Lax-Friedrichs scheme into a second-order TVD Lax-Friedrichs (TVDLF) scheme [53, 80],

$$U_j^{n+1} = U_j^n - \frac{\Delta t}{\Delta x}\left(\mathcal{F}_{j+1/2} - \mathcal{F}_{j-1/2}\right), \tag{3.49}$$

where the flux is given by

$$\mathcal{F}_{j+1/2} = \frac{1}{2}\left\{ f\left(U_{j+1/2}^R\right) + f\left(U_{j+1/2}^L\right) - \frac{\Delta x}{\Delta t}\triangle U_{j+1/2}^{RL}\right\}. \tag{3.50}$$

The associated dissipative limiter of the TVDLF scheme is given by

$$\phi_{j+1/2}^{TVDLF} = \frac{\Delta x}{\Delta t}\left(U_{j+1/2}^R - U_{j+1/2}^L\right) = \frac{\Delta x}{\Delta t}\triangle U_{j+1/2}^{RL}. \tag{3.51}$$

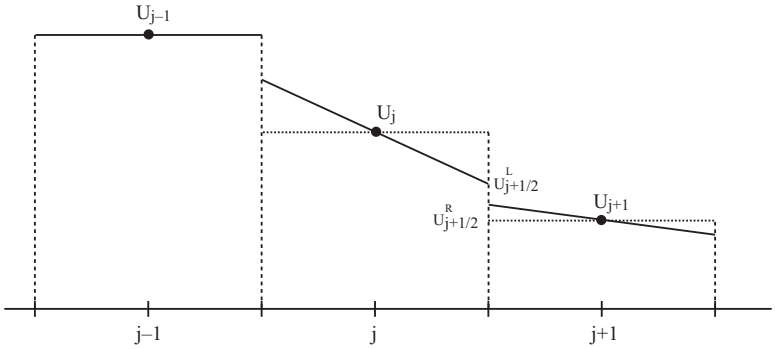

Figure 3.1: Schematic diagram for the cell average physical values U_j (dashed lines) and their linear piecewise cell reconstructions (solid lines). For each interface (e.g., between U_j and U_{j+1}) there are two values: $U^L_{j+1/2} = U_j + U'_j/2$ from the left-side of the cell and $U^R_{j+1/2} = U_{j+1} - U'_{j+1}/2$ from the right-side of the cell with the corresponding approximate derivatives U'_j and U'_{j+1}, respectively. This figure has been reproduced from Pudasaini and Hutter 2007 [80].

3.5 Non-Oscillatory Central Schemes

Here, some basic concepts are presented, and Non-Oscillatory Central Schemes are constructed. The classical second-order accurate Lax-Friedrichs scheme [53] was extended by Nessyahu and Tadmor (1990) [65] to develop the one-dimensional Non-Oscillatory Central Differencing (NOC) scheme. This is a high-resolution (higher-order) scheme that satisfies the TVD requirement (3.20). The NOC scheme utilizes the TVD limiter for the cell reconstructions [53, 80, 97, 98]. The main concept of the NOC scheme is that this is based

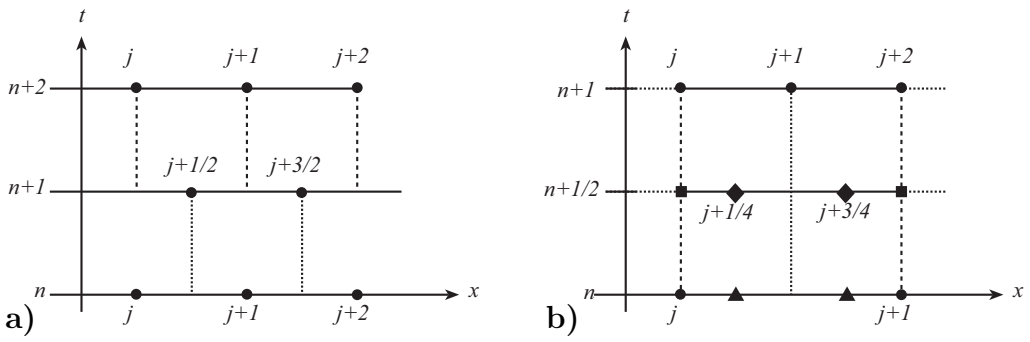

Figure 3.2: Diagram of the NOC scheme. **a)** Grid points computed in the NOC method. **b)** NOC computational diagram. Here, • indicate the grid points at time level n, $n+1$ and $n+2$. ■ represent the positions where the fluxes $\mathcal{F}$ at time level $n+1/2$ are approximated, ♦ are for the source terms s and ▲ denote the quarter and three-quarter points, e.g., $U^n_{j+1/4}$, $U^n_{j+3/4}$. This figure has been reproduced from [80].

on a two-steps *predictor-corrector* method with a *staggered grid* [80]. The essence of this method is that at time $t^{n+1} = t^n + \Delta t$, the cell averages $U^{n+1}_{j+1/2}$ are evaluated over the bounded region $[x_j, x_{j+1}]$, see, Fig. 3.2. Therefore, the boundaries of the cells at the new time level are the centers of the cells at the old time level. Importantly, at these boundary points, the piecewise polynomial reconstruction of the cell averages at the old time level t^n is smooth, and still remains smooth for $t < t^{n+1}$ under an appropriate restriction of the time step [65, 80].

In order to develop a NOC scheme, a scalar hyperbolic differential equation is considered:

$$\frac{\partial w}{\partial t} + \frac{\partial f(w)}{\partial x} = s(w), \tag{3.52}$$

where, $f(w)$ is the transport flux and $s(w)$ is the source term. Integrating (3.52) we obtain

$$\begin{aligned}\int_{x_j}^{x_{j+1}} w(x,\, t^{n+1})\, dx = \int_{x_j}^{x_{j+1}} w(x,\, t^n)\, dx - \int_{t^n}^{t^{n+1}} \left(f(x_{j+1},\, t) - f(x_j,\, t)\right)\, dt \\ + \int_{x_j}^{x_{j+1}} \int_{t^n}^{t^{n+1}} s(x,\, t)\, dt\, dx,\end{aligned} \tag{3.53}$$

or,

$$\Delta x\, U^{n+1}_{j+1/2} = \frac{\Delta x}{2}\left(U^n_{j+1/4} + U^n_{j+3/4}\right) - \triangle t\left(f^{n+1/2}_{j+1} - f^{n+1/2}_{j}\right) + \frac{\Delta t\, \Delta x}{2}\left(s^{n+1/2}_{j+1/4} + s^{n+1/2}_{j+3/4}\right), \tag{3.54}$$

where $U_{j+1/2}$ is the cell average over $[x_j,\, x_{j+1}]$. Dividing (3.54) by Δx produces a scheme [80]:

$$U^{n+1}_{j+1/2} = \frac{1}{2}\left(U^n_{j+1/4} + U^n_{j+3/4}\right) - \frac{\triangle t}{\triangle x}\left(f^{n+1/2}_{j+1} - f^{n+1/2}_{j}\right) + \frac{\triangle t}{2}\left(s^{n+1/2}_{j+1/4} + s^{n+1/2}_{j+3/4}\right), \tag{3.55}$$

see Fig. 3.2b. Using the TVD slope limiter σ^n_j, the values of $U^n_{j+1/4}$ and $U^n_{j+3/4}$ are determined by the reconstruction over the j^{th} and $(j+1)^{th}$ cell:

$$U^n_{j+1/4} = U^n_j + \frac{\Delta x}{4}\sigma^n_j, \quad U^n_{j+3/4} = U^n_{j+1} - \frac{\Delta x}{4}\sigma^n_{j+1}. \tag{3.56}$$

The integral of f is approximated by the physical values [80]:

$$f^{n+1/2}_j = f\left(U^{n+1/2}_j\right), \qquad f^{n+1/2}_{j+1} = f\left(U^{n+1/2}_{j+1}\right), \tag{3.57}$$

where,

$$U^{n+1/2}_j = U^n_j + \frac{\triangle t}{2}\left(\partial U/\partial t\right)^n_j, \;\; U^{n+1/2}_{j+1} = U^n_{j+1} + \frac{\triangle t}{2}\left(\partial U/\partial t\right)^n_{j+1}. \tag{3.58}$$

Similarly, the integral of s is approximated by

$$s^{n+1/2}_{j+1/4} = s\left(U^{n+1/2}_{j+1/4}\right), \quad s^{n+1/2}_{j+3/4} = s\left(U^{n+1/2}_{j+3/4}\right). \tag{3.59}$$

And, the grid values are approximated by the cell reconstructions [80]:

$$\begin{aligned} U_{j+1/4}^{n+1/2} &= U_j^n + \tfrac{\triangle t}{2} \left(\partial U/\partial t\right)_j^n + \tfrac{\Delta x}{4}\sigma_j^n, \\ U_{j+3/4}^{n+1/2} &= U_{j+1}^n + \tfrac{\triangle t}{2} \left(\partial U/\partial t\right)_{j+1}^n - \tfrac{\Delta x}{4}\sigma_{j+1}^n. \end{aligned} \tag{3.60}$$

Since,

$$\partial f/\partial x = \left(\partial f/\partial w\right)\left(\partial w/\partial x\right), \quad a = \partial f/\partial w, \quad \sigma = \partial w/\partial x, \tag{3.61}$$

the conservation law (3.52) provides the temporal derivatives in (3.58) and (3.60):

$$\left(\partial w/\partial t\right)_j^n = -\left(\partial f/\partial x\right)_j^n + s_j^n = -a_j^n\,\sigma_j^n + s_j^n. \tag{3.62}$$

The CFL Condition: For homogeneous problem, substituting the TVD cell reconstruction by the midpoint rule and using the one-step scheme, (3.55) reduces to

$$U_{j+1/2}^{n+1} = \frac{1}{2}\left(U_j^n + U_{j+1}^n\right) - \frac{\triangle t}{\triangle x}\left(f_{j+1}^n - f_j^n\right). \tag{3.63}$$

This scheme satisfies the TVD requirement (3.18) with the CFL condition

$$\frac{\Delta t}{\Delta x}\left|\frac{f_{j+1} - f_j}{U_{j+1} - U_j}\right| \le \frac{1}{2}, \quad \Rightarrow \quad \frac{\Delta t}{\Delta x}\left|a^{\max}\right| < \frac{1}{2}, \quad \text{for all} \quad j, \tag{3.64}$$

where $a^{\max}$ is the maximum wave speed. With the CFL condition (3.64) the NOC scheme (3.55) possesses the TVD property for the conservative law $\partial w/\partial t + \partial f/\partial x = 0$ [65, 80, 97].

Chapter 4

Numerical Simulations of Sub-diffusion and Sub-advection

We will see in Chapter 5 that, with our present knowledge, it is not possible to fully and analytically solve the sub-diffusive and sub-advective fluid flows in porous media. So, here, a high resolution numerical solutions are presented for the full sub-diffusion and sub-advection model (2.31), which is then compared with the solution of the classical diffusion and advection model solution. Furthermore, the full sub-diffusion and sub-advection model solutions are presented both for the linear and quadratic drags, which reveal that the generalized drag plays important role in the form and propagation speed of the diffusion-advection waves. It is also demonstrated that the long time solution to sub-diffusive and sub-advective fluid flow through porous media is largely independent of the initial fluid profile [78]. Moreover, our numerical simulation results are also compared with that of Lutsko and Boon (2008) [60].

4.1 Numerical Method, Simulation Parameters

It is a great mathematical challenge to construct exact solutions to the full model equation (2.31), the sub-diffusion and sub-advection fluid flows in porous media [78]. In Chapter 5, semi-exact solutions have been constructed by reducing the model equation (2.31) to the classical advection-diffusion equation, and by using the separation of variables leading to special ordinary differential equations in the form of Lienard equation and Abel equation in canonical form and linearization of the model equation. Numerical solutions is today probably the most popular and convenient way for complex systems, one seeks to solve the complicated system of equations by numerical techniques. With the growing

development of hardware and software, and with the rapid increase of numerical and scientific computing techniques [25, 26, 80], numerical method has become the dominant approach in analyzing systems expressible in standard mathematical form. Here, focus is made on the numerical solution of the full model (2.31). The parameter values chosen for the simulation are $C = 2.5$ and $D = 0.1329$, respectively. The simulations are based on the TVD-NOC methods presented in Chapter 3.

4.2 Linear and Quadratic Drags

The drag can be linear ($J = 1$) or quadratic ($J = 2$):

$$u_f = \left[\frac{\gamma \cos\zeta}{C_{DG}}\alpha_f \left(\tan\zeta - \frac{\partial h}{\partial x}\right)\right]^{1/J}, \tag{4.1}$$

which is the generalized Darcy expression for the fluid velocity [24, 77, 78]. Then, the mass balance equation for fluid (2.24) becomes

$$\frac{\partial H}{\partial t} + \frac{\partial}{\partial x}\left(\left[CH^{J+1} - \frac{D}{J+1}\frac{\partial H^{J+1}}{\partial x}\right]^{1/J}\right) = 0, \tag{4.2}$$

where, in the present form, $C = \gamma \sin\zeta / C_{DG}$ and $D = \gamma \cos\zeta / C_{DG}$. This can be written in more convenient form as follows:

$$\frac{\partial H}{\partial t} + \frac{1}{J}\left[CH^{J+1} - \frac{D}{J+1}\frac{\partial H^{J+1}}{\partial x}\right]^{\frac{1}{J}-1}\left[C\frac{\partial H^{J+1}}{\partial x} - \frac{D}{J+1}\frac{\partial^2 H^{J+1}}{\partial x^2}\right] = 0. \tag{4.3}$$

or,

$$\frac{\partial H}{\partial t} + \frac{1}{J}\left[CH^{J+1} - \frac{D}{J+1}\frac{\partial H^{J+1}}{\partial x}\right]^{\frac{1}{J}-1}\frac{\partial}{\partial x}\left[CH^{J+1} - \frac{D}{J+1}(J+1)H^J\frac{\partial H}{\partial x}\right]. \tag{4.4}$$

We see that, for $J = 1$, the first square bracket in (4.4) becomes unity, and reduces to equation (2.31) with $\alpha = 2$. The numerical solutions for (2.31), with $J = 1$ (linear drag), and $J = 2$ (quadratic drag) are shown in Fig. 4.3 and Fig. 4.5 respectively.

4.3 Simulation Results and Discussion

Figure 4.1 shows the numerical solution of classical advective and diffusive equation which is Gaussian in shape. Figure 4.2 plots the time evolution of the *sub-diffusive fluid flow in porous and debris material* ($\alpha = 2$). The exact solution (solid lines) is compared directly with the numerical solution (open circles). For exact solutions of sub-diffusion model (5.11), we refer to §5.2. They match almost perfectly. In contrast to the classical *Gaussian*

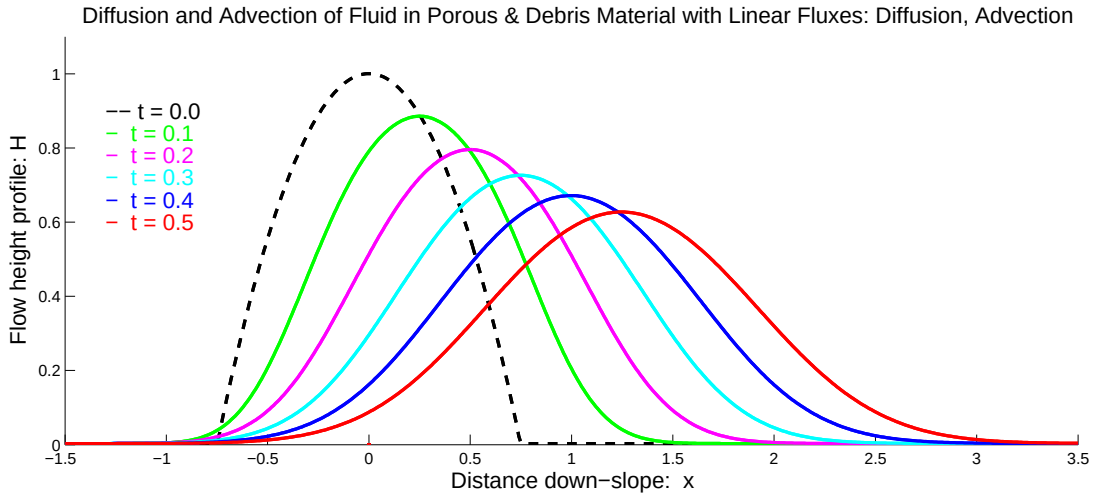

Figure 4.1: Advective-diffusive fluid flows with classical model: linear diffusion-advection fluxes [78].

solution, the solution (5.12) possesses some special properties [78]. For example, (i) these solutions have compact supports, and (ii) the front travels with finite speed, unlike other parabolic solutions [101, 102].

From Fig. 4.2, it is evident that, the solution to sub-diffusive fluid flow in porous media is fundamentally different than the diffusive fluid flow or diffusion of heat, pollutant and tracer particles in fluid. In the later case, the diffusion is linear, and the solution is represented by the classical Gaussian distribution whereas in the former case, the fluid diffuses slowly in time, and thus to maintain the mass balance, the flow (substance) is less spread in the lateral direction [78]. The *generalized diffusion equation* is in some ways similar to the fractional Fokker Planck equation [59]: both describe sub-diffusion.

Figure 4.3 presents the high-resolution numerical results for the sub-diffusion and sub-advection models [78]. The sub-advective and sub-diffusive flow behaviour is revealed by Figure 4.3. As the flow becomes more sharp (bore-type) in the front and it also elongates in the down-slope direction. The front advects continuously whereas the tail remains effectively unmoved. This is a typical behaviour of sub-advective flow [76, 78]. Since the flow is sub-diffusive, the flow does not spread laterally (here, in x-direction) which would be the case in the classical diffusion and advection processes. This solution is completely different from the solution for the classical diffusion-advection equation, where the entire fluid pocket would advect in the down-slope direction, which at the same time also diffuses with spreading Gaussian profile (Fig. 4.1). In contrast to the classical advection-diffusion of fluid in open environment, or transport of tracer particles and other substances by transporting fluid, where the tail of the initial substance distribution also

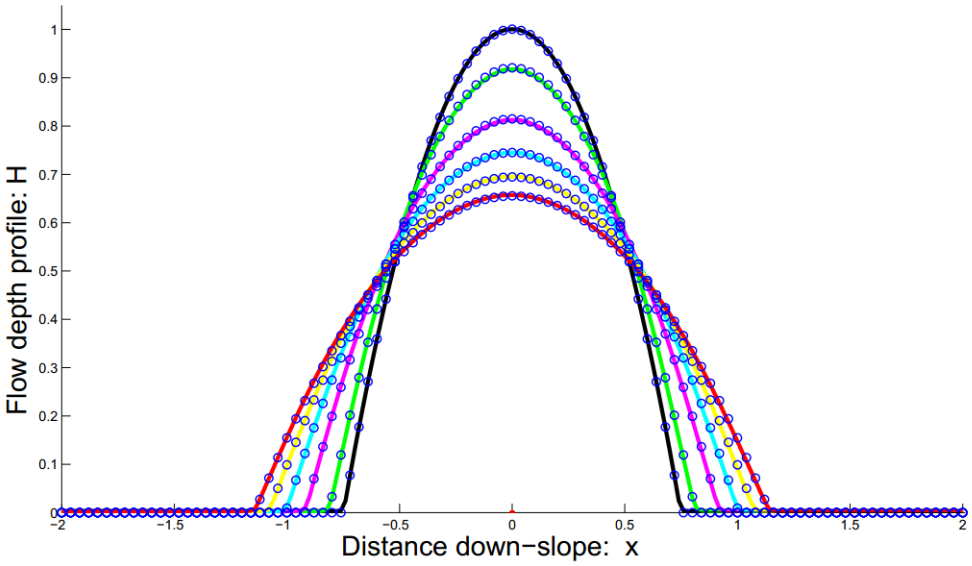

Figure 4.2: Time evolution of the sub-diffusive (so, $C = 0$) fluid flow in porous and debris material ($\alpha = 2$). The exact solution (solid lines, given by (5.12)) is compared directly with the numerical solution (open circles). Both solutions are presented for time slices $t_0 + [0.1, 0.3, 0.5, 0.7, 0.9]$, where $t_0 = 0.352$ is the reference time with $H_0 = H(t_0, x)$, the dark curve. Numerical solutions are found to match perfectly with the exact solutions [78].

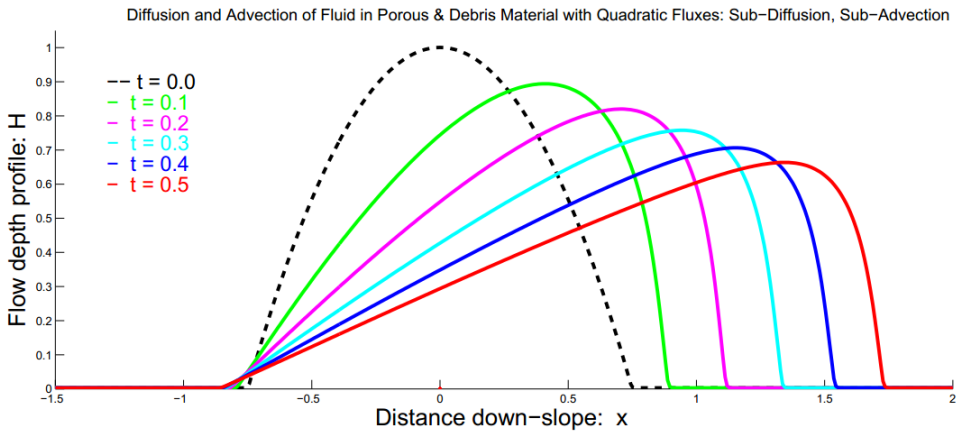

Figure 4.3: Sub-diffusion and sub-advection of a fluid through a porous media: Simulation for the new model (2.31), [78].

advects (with the speed of the transporting background fluid) in the down-slope direction, here for the viscous fluid flow through porous media, the tail, although less in intensity, always remains in its original position. This happens as some viscous fluid must stick at its original position. This is the most likely scenario for fluid flow in porous media [78]. This is due to the fact that, here, the solid porous skeleton is effectively stationary (unlike

the moving background fluid that transports tracer particles in usual advective-diffusive flow) and, in this flow situation, the advection of the fluid is due to the gravity force on the fluid.

The solution similar to that in Fig. 4.3 has also been presented by Lutsko and Boon (2008) [60] for their sub-diffusion, sub-advection model that emerged from generalized form of the classical Fokker-Planck equation with the effect of drift. They solved their model by applying the Monte Carlo numerical simulation technique, as shown in Fig. 4.4. The similarity in the numerical solution of sub-diffusive and sub-advective, in our result Fig. 4.3, and that in Lutsko and Boon (2008) [60], Fig. 4.4, is that the solution is more and more asymmetric as time progresses. Moreover, the velocity of the peak of the distribution also decreases.

As the numerical solution in Fig. 4.2 fits exactly with the true and analytical solution, this implies that, the numerical solution presented in Fig. 4.3 for the full sub-diffusion and sub-advection model most likely presents the reality. So, this also indicates the high performance and high accuracy of our numerical simulation method (TVD-NOC) Fig. 4.2. And that result presented in Fig. 4.3, Fig. 4.5, and Fig. 4.6 (see later) most

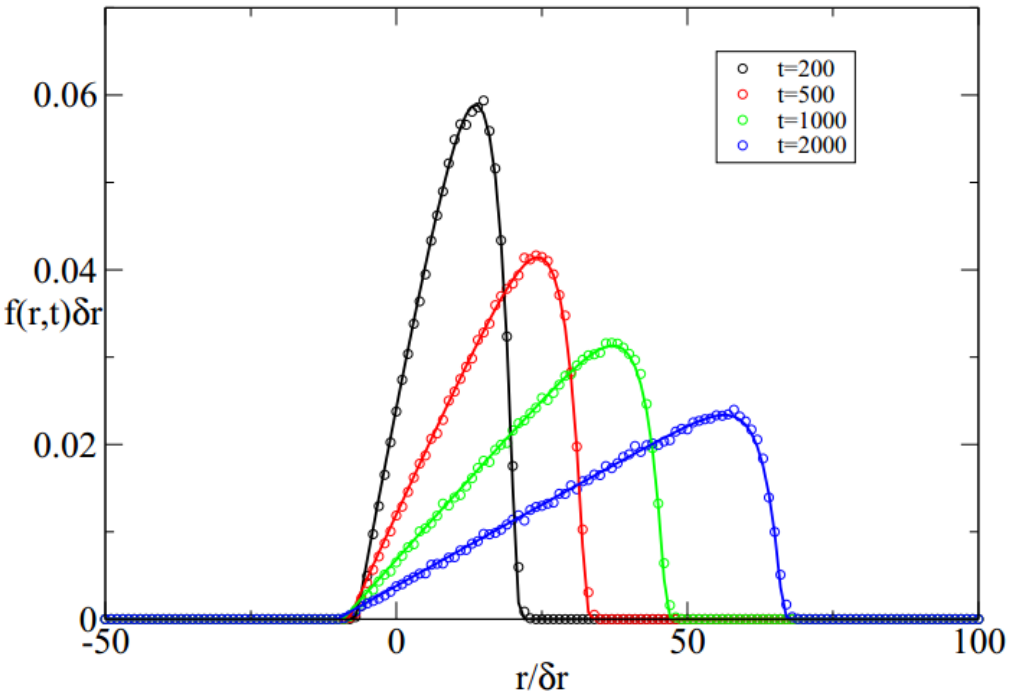

Figure 4.4: Time evolution of the sub-diffusive and sub-advective fluid flow in porous media for $q = 0$. The symbols are from Monte Carlo simulation of the random-walk (Lutsko and Boon, 2008) [60].

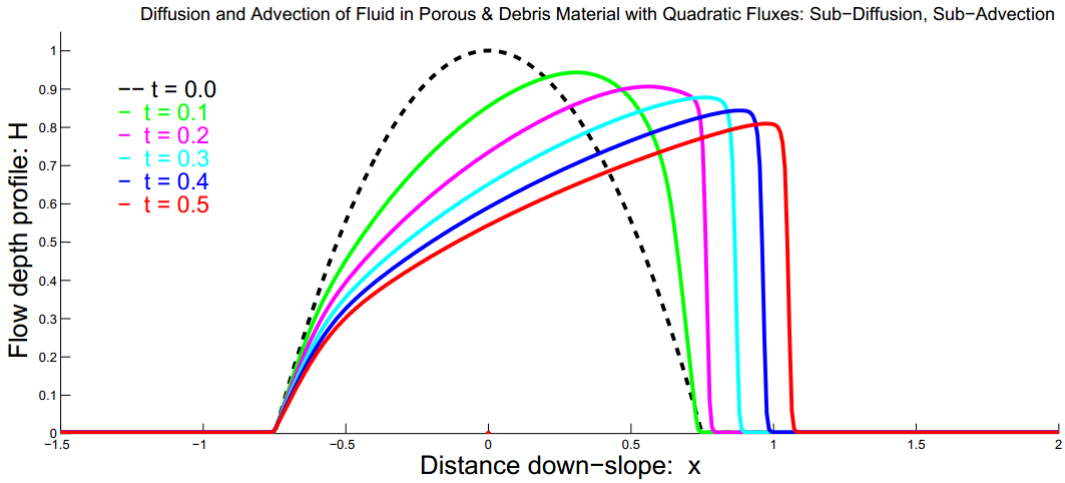

Figure 4.5: Same as in Fig. 4.3 but now with quadratic drag [78].

likely provides us with real sub-diffusive and sub-advection flow situations in general porous media. However, this must be verified with observation.

Figure 4.5 displays the effect of the quadratic drag in the sub-diffusive and sub-advective fluid flow in porous and debris material. Quadratic drag increases the exponents in the sub-advective and sub-diffusive fluxes, and effectively reduces the wave speed (of fluid flow). This resulted in the slow motion and deformation. As compared with the linear drag (Fig. 4.3), with the quadratic drag, the front is much sharper, flow depth is larger, the fluid body is amplified in the tail, the solution there is also strongly curved, and the flow is less stretched [78].

Numerical simulations reveal that, after certain time, solutions for the sub-diffusion and sub-advection are largely independent of their initial profiles as shows in Fig. 4.6, where the considered initial profiles were triangular (dashed line), Gaussian point source (solid line), and rectangular (dashed-dotted line). The figure shows that the initial fluid profiles do not substantially influence the time evolution of the fluid profiles through the porous and debris material. However, as evident from the initial profiles, the solutions with the Gaussian profile mainly lies in between the rectangular and triangular (in the front) and triangular and rectangular (in the back) solutions. So, the accurate knowledge of the initial profile of the fluid in the porous media may not necessary for the long time evolution of the sub-diffusive and sub-advective flows. This is an important and novel information in understanding the intrinsically complex behavior of diffusive and advective fluid flow in porous and debris materials [78].

It is to mention that some of the simulation results have already been presented in Khattri

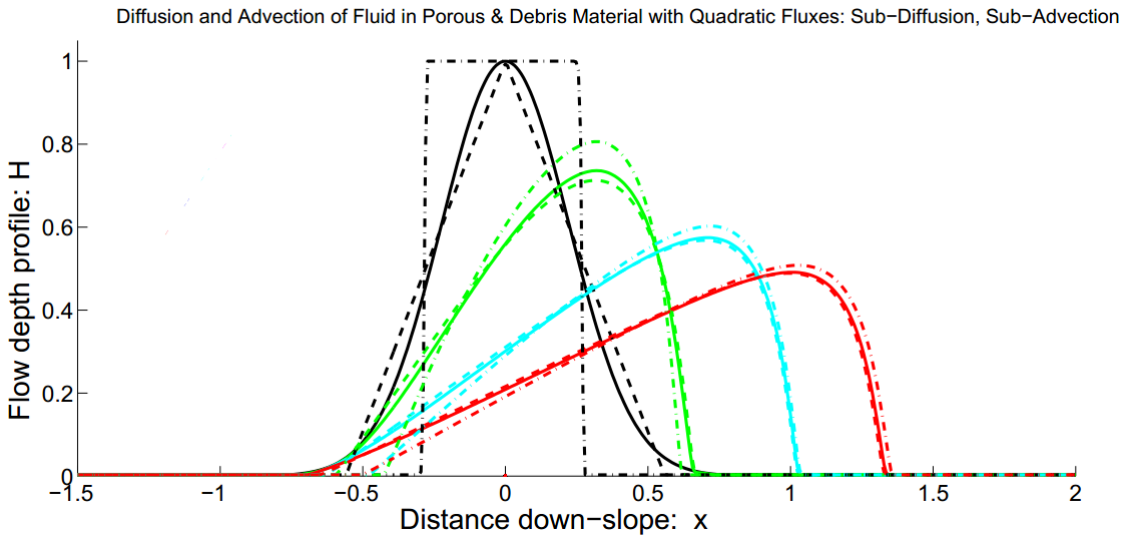

Figure 4.6: Sub-diffusive and sub-advective fluid flow through porous media with three different initial fluid profiles: smooth Gaussian (solid line), triangle (dashed line) and rectangle (dashed-dotted line) [78].

et al. (2013, 2014) [49, 50]. For effectively two-phase and geometrically three-dimensional debris flow, some simulation results have been presented in Kattel et al. (2013, 2014) [47, 48] and Kattel (2014) [46]. More advanced simulations with more complex eigenvalues of the model system due to Pudasaini (2012) [77], the three-dimensional subaerial debris flows impacting a fluid reservoir and thus generating tsunami waves can be found in Pokhrel et al. (2013, 2014) [69, 70] and Pokhrel (2014) [68]; and Kafle et al. (2013, 2014) [44, 45], respectively.

Chapter 5

Some Exact Solutions for Sub-diffusion & Sub-advection Flows

Here, some exact analytical solutions to the model equation (2.31) are presented. The complete solutions are derived for the reduced classical diffusion-advection fluid flows with linear fluxes, and the full sub-diffusive fluid flows [78]. Solutions for the classical linear diffusion and the new sub-diffusion with quadratic diffusive fluxes are compared. The similarities and differences in the solutions are discussed. Some exact solutions for the full sub-diffusion and sub-advection equation are constructed, including the solutions for the reduced models in the form of the classical diffusion and advection equation, and with separation of variables leading to special ordinary differential equations in the form of Lienard and Abel canonical equations, and linearization of the model equation. Exact analytical solution are obtained for each of these special situations.

5.1 Classical Diffusion-Advection Model

For $\alpha = 1$, equation (2.31) reduces to the classical diffusion-advection equation [23, 94] for which exact solutions can be constructed in the form of Gaussian distribution, which also takes into account the advection part, as done usually by proper coordinate transformation. For either $C = 0$ (diffusion only), or $D = 0$ (advection only) general exact solutions can be constructed [78]. $C = 0$ is equivalent to $\zeta = 0$, which means there is no advection because the debris material is not inclined and there is no gravity to pull the fluid down.

For $\alpha = 2$, and $C = 0$ equation (2.31) reduces to the generalized diffusion equation [12, 59, 78] for which exact solutions can be constructed in the form of q-Gaussian distribution. However, for $\alpha \neq 1$, it is a great mathematical challenge (even for $\alpha = 2$, our

particular interest) to construct exact solutions to equation (2.31), when $D \neq 0$, $C \neq 0$. The simple situation is considered by assuming that $\alpha = 1$ and $C \neq 0$, $D \neq 0$. Then, equation (2.31) becomes

$$\frac{\partial H}{\partial t} + C\frac{\partial H}{\partial x} - D\frac{\partial^2 H}{\partial x^2} = 0. \tag{5.1}$$

This is the classical diffusion-advection equation [23, 94]. Note that the advection term $C\partial H/\partial x$, has a first order derivative, which means that if x is replaced by $-x$ the term changes sign (anti-symmetry), because it involves only the first order spatial derivative. Therefore, advection occurs in the flow direction (for $C > 0$, in the direction of increasing x) whereas, the diffusion term, $D(\partial^2 H/\partial x^2)$, has a second order spatial derivative, which means that if x is replaced by $-x$ the term does not changes the sign (symmetry) [22]. Physically, this means that diffusion takes place in both the upstream and downstream directions.

Exact analytical solutions exist for simple model (5.1). We construct the solution by using coordinate transformation for the moving coordinate system. Assume that an instantaneous point source of mass $\mathcal{M} = M/A$ is released at location x_0 and time t_0. A coordinate transformation $(x, t) \to (\xi, \tau)$ for moving (with C) system can be introduced: $\xi = (x - x_0) - C(t - t_0)$ and $\tau = t$. Then, by using the chain rule of differentiation, (5.1) becomes:

$$\frac{\partial H}{\partial \xi}\frac{\partial \xi}{\partial t} + \frac{\partial H}{\partial \tau}\frac{\partial \tau}{\partial t} + C\left(\frac{\partial H}{\partial \xi}\frac{\partial \xi}{\partial x} + \frac{\partial H}{\partial \tau}\frac{\partial \tau}{\partial x}\right) - D\frac{\partial}{\partial x}\left(\frac{\partial H}{\partial \xi}\frac{\partial \xi}{\partial x}\right) = 0,$$

which reduces to classical diffusion equation in the coordinates ξ and τ:

$$\frac{\partial H}{\partial \tau} = D\frac{\partial^2 H}{\partial \xi^2}. \tag{5.2}$$

The boundary conditions can be set [22, 94]:

$$H(\pm\infty, \tau) = 0,$$

meaning that H at $\pm\infty$ is zero. This is meaningful as the intensity of any substance vanishes at infinity. As initial condition, one may take [94]:

$$H(\xi, 0) = (M/A)\delta(\xi),$$

where, δ is the Dirac delta functional, which is zero everywhere except at $\xi = 0$, where it is infinite. This means that H has a point source at ξ at the initial time with the value $\mathcal{M} = M/A$. The integral of the delta function from $-\infty$ to ∞ is 1.

Similarity method is adopted to obtain the solution of (5.2) [22, 23, 94]. Let us introduce the new similarity variable $\eta = \xi/\sqrt{D\tau}$. For this variable, we have:

$$\frac{\partial \eta}{\partial \tau} = -\frac{\eta}{2\tau}, \quad \frac{\partial \eta}{\partial \xi} = \frac{1}{\sqrt{D\tau}}\cdot$$

Now, the following substitutions are made:

$$H = \frac{M}{A\sqrt{D\tau}} f\big(\xi/\sqrt{D\tau}\big), \quad \text{and} \quad \eta = \xi/\sqrt{D\tau}, \tag{5.3}$$

where, f is a function to be determined. Using the chain rule of differentiation, we have

$$\begin{aligned} \frac{\partial H}{\partial \tau} &= \frac{\partial}{\partial \tau}\left[\frac{M}{A\sqrt{D\tau}} f(\eta)\right] \\ &= \frac{M}{A\sqrt{D\tau}}\left(-\frac{1}{2}\right)\frac{1}{\tau} f(\eta) + \frac{M}{A\sqrt{D\tau}}\frac{\partial f}{\partial \eta}\frac{\partial \eta}{\partial \tau} \\ &= -\frac{M}{2\,A\,\tau\sqrt{D\tau}}\left(f + \eta\frac{\partial f}{\partial \eta}\right). \end{aligned} \tag{5.4}$$

Again, by using chain rule, we have for the diffusion term in (5.2):

$$\begin{aligned} \frac{\partial^2 H}{\partial \xi^2} &= \frac{\partial}{\partial \xi}\left[\frac{\partial}{\partial \xi}\left(\frac{M}{A\sqrt{D\tau}} f(\eta)\right)\right] \\ &= \frac{\partial}{\partial \xi}\left[\frac{\partial \eta}{\partial \xi}\frac{\partial f}{\partial \eta}\frac{M}{A\sqrt{D\tau}}\right] \\ &= \frac{M}{A\,D\tau\sqrt{D\tau}}\frac{\partial^2 f}{\partial \eta^2}\cdot \end{aligned} \tag{5.5}$$

Substituting (5.4)-(5.5) in the diffusion equation (5.2), we get

$$\frac{d^2 f}{d\eta^2} + \frac{1}{2}\left(f + \eta\frac{df}{d\eta}\right) = 0, \tag{5.6}$$

which is an *ordinary differential equation*. This shows that the great advantage of using a similarity variable and function is that it reduces the complex partial differential equation into a relatively simple ordinary differential equation.

To solve (5.6), we first make use of the identity

$$\frac{d(f\eta)}{d\eta} = f + \eta\frac{df}{d\eta}\cdot$$

Substitution gives us

$$\frac{d}{d\eta}\left[\frac{df}{d\eta} + \frac{1}{2} f\eta\right] = 0\cdot$$

Integrating with respect to η, we get

$$\frac{df}{d\eta} + \frac{1}{2} f\eta = N, \tag{5.7}$$

where, the constant N is to be determined by using initial and boundary conditions. The boundary conditions for the original partial differential equation are [23, 94]:

$$H,\ \frac{\partial H}{\partial \xi} \to 0 \text{ for } \xi \to \pm\infty\cdot$$

Since $\eta = \xi/\sqrt{D\tau},\ \eta \to \pm\infty$ as $\xi \to \pm\infty$, and since

$$f(\eta) = \frac{\sqrt{D\tau}}{M/A} H(\xi, \eta),\ \ \frac{df}{d\eta} = \frac{\sqrt{D\tau}}{M/A} \frac{\partial H}{\partial \xi},$$

$f,\ \partial f/\partial \eta \to 0$ as $H,\ \partial H/\partial \xi \to 0$. So, the boundary conditions for ordinary differential equation are $f,\ \partial f/\partial \eta \to 0$ as $\eta \to \pm\infty$. This boundary condition requires that $N = 0$. So, (5.7) becomes

$$\frac{df}{d\eta} = -\frac{1}{2} f\eta,$$

or,

$$\frac{df}{f} = -\frac{1}{2}\eta d\eta,$$

This is an ordinary differential equation in which the variables are separated that can immediately be integrated to obtain:

$$f = C_1 \exp(-\eta^2/4),$$

where, C_1 is a constant of integration. Transforming back to the original coordinate $(\xi, \eta) \to (\xi, \tau)$. Since, $\eta = \xi/\sqrt{D\tau}$, we obtain

$$\begin{aligned} H &= \frac{M}{A\sqrt{D\tau}} f(\eta), \\ &= \frac{C_1 M}{A\sqrt{D\tau}} \exp\left(\frac{-\xi^2}{4D\tau}\right)\cdot \end{aligned}$$

To find the constant C_1, the conservation of mass [23, 94] is imposed as:

$$\int_{-\infty}^{\infty} H(\xi, \tau) d\xi = \frac{M}{A}\cdot \tag{5.8}$$

Integration of $H(\xi, \tau)$ in space is straightforward. Substituting $H(\xi, \tau)$ in equation (5.8)

$$\int_{-\infty}^{\infty} \frac{C_1 M}{A\sqrt{D\tau}} \exp\left(\frac{-\xi^2}{4D\tau}\right) d\xi = \frac{M}{A}$$

$$\text{or,}\ \ \frac{C_1}{\sqrt{D\tau}} \int_{-\infty}^{\infty} \exp\left(\frac{-\xi^2}{4D\tau}\right) d\xi = 1\cdot$$

With substitution, $y = \xi/2\sqrt{D\tau}$, implies $d\xi = 2\sqrt{D\tau}dy$. So,

$$2C_1 \int_{-\infty}^{\infty} \exp(-y^2)dy = 1 \cdot$$
$$\therefore \quad C_1 = \frac{1}{2\sqrt{\pi}}.$$

Thus, the similarity solution for (5.2) is

$$H(\xi, \tau) = \frac{\mathcal{M}}{\sqrt{4\pi D\tau}} \exp\left[-\frac{\xi^2}{4D\tau}\right]. \tag{5.9}$$

Substituting back to the original coordinates $(\xi, \tau) \rightarrow (x, t)$, we obtain the solution of (5.1) [23, 30, 94]:

$$H(t, x) = \frac{\mathcal{M}}{\sqrt{4\pi D(t - t_0)}} \exp\left[-\frac{((x - x_0) - C(t - t_0))^2}{4D(t - t_0)}\right]. \tag{5.10}$$

Figure 5.1 and Fig. 5.2 show the time evolution of the solution (5.10) of the diffusion only and diffusion-advection equation, respectively, with $\mathcal{M} = 2.9$, $D = 0.2167$, and $C = 0$ (Fig. 5.1) and $C = 0.3$ (Fig. 5.2). The solution (5.10) generates advective-diffusive fluid flow. However, the question remains: if this solution is physically meaningful for fluid flows through porous and debris materials [78].

Here, the terms associated with D and C represent the classical linear diffusion and linear advection process, because the advection and diffusion fluxes (CH and DH, respectively) are linear in H. In Fig. 5.2, the fluid pocket advects with the speed C in the flow direction (here, the down-slope direction), whereas at the same time, the fluid diffuses in

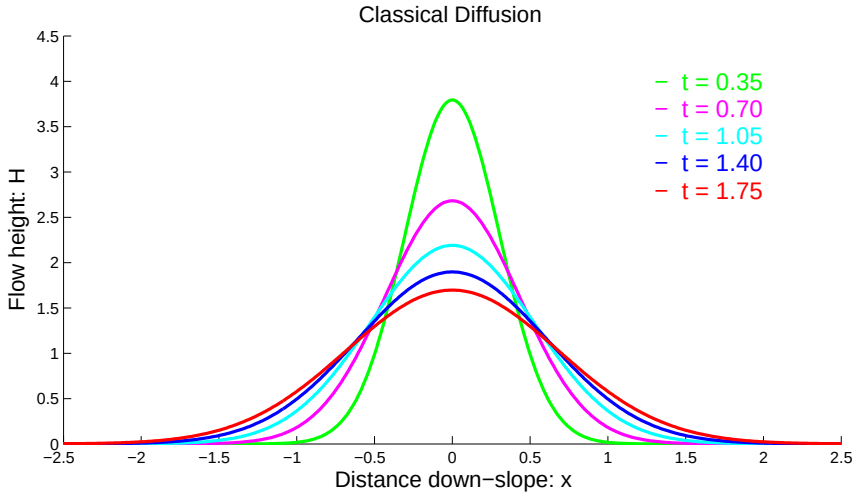

Figure 5.1: Analytical solutions for classical diffusive equation (solution with $C = 0$ in (5.10)).

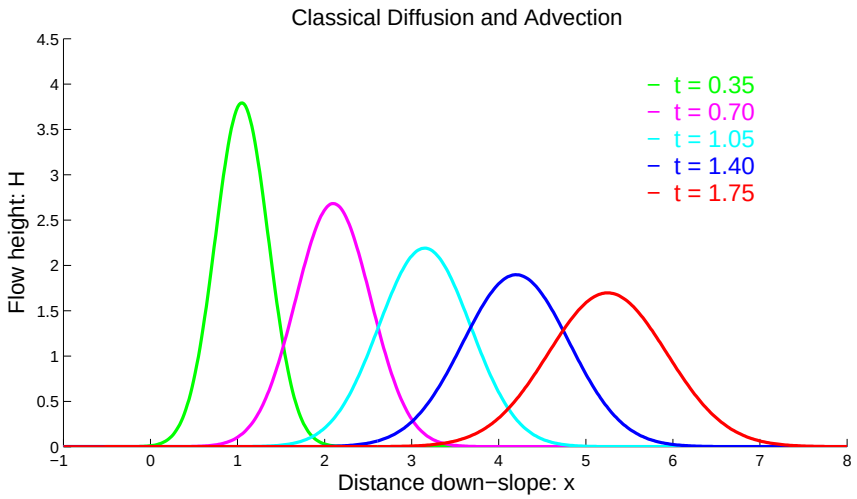

Figure 5.2: Analytical solution of the classical advection and diffusive equation (5.1). The solutions (5.10) are symmetrical.

both the upstream and downstream directions as controlled and described by the diffusion coefficient D [78]. At any time ($t > 0$), the evolving flow profile is a symmetric Gaussian, without finite support.

5.2 Generalized Diffusion, Porous Media Equation

Here, the main concern is with the physically advanced models and their solutions. For this reason, next, assume that $\alpha > 1$ (otherwise, say, general), $C = 0$, and $D \neq 0$. Then, the model (2.31) reduces to a special porous media equation with diffusion flux of order α in H:

$$\frac{\partial H}{\partial t} - D\frac{\partial^2 H^\alpha}{\partial x^2} = 0\cdot \tag{5.11}$$

Note that, in contrast to the classical porous media equation where the exponent α is determined by an exponent relationship between the fluid pressure and density, and the exponent is either pre-described or calibrated, here $\alpha = 2$ appears systematically [78]. Equation (5.11) is similar to Richards equation for water flow in unsaturated soil [86], where $H(= \theta)$ is the moisture content (i.e., the percentage of pore space at location x filled with fluid at time t). In Richards equation, $D(\theta) = D\theta$ is assumed. In the derivation of (5.11), we do not need to assume this, see Chapter 2.

Exact solution to (5.11) exists [6, 7, 12, 13, 59, 78, 101, 102] and can be written in the

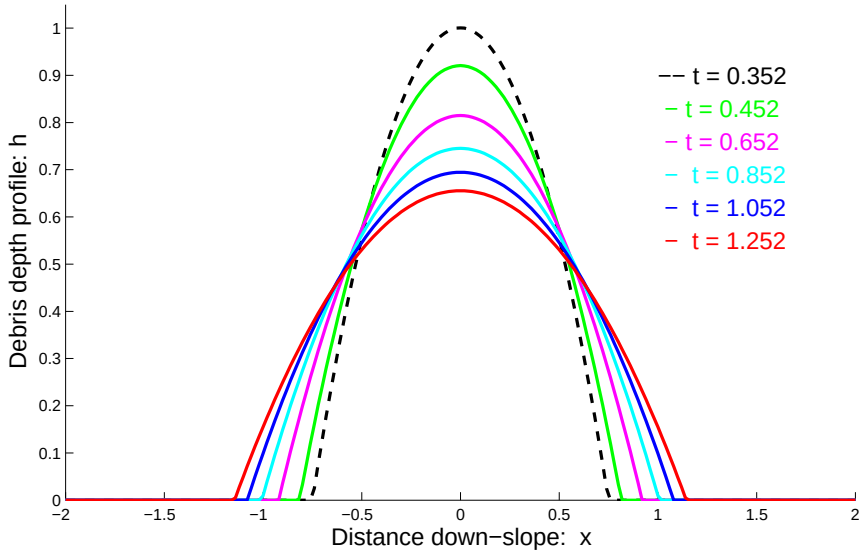

Figure 5.3: Time evolution of the sub-diffusive fluid flow in porous and debris material with parameters $q = 1$, $m_0 = 2$, $D = 0.1329$. The solution is based on the Lutsko and Boon (2008) [60], equation (5.12) for the generalized porous media flow diffusion equation based on Pudasaini (2012)[77].

form of the $q-$Gaussian [78]:

$$H(t,x) = t^{-\gamma/2}\left[\mathcal{B}^{\frac{1}{1-q}}\left(1 - \frac{1}{2m_0\mathcal{B}D}\frac{(1-q)}{(3-q)}\frac{x^2}{t^\gamma}\right)^{\frac{1}{1-q}}\Theta\left(1 - \frac{1}{2m_0\mathcal{B}D}\frac{(1-q)}{(3-q)}\frac{x^2}{t^\gamma}\right)\right], \quad (5.12)$$

where Θ is the step function and m_0 is a constant. In (5.12), $\mathcal{B}$ is the normalization factor given by

$$\mathcal{B} = \left(\frac{\eta(\eta+2)}{8m_0D}\right)^{\frac{\eta}{\eta+2}} B\left(\frac{1}{\eta}, \frac{1}{2}\right)^{-\frac{2\eta}{\eta+2}}, \quad (5.13)$$

where $\eta = 1 - q$, $\gamma = 2/(2+\eta)$, B is the beta function, and $q \to 0$ corresponds to $\alpha \to 2$. In the limit, $q \to 1$, equation (5.12) approaches the classical Gaussian solution given by (5.10), with $C = 0$.

Figure 5.3 shows the time evolution of the generalized diffusion solution with $m_0 = 2$, $D = 0.1329$, $\alpha = 2$. The sub-diffusive solution ($q = 0$), approaching the classical Gaussian solution by the sub-diffusive solution ($q \to 1$), and the classical Gaussian solution are plotted in Fig. 5.4. Here, parameter values are $D = 0.3542$ (which corresponds to $\zeta = 15°$, $C_{DG} = 0.6$, $\gamma = 1100/2500$), $t = 500$, $M = 1$, $A = 1$, and the constant of integration (Boon and Lutsko, 2007)[59] as unity. The initial profile ($t = 0$) is a point source. So, to match the reference solution, we multiply the approached classical Gaussian solution by

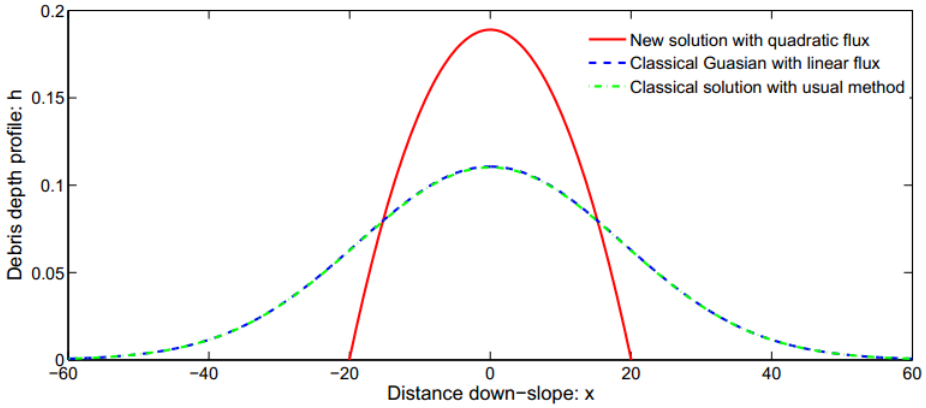

Figure 5.4: The sub-diffusive solution (solid red line, $q = 0$, i.e., quadratic flux, $\alpha = 2$), approximation of the classical Gaussian solution by the sub-diffusive solution (dashed blue line, $q \to 1$) and the classical Gaussian solution (dashed green line) are plotted together. There is a large difference between the sub-diffusive solution and solution with classical (linear flux) diffusion model [78].

a factor 0.91, and at the same time the usual classical Gaussian solution is multiplied by the factor 5.1981 [78]. On doing this, the solution behaviors remain unaltered for all the times (e.g., $t = 100, 600, 1500, 5000$, etc., not shown here).

There is a large difference between the quadratic *sub-diffusive solution* and solution with classical linear diffusion model (Pudasaini, 2014) [78]. However, in the limit, $q \to 1$, *sub-diffusive solution* exactly recovers the *classical Gaussian solution*. It seems that the solution with quadratic flux is more ellipsoidal rather than Mexican-hat type, corresponding to the solution of the classical diffusion equation with linear flux. Also, we note that, with the sub-diffusive model, the diffusion and dispersion is much slow and much less spread than the same with the linear flux (the classical diffusion model) [78]. In fact, the time scale for the quadratic flux is fundamentally different than the time scale in the classical (linear flux) diffusion equation. This finally leads to two completely different solutions as presented here. The new sub-diffusive solution reveals that the flow of fluid through the porous and debris material should be modelled with the non-linear (quadratic) flux diffusion equation rather than the classical linear diffusion equation [78]. Such a special phenomenon for generalized porous medium flow is revealed by Pudasaini (2014) [78] for the first time for the flow of fluid in the debris bulk. With appropriate values of D and α, the same model may find applications for the diffusion of fluid through skin and bone in bio-medical sciences [61].

5.3 Sub-diffusive and Sub-advective Equation

For simplicity, assume that $\alpha = 2$, then equation (2.31) becomes

$$\frac{\partial H}{\partial t} + C\frac{\partial H^2}{\partial x} - D\frac{\partial^2 H^2}{\partial x^2} = 0\cdot \tag{5.14}$$

The most interesting aspect in (5.14) is that $\alpha = 2$ emerges systematically from the derivation of the model equation [78]. It is a great challenge to construct exact analytical solutions, even to seemingly simple sub-diffusion and sub-advection equation (5.14). Here, some possible ways to construct exact solutions are outlined. Equation (5.14) can most probably be not solved directly and fully in this form. Based on our physical intuition, at this point, we need to apply some special mathematical tools to reduce the complexity. To do so, in what follows, the model equation is reduced in the form of the classical diffusion-advection equation, separation of variables is utilized, and linearization techniques are adopted, together with the associated fixed point, to construct some exact analytical solutions. Furthermore, we construct advanced exact solutions by using the Bring ultraradical [16] and higher-order hypergeometric function. In this course, Lienard and Abel equation will also be generated in canonical form, and provide other set of exact solutions are also generated[57, 78].

5.3.1 Reduction to Classical Diffusion-Advection Equation (I)

With the substitution

$$H^2 = \mathcal{H}, \quad 2\sqrt{\mathcal{H}}\partial t = \partial\tau, \tag{5.15}$$

the model (5.14) reduces, in the form, to the usual diffusion-advection equation

$$\frac{\partial \mathcal{H}}{\partial \tau} + C\frac{\partial \mathcal{H}}{\partial x} - D\frac{\partial^2 \mathcal{H}}{\partial x^2} = 0, \tag{5.16}$$

where, τ is a new 'time' variable. Now, we wish to solve (5.16) by the method of separation of variables. Because, this will provide us with solution in the original variables, t and x. Assume that the spatial and time components of the function $\mathcal{H}$ can be separated as:

$$\mathcal{H}(\tau, x) = \frac{X(x)}{T(\tau)}, \tag{5.17}$$

where, $X = X(x)$ and $T = T(\tau)$ are the two new functions in space (x) and time (τ) which are to be determined. Then, by substituting (5.17), equation (5.16) reduces to

$$\frac{1}{DT}\frac{\partial T}{\partial \tau} = \frac{1}{X}\left[\mathcal{C}\frac{\partial X}{\partial x} - \frac{\partial^2 X}{\partial x^2}\right], \tag{5.18}$$

where, $\mathcal{C} = C/D$. In (5.18), the left hand side is only a function of τ (or, T), and the right hand side is a function of x (or, X) alone. Thus, the variables are separated. So, (5.18) implies that there must exist a constant K such that

$$\frac{1}{DT}\frac{\partial T}{\partial \tau} = -K = \frac{1}{X}\left[\mathcal{C}\frac{\partial X}{\partial x} - \frac{\partial^2 X}{\partial x^2}\right]. \tag{5.19}$$

The constant K is to be determined from the solution for T and X, and other conditions associated with the model equation (5.16). Equation (5.19) now represents a set of two ordinary differential equations, one for T, and the other for X. This is a great advantage associated with the method of separation of variables. As this method transforms the characteristically much more complicated, perhaps in many cases exactly unsolvable, partial differential equations to much simpler, readily and exactly solvable set of ordinary differential equations [71, 78].

Now, taking the left and the middle terms in (5.19), we obtain:

$$\frac{\partial T}{\partial \tau} = -KDT. \tag{5.20}$$

This equation can be solved exactly, and the solution is:

$$T = \exp(K_1 - KD\tau), \tag{5.21}$$

or,

$$\tau = \frac{-\ln T + K_1}{DK}, \tag{5.22}$$

where, K_1 is a constant of integration. So, T is an exponential function of the new time variable, τ.

Again, taking the middle and the right terms in (5.19), we get

$$\frac{d^2X}{dx^2} - \mathcal{C}\frac{dX}{dx} = KX\cdot \tag{5.23}$$

This is a second order linear ordinary differential equation which can be solved exactly [52, 95] by assuming the solution of the form:

$$X = e^{\lambda x}, \tag{5.24}$$

where, λ is a parameter whose values are to be determined. Substituting (5.24) into (5.23), we obtain

$$(\lambda^2 - \mathcal{C}\lambda - K)e^{\lambda x} = 0,$$

which is the characteristic equation associated with the ordinary differential equation (5.23). Since $e^{\lambda x} \neq 0$, because $X \neq 0$, we must have

$$\lambda^2 - \mathcal{C}\lambda - K = 0\cdot$$

So, the roots of the characteristic equation are

$$\lambda = \frac{\mathcal{C} \pm \sqrt{\mathcal{C}^2 + 4K}}{2}\cdot \tag{5.25}$$

Therefore, from (5.24) and (5.25) the general solution of (5.23) is given by the superposition:

$$X = C_1 \exp\left(-\frac{1}{2}x\left(\sqrt{\mathcal{C}^2 + 4K} - \mathcal{C}\right)\right) + C_2 \exp\left(\frac{1}{2}x\left(\sqrt{\mathcal{C}^2 + 4K} + \mathcal{C}\right)\right)\cdot \tag{5.26}$$

Where C_1 and C_2 are constants of integration.

However, it still remains to determine τ in terms of the original time variable, t. From (5.15) and (5.21), we obtain

$$\partial\tau = \frac{2\sqrt{X}}{\sqrt{T}}\partial t,$$

$$\text{or,} \qquad \partial\tau = \frac{2\sqrt{X}}{\sqrt{\exp(K_1 - DK\tau)}}\partial t\cdot$$

Since the space and time variables are separated, in this equation X plays the role of a parameter, and thus can be solved as the variables τ and t are separated:

$$2\sqrt{X}\partial t = \exp(K_1/2)\exp(-DK\tau/2)\partial\tau,$$

$$\text{or,} \qquad 2\sqrt{X}t = \exp(K_1/2)\left(\frac{\exp(-DK\tau/2)}{-DK/2} + \frac{K_2}{DK/2\exp(K_1/2)}\right),$$

$$\text{or,} \qquad \frac{2\sqrt{X}t}{\exp(K_1/2)} = \frac{\exp(-DK\tau/2)}{-DK/2} + \frac{K_2}{DK/2\exp(K_1/2)},$$

$$\text{or,} \qquad \frac{-DK\sqrt{X}t}{\exp(K_1/2)} + K_2 = \exp(-DK\tau/2)\cdot$$

So, τ can be expressed in terms of t as

$$\tau = \frac{-2}{DK}\ln\left(\frac{-DK\sqrt{X}t}{\exp(K_1/2)} + K_2\right), \tag{5.27}$$

where K_2 is a constant of integration. Therefore, from (5.17), (5.21), and (5.26) an exact analytical solution for (5.14) is obtained:

$$H = \sqrt{\frac{C_1 \exp\left(-\frac{1}{2}x\left(\sqrt{\mathcal{C}^2 + 4K} - \mathcal{C}\right)\right) + C_2 \exp\left(\frac{1}{2}x\left(\sqrt{\mathcal{C}^2 + 4K} + \mathcal{C}\right)\right)}{\exp(K_1 - KD\tau)}}, \tag{5.28}$$

where, τ is given by (5.27). Note that, in the exact solution (5.28), the constant K, and the constants of integration K_1, K_2, C_1 and C_2 must be determined from the underlying configuration and the physics of the problem. Otherwise, for simulation purpose, the parameter values for these constants can be chosen properly.

Figure 5.5 plots the analytical solutions (5.27) and (5.28) for the time evolution of the sub-diffusive and sub-advective fluid flow in porous media with parameters $C = 1.12$, $D = 0.01$, $K = -0.4$, $K_1 = 10.01$, and $C_2 = 1.35$. Panel **a** corresponds to $C_1 = 1.012$ and panel **b** corresponds to $C_1 = 2$. The solutions are non-symmetrical which is the characteristics of the sub-diffusive and sub-advective flows. In both panels **a** and **b**, the front and tail remain effectively unmoved. The flow becomes more sharp in the front and

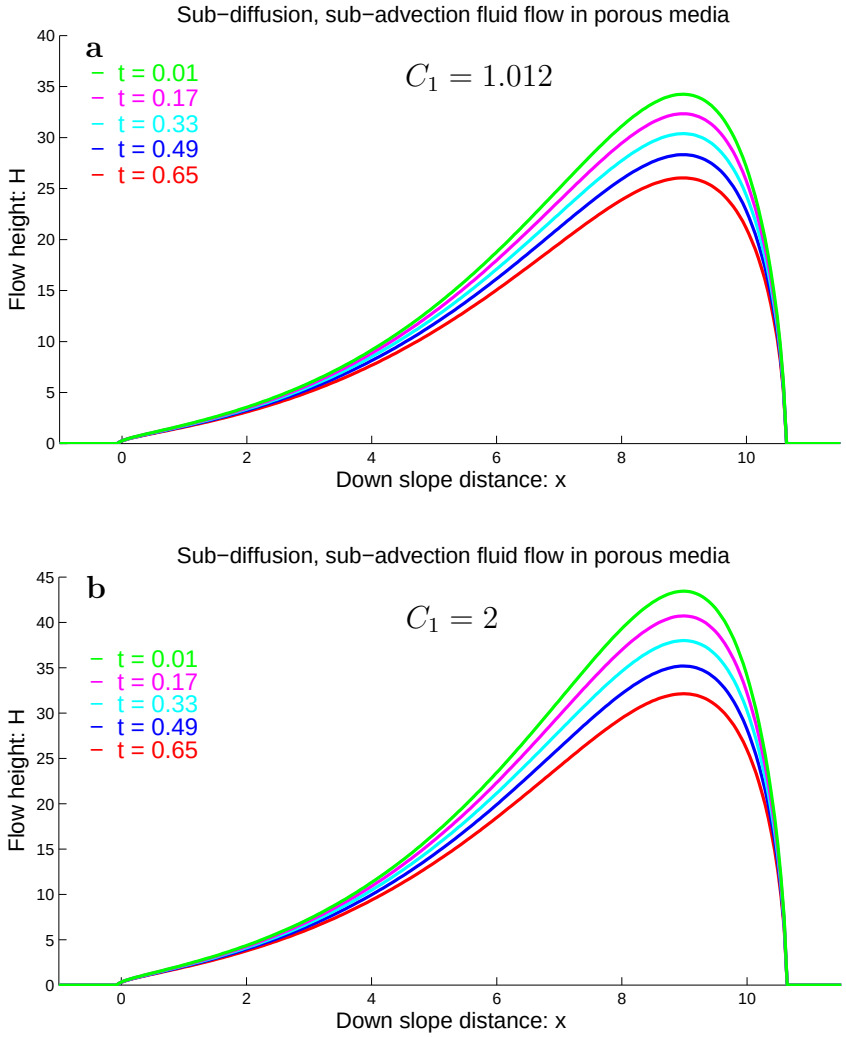

Figure 5.5: Sub-diffusive and sub-advective fluid flow through porous media: analytical solutions (5.27) and (5.28) with parameters are $C = 1.12$, $D = 0.01$, $K = -0.4$, $K_1 = 10.01$, and $C_2 = 1.35$.

elongates in the upslope direction. The effect of the parameter value C_1 is that, for larger value of C_1, the flow height is greater and sharper in upslope direction. This solution is completely different from the solution for the classical diffusion-advection equation (Fig. 5.2), where the front and tail effectively moved with Gaussian profile.

5.3.2 Reduction to Classical Diffusion-Advection Equation (II)

Exact solution for the equation (5.16) exists and takes the form,

$$\mathcal{H}(\tau, x) = \frac{\mathcal{M}}{\sqrt{4\pi D\tau}} \exp\left[-\frac{(x - C\tau)^2}{4D\tau}\right], \tag{5.29}$$

where $\mathcal{M}$ is the mass from an instantaneous point source that is released at location $x_0 = 0$ and time $t_0 = 0$. However, here, the solution $\mathcal{H}$ has been expressed in terms of τ, which is related to the time variable t by the equation, see (5.15):

$$H^2 = \mathcal{H}, \quad \partial t = \left(1/2\sqrt{\mathcal{H}}\right) \partial\tau\cdot \tag{5.30}$$

Since $\mathcal{H}$ is known in terms of τ, we may use (5.30) to find a functional relationship for τ in terms of t. However, although desirable, it may be very difficult, if not impossible, to explicitly convert the analytical solution (5.29) in terms of the original variables t and x.

Without any further reduction, it may not be possible to find exact solution in the form (5.29) that takes into account, in the classical form, the diffusion and advection of the sub-diffusion and sub-advection flow process. However, since a functional relationship for τ in terms of t is already been developed in (5.27) and the solution for X in (5.26):

$$\tau = \frac{-2}{DK} \ln\left(\frac{-DK\sqrt{X}t}{\exp(K_1/2)} + K_2\right), \tag{5.31}$$

and,

$$X = C_1 \exp\left(-\frac{1}{2}x\left(\sqrt{\mathcal{C}^2 + 4K} - \mathcal{C}\right)\right) + C_2 \exp\left(\frac{1}{2}x\left(\sqrt{\mathcal{C}^2 + 4K} + \mathcal{C}\right)\right), \tag{5.32}$$

Those solutions may be utilized to close (5.29). Therefore, the analytical solution for (5.14) is given by (5.29)-(5.32). Note that, here, X plays the role of a parameter.

Figure 5.6 shows the results given by the analytical solutions (5.29)-(5.32) with the parameters $C = 1.42$, $D = 1.01$, $K = 0.4$, $K_1 = 10.01$, $C_2 = 1.35$. Panel **a** corresponds to $C_1 = 1.0120$, and panel **b** corresponds to $C_1 = 1.3156$. It is to note that T is an exponential function of a new variable τ. In solutions (5.29)-(5.32), somehow, two solutions are super-imposed. This is mainly to get τ in terms of t. The flow height decreases

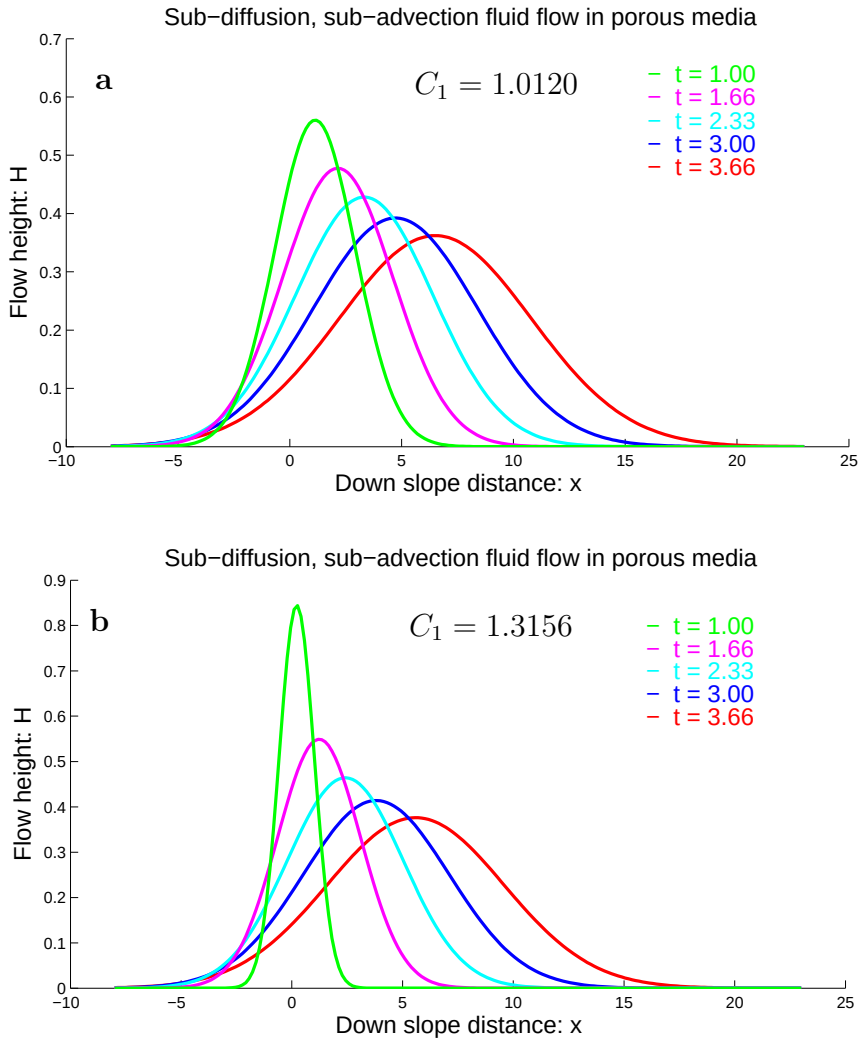

Figure 5.6: Sub-diffusive and sub-advective fluid flow through porous media: from analytical solution (5.29)-(5.32) with parameters $C = 1.42$, $D = 1.01$, $K = 0.4$, $K_1 = 10.01$, $C_2 = 1.35$.

with increasing time to get advecting solutions. In both panels **a** and **b**, the tails are somewhat unmoved but the fronts are moving forward. The effect of the parameter value C_1 is that, for larger value of C_1, the flow height is greater and there is less advection in the flow direction. These results are closed as presented in Fig. 4.3 and Fig. 4.4 in terms of advection and diffusion, but the tail remain effectively unmoved. Nevertheless, the solutions in Fig. 5.5 are more closer in the form with sub-diffusion and sub-advection solution in Fig. 4.3 and Fig. 4.4.

To further analyze the solutions (5.29)-(5.32) in detail, the focus is made on only at the sub-diffusive part of the solution. Figure 5.7 plots the time evolution of the solution (5.29)-(5.32) with $C = 0$. This solution reduces to *generalized diffusion solution* which is

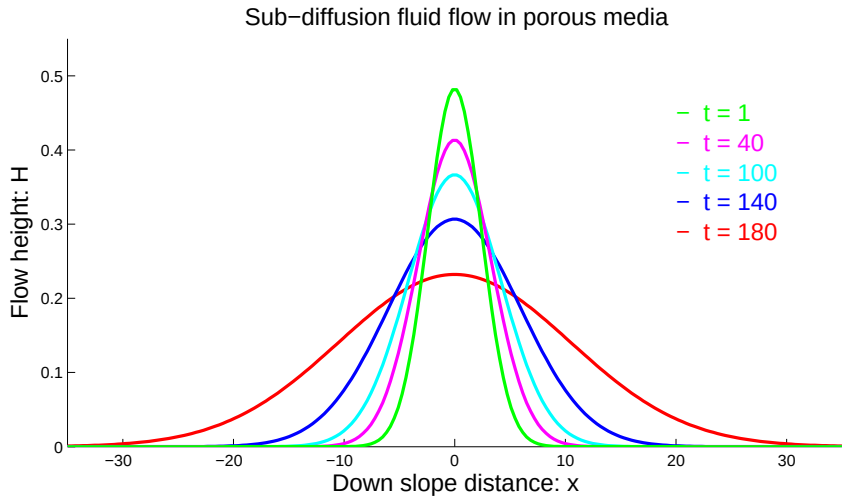

Figure 5.7: Time evolution of sub-diffusive fluid flow through porous media: analytical solution (5.29)-(5.32) with parameters $C_1 = 1.42$, $D = 1.01$, $K = 0.4$, $K_1 = 10.01$, $C_2 = 1.35$ and $C = 0$. The solution is somehow q-Gaussian similar to that presented by Fig. 5.3. However, the solution here is a bit flat and dispersed.

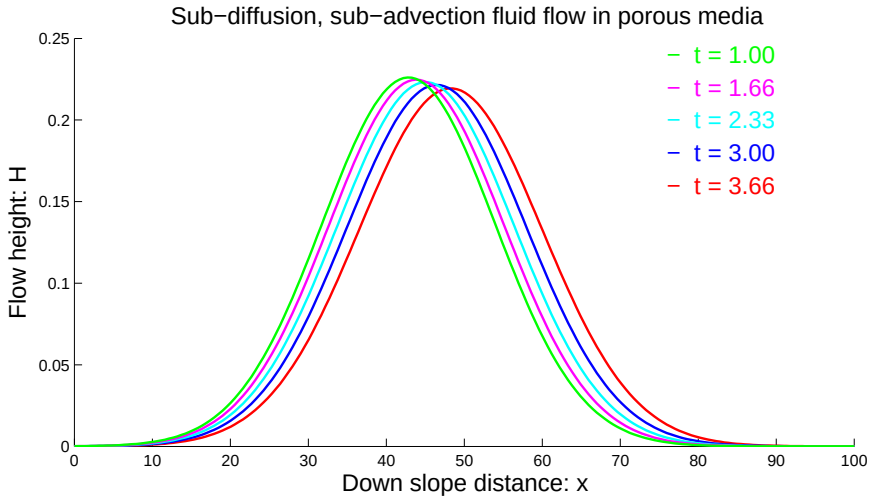

Figure 5.8: Sub-diffusive and sub-advective fluid flow through porous media: analytical solution (5.29)-(5.32) taking with $X(20)$, with parameters $C_1 = 1.012$, $C_2 = 1.35$, $K_1 = 10.01$, $C = 2.0$, $D = 1.01$ and $K = 0.4$.

similar to that produced by Pudasaini (2014) [78] and Boon and Lutsko [12] solution for sub-diffusion problem (see, Fig. 4.2 ans Fig. 5.3). So, the Barenblatt [6, 7] and Boon and Lutsko [12] solution have somehow been extended by constructing the exact solution to the sub-diffusive and sub-advective equation. It is to note that *Porous Media Equation* is reduced to generalized diffusion equation when $C = 0$. The solution has q-Gaussian shape. In solutions (5.29)-(5.32), X is taken as a parameter. Figures 5.6 and 5.7 are produced by taking $X(1)$.

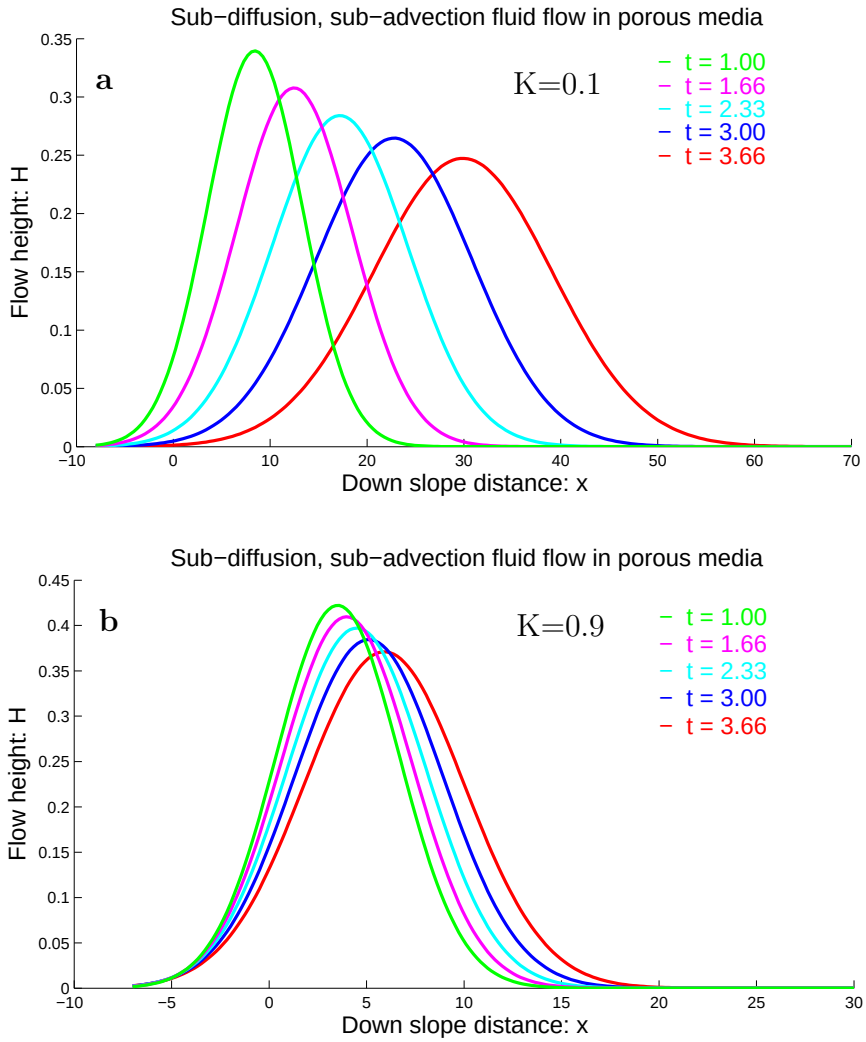

Figure 5.9: Sub-diffusive and sub-advective fluid flow through porous media: analytical solutions (5.29)-(5.32) with parameters $C_1 = 1.012$, $C_2 = 1.35$, $K_1 = 10.01$, $C = 1.42$ and $D = 1.01$.

In Fig. 5.8, it has been chosen $X(20)$ and other parameters are $C_1 = 1.012$, $C_2 = 1.35$, $K_1 = 10.01$, $C = 2.0$, $D = 1.01$ and $K = 0.4$. The solutions get closer with almost the same peaks of flow heights. More interesting fact is that in $X(n)$, higher the values of n, the solutions get closer and closer.

Another important parameter is K that emerged in (5.19) while separating the variables. This parameter can be of fundamental importance in controlling the flow dynamics. Time evolutions of analytical solutions (5.29)-(5.32) of sub-diffusive and sub-advective fluid flows in porous media are presented in Fig. 5.9 with the parameter values $C_1 = 1.012$, $C_2 = 1.35$, $K_1 = 10.01$, $C = 1.42$ and $D = 1.01$. Panel **a** corresponds to $K = 0.1$, and panel **b** corresponds to $K = 0.9$. In panel **a**, the solutions are advecting substantially

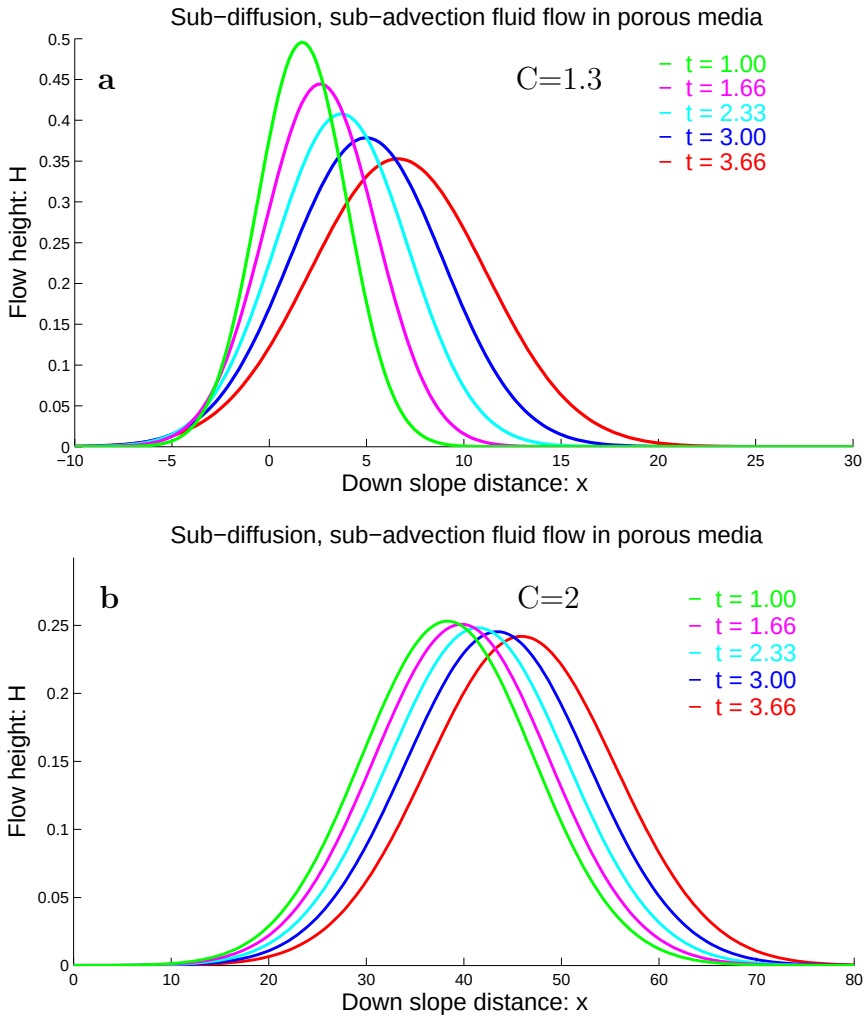

Figure 5.10: Sub-diffusive and sub-advective fluid flow through porous media as modelled by the analytical solution (5.29)-(5.32) with parameters $C_1 = 1.012$, $C_2 = 1.35$, $K_1 = 10.01$, $K = 0.4$ and $D = 1.01$. The flow fronts are moving in down-slope direction, whereas the rear positions remain effectively very close to the initial position.

farther down-slope direction. However, the rears remain very close to original position. This characterizes sub-diffusive and sub-advective fluid flow in porous media. Panel **b** corresponds to a bit different peaks for flow heights and advection of the front is less as compared to panel **a**. The solutions get closer and closer if we increase the value of K. Higher the value of K, higher will be the flow height and lesser is the advection. Thus, the values of K somehow controls advection.

Figures 5.10 plots the solution (5.29)-(5.32) for sub-diffusive and sub-advective equations with different values of C, namely $C = 1.3$ (panel **a**) and $C = 2$ (panel **b**). In panel **b**, the solutions for different times are very close to each other and the fronts are also

not advecting substantially. However, the amplitudes and the positions of solutions in panel **a** and **b** are different. The effect of the parameter C is that larger value of C, more advection in the flow direction. In both panels flow advects in the down-slope in the front and also diffuses somehow; this indicates the solution represented by (5.29)-(5.32) somehow captures the basic features of sub-diffusive and sub-advective solutions as in Fig. 4.3 and Fig. 4.5. Comparing between Fig. 5.5 and Fig. 5.6-Fig. 5.10; fronts and tails remain effectively unmoved and the flow elongates in the up-slope direction in Fig. 5.5, whereas in Fig. 5.6-Fig. 5.10, tails remain almost unmoved but fronts advects in the flow direction.

5.3.3 Reduction to Classical Diffusion-Advection Equation (III)

Here, two exact solutions constructed by Pudasaini (2014) [78] in reduced forms are discussed: simple analytical solution, and a bit more complex solution with the Bring radical (ultraradical), that is expressed in terms of a hypergeometric function. Again, consider (5.29)-(5.30). For simplicity, we set $\xi = x - Ct$, which is a new spatial coordinate. With this, $\partial t = \left(1/2\sqrt{\mathcal{H}}\right)\partial\tau$ reduces to

$$\partial t = \frac{1}{K_2}\left(\tau^{\frac{1}{4}}\exp(K_1/\tau)\right)\partial\tau, \tag{5.33}$$

where,

$$K_2 = 2\mathcal{M}^{1/2}/\left(4\pi D\right)^{1/4}, \text{ and } K_1 = \frac{\xi^2}{8D}.$$

Equation (5.33) possesses exact solution for t in τ

$$t = \frac{4}{5K_2}\left[\exp\left(K_1/\tau\right)\left\{4K_1\tau^{\frac{1}{4}} + \tau^{\frac{5}{4}}\right\} + \frac{4K_1^2\Gamma\left(\frac{3}{4}, -\frac{K_1}{\tau}\right)}{\tau^{\frac{3}{4}}\left(-\frac{K_1}{\tau}\right)^{3/4}}\right]. \tag{5.34}$$

However, it is still difficult to obtain an explicit expression for τ in terms of t from (5.34), which demands a very complicated inversion technique. Here, we aim, only to capture some basic features of the model by assuming that the higher order terms (associated with the Γ function), the non-linear terms in the exponential function and that the term $\tau^{5/4}$ can be neglected. With this, a simple explicit solution is obtained that may be useful [78]:

$$\tau = \left[\frac{5}{16}\frac{K_2}{K_1}t\right]^4. \tag{5.35}$$

The advantage with this solution is that it includes both K_1 and K_2. Solution (5.35) can be written in the original coordinate and in terms of D and C as

$$\tau = \frac{5^4\mathcal{M}^2D^3}{4\pi}\left[\frac{t}{(x-Ct)^2}\right]^4. \tag{5.36}$$

A simple analytical solution is then given explicitly by (5.29), (5.36) and $H^2 = \mathcal{H}$ [78]. These solutions can however, be improved by assuming that the higher order terms (associated with the Γ function) and the non-linear terms (which can also be called the lower order terms) in the exponential function can be neglected. Here, a solution procedure developed by Pudasaini (2014) [78] is outlined. With the substitutions,

$$\tilde{t} = -5K_2 t/4,\ a = 4K_1,\ \text{and}\ \tau^{1/4} = T,$$

equation (5.34) reduces to

$$T^5 + aT + \tilde{t} = 0, \tag{5.37}$$

which takes the form of a reduced quintic polynomial, in the Bring-Jerrard normal form [16]. The roots of (5.37) can be written in the Bring radical (ultraradical), that is expressed in terms of a hypergeometric function, ${}_4F_3$ as

$$T = \left[-\frac{a}{5}\right]^4 B_R\left(-\frac{1}{4}\left[\frac{5^5}{-a^5}\right]^4 \tilde{t}\right), \tag{5.38}$$

where B_R is the Bring radical [16], given by

$$B_R(\lambda) = -\lambda\, {}_4F_3\left(\frac{1}{5}, \frac{2}{5}, \frac{3}{5}, \frac{4}{5}; \frac{1}{2}, \frac{3}{4}, \frac{5}{4}; -\left[\frac{5\lambda}{4}\right]^4\right). \tag{5.39}$$

The convergence condition of (5.39) is $|\lambda| < 4/5^{5/4}$ for the associated series to the hypergeometric function ${}_4F_3$. Even in this reduced form, the explicit solution for τ in terms of t is still complicated. Note that, the solution techniques presented here may in principle be extended for any α. However, for the more complete and accurate results, we must use (5.29) together with (5.34) with the full relationship between t and τ [78]. For detailed discussion, we refer to Pudasaini (2014) [78].

5.3.4 Direct Application of Separation of Variables

In §5.3.1, the separation of variables method was applied to already reduced classical diffusion-advection equation, and the solution obtained from the separation of variables were also utilized to close the solution appearing in the reduced from in the classical solution to the advection-diffusion problem. Here, further advancing is made by applying the separation of variables method directly to the full sub-diffusion and sub-advection model (5.14) without any further reduction. Again, let us assume that the separation of variable is feasible for the original unknown variable, H:

$$H(t, x) = \frac{X(x)}{T(t)}, \tag{5.40}$$

where, as before, $X = X(x)$, and $T = T(t)$ are the two new functions to be determined in the course of the solution development. Unlike the separation applied in §5.3.1, here, (the time function) T is a function of the original time variable, t. This is due to the fact that here the separation is applied to the full and original model equation (5.14).

The separation (5.40) reduces (5.14) to

$$\frac{1}{D}\frac{\partial T}{\partial t} = \frac{1}{X}\left[\mathcal{C}\frac{\partial X^2}{\partial x} - \frac{\partial^2 X^2}{\partial x^2}\right], \tag{5.41}$$

where, $\mathcal{C} = C/D$. In (5.41), the left hand side is only a function of t and the right hand side is an expression only in x, because $X = X(x)$. Thus, the variables are separated. Equation (5.41) implies that there must exist a constant K, such that,

$$\frac{1}{D}\frac{\partial T}{\partial t} = -K = \frac{1}{X}\left[\mathcal{C}\frac{\partial X^2}{\partial x} - \frac{\partial^2 X^2}{\partial x^2}\right]. \tag{5.42}$$

The constant K should be determined from the solution for T and X, and other conditions associated with the model equation. Equation (5.42) now represents two ordinary differential equations, one for T, and the other for X. The left and middle expressions in (5.42) imply a solution for T:

$$T = K_0 - DKt, \tag{5.43}$$

where, K_0 is a constant of integration. Therefore, T is linear in t, which in (5.21) was an exponential in τ. So, they behave differently.

The middle and right expressions in (5.42) leads to the *second order ordinary differential equation* for X in x

$$\frac{d^2 X^2}{dx^2} - \mathcal{C}\frac{dX^2}{dx} = KX\cdot \tag{5.44}$$

The great complexity in solving (5.44) is due to the fact that the right hand side is only linear in X, whereas the unknown variable X is in quadratic form in the left within the differential operators. For the sake of simplicity, we substitute $X^2 = y$. Then, (5.44) becomes

$$\frac{d^2 y}{dx^2} - \mathcal{C}\frac{dy}{dx} - K\sqrt{y} = 0. \tag{5.45}$$

or,

$$y''_{xx} - \mathcal{C}y'_x = K\sqrt{y}, \tag{5.46}$$

which is the Lienard equation [57, 72]. This can be reduced to Abel equation in canonical form [72], which may possess an exact solution, but in very complicated form (Pudasaini,

2014) [78]. In contrast to (5.23), this is a second order non-linear ordinary differential equation. This non-linearity is posing the great problem to find the solution to (5.45) [78].

Setting $dy/dx = u$, the Lienard equation (5.45) reduces to

$$u\frac{du}{dy} - \mathcal{C}u = K\sqrt{y}. \tag{5.47}$$

By introducing a new dependent variable $v = 1/u$, equation (5.47) takes the form of the standard second kind Abel differential equation [36],

$$\frac{dv}{dy} = -\mathcal{C}v^2 - K\sqrt{y}v^3. \tag{5.48}$$

An exact integrability condition for the Abel equation (5.48) may be obtained by Chiellini Lemma [36]:

Chiellini Lemma: *If the coefficients $f(x)$ and $g(x)$ of a second kind Abel differential equation of the form*

$$\frac{dv}{dx} = f(x)v^2 + g(x)v^3, \tag{5.49}$$

satisfy the condition

$$\frac{d}{dx}\left(\frac{g(x)}{f(x)}\right) = A\, f(x), \quad A \neq 0,$$

then, the Abel equation (5.49) *can be exactly integrated.*

However, the Chielleni condition is not satisfied by (5.48). To the best of our knowledge, (construct) the exact solution to the model equation (5.45) could not be found.

The above complexity associated with the non-linearity somehow urged us to reduce the model equation and find some exact analytical solutions to that reduced system. Although, reduced, such analytical solutions may provide us with some important insights into the physics of the flow associated with the complex system. One way to exit from this complexity is to linearizing the non-linear equation (5.45) [52]. This is achieved by converting (5.45) into a Lienard system of equations [17, 52]. For this purpose, we set

$$\begin{aligned} y_1 &= y, \\ y_2 &= \frac{dy}{dx} + \mathcal{C}y. \end{aligned} \tag{5.50}$$

Then, from equation (5.45) we obtain a nonlinear system [52] of the form

$$\begin{aligned} \frac{dy_1}{dx} &= y_2 - \mathcal{C}y_1, \\ \frac{dy_2}{dx} &= -K\sqrt{y_1}. \end{aligned} \tag{5.51}$$

The right hand sides of the system of equation (5.51) are zero when $y_1 = 0$ and $y_2 = 0$. The *nullclines* (zero gradients) are $y_2 = \mathcal{C}y_1$ and $y_1 = 0$. Nucllines is the set of points which satisfy the given system of ordinary differential equations. The intersection point of all the nullclines is called an equilibrium point or *fixed point* of the system, or, which, for our problem, is $(0, 0)$. Near a fixed point, the dynamics of the nonlinear system are qualitatively similar to the dynamics of the linear system associated with the Jacobian matrix provided its eigenvalues have nonzero real parts [36].

The associated Jacobian matrix is

$$\begin{bmatrix} -\mathcal{C} & 1 \\ -K & 0 \end{bmatrix}.$$

The linearized system at $(0, 0)$ is

$$\begin{bmatrix} y_1' \\ y_2' \end{bmatrix} = \begin{bmatrix} -\mathcal{C} & 1 \\ -K & 0 \end{bmatrix} \begin{bmatrix} y_1 - 0 \\ y_2 - 0 \end{bmatrix}.$$

Now, the second order non-linear ordinary differential equation (5.45) formally reduces to *a system of first order linear ordinary differential equations*

$$\begin{aligned} \frac{dy_1}{dx} &= -\mathcal{C}y_1 + y_2, \\ \frac{dy_2}{dx} &= -Ky_1. \end{aligned} \tag{5.52}$$

Differentiating $(5.52)_1$ with respect to x and using $(5.52)_2$, we get

$$\frac{d^2y_1}{dx^2} - \mathcal{C}\frac{dy_1}{dx} - Ky_1 = 0, \tag{5.53}$$

which is *a second order linear ordinary differential equation*. Which, seems to be directly linearized from (5.45) just by replacing the quadratic term $\sqrt{y}$ by the linear term y. However, here, (5.53) is obtained by a formal linearization around the fixed point. Writing back y for y_1, the solution for (5.45) is

$$y(x) = C_1 \exp\left(-\frac{1}{2}x\left(\sqrt{\mathcal{C}^2 + 4K} + \mathcal{C}\right)\right) + C_2 \exp\left(\frac{1}{2}x\left(\sqrt{\mathcal{C}^2 + 4K} + \mathcal{C}\right)\right).$$

Thus, the another unknown function $(X = X(x), X^2 = y)$ is determined:

$$X = \sqrt{C_1 \exp\left(-\frac{1}{2}x\left(\sqrt{\mathcal{C}^2 + 4K} + \mathcal{C}\right)\right) + C_2 \exp\left(\frac{1}{2}x\left(\sqrt{\mathcal{C}^2 + 4K} + \mathcal{C}\right)\right)}. \tag{5.54}$$

Hence, the analytical solution for (5.14) is given by the solutions (5.40), (5.43) and (5.54).

Note that, the parameters K_0, K, C_1 and C_2 must be constrained from the physics of the

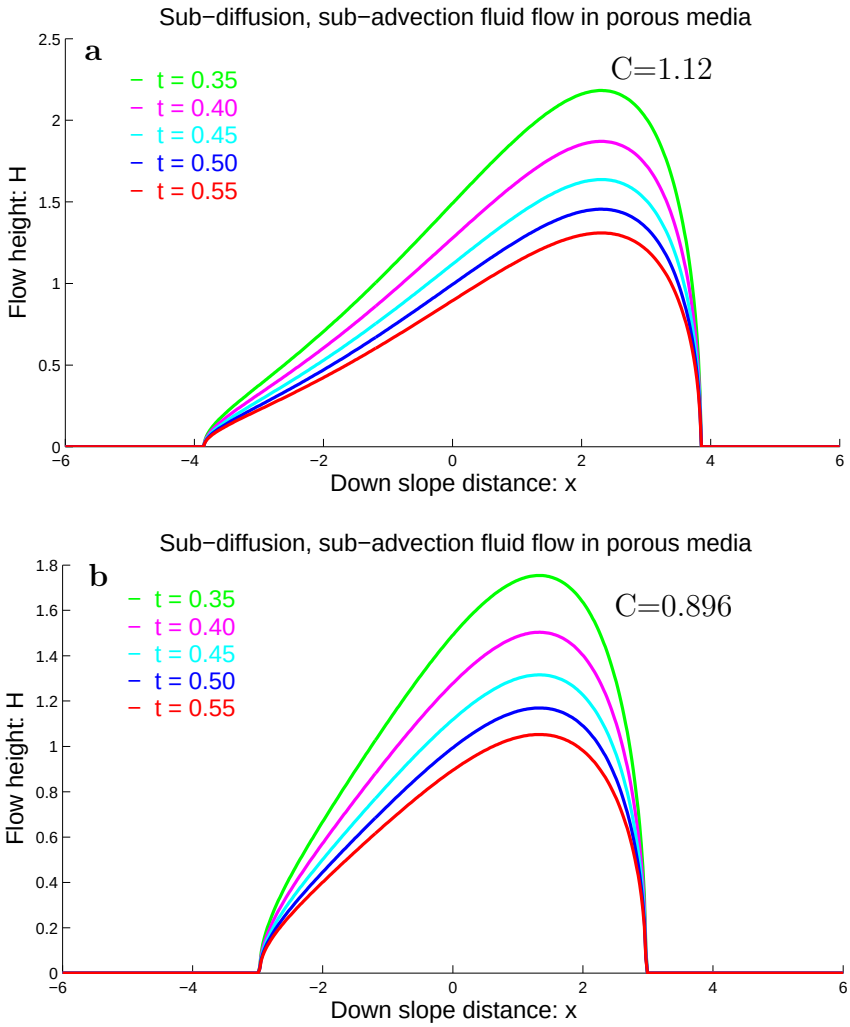

Figure 5.11: Time evolution of sub-diffusive and sub-advective fluid flow through porous media (5.40), (5.43) and (5.54) with parameters $C_1 = 0.1$, $C_2 = 0.1$ and $K = 0.48$.

problem (including the initial and boundary conditions, physical parameters involved in the model equations, etc.). For simplicity, for simulation purpose, numerical values for these parameters can also be chosen appropriately. Furthermore, the solution constructed here is fully valid and exact in the vicinity of the fixed point. However, depending on the required accuracy, this solution can still be a good approximation in the larger problem domain.

The Linearized solution for the sub-diffusion and sub-advection problem with separation of variables, resulted in similarity solutions. From the mathematical rigorous, they are the best solutions. These are the most advanced exact solutions for the sub-diffusion and sub-advection problems constructed and mentioned here.

Figures 5.11 describes the solution to the sub-diffusion and sub-advection model as con-

structed by using separation of variables and linearization. The solutions are given by (5.40), (5.43) and (5.54). The chosen parameters are $C_1 = 0.1$, $C_2 = 0.1$ and $K = 0.48$. Panel **a** corresponds to $C = 1.12$, and panel **b** corresponds to $C = 0.896$. In both panels **a** and **b**, the solutions are non-symmetrical. The front and tail are effectively unmoved and flow elongates in the upslope direction as Fig. 5.5. The effect of the parameter C is that, for larger the value of C, advection and stretching in the flow direction.

Comparison between Fig. 5.5, Fig. 5.6, and Fig. 5.11 indicate that the rear position which is effectively moved may be better modelled by Fig. 5.6, whereas the upslope elongation is better described by Fig. 5.5 and Fig. 5.11. The similarity in the solutions in Fig. 5.5 and Fig. 5.11 is that fronts and rear parts are effectively unmoved.

Chapter 6

Summary

The newly developed sub-advection and sub-diffusion model [78], showed that a number of important physical processes, such as the flow of a fluid through porous landscape and debris materials, are governed by the nonlinear advection and diffusion processes. The sub-diffusion and sub-advection model describes the fluid flows through inclined porous landscape and debris material with systematically derived non-linear (quadratic) diffusion and advection fluxes. The new equation is derived based on the two-phase mass flow model [77]. Then, the properties and the significance of the sub-diffusion and sub-advection was discussed in detail from the physical and application point of view. It turned out that it was not possible to solve the full sub-diffusion and sub-advection model with analytical methods. For this, higher-resolution shock capturing numerical methods were presented to appropriately integrate the model equation numerically. Some exact solutions and numerical solutions to the sub-diffusion and sub-advection model have already been constructed [78].

Here, further advancement is made by constructing some additional exact solutions to the model equation for the sub-diffusion and sub-advection fluid flows in porous landscape and debris materials. Three fundamental processes are involved in the construction of the exact solutions. The exact solutions are constructed by transforming the model equation to the classical diffusion-advection equation, considering the separation of the variables techniques, and also linearizing the non-linear model equation. All the exact solutions reveal important insights into the underlying physics of fluid flows, and thus, may play important role in advanced and accurate descriptions of fluid flows in the porous landscape and the debris materials, and in general porous media. The new exact solutions are compared with the high-resolution numerical solutions of the full sub-diffusion and sub-advection equations, and other numerical solutions available in literature [59]. The new exact solutions capture basic features of the full model equations as revealed by the numerical simulations.

The subdiffusive and sub-advective fluid flow in porous media is fundamentally different than the diffusive and advective fluid flow or diffusion of heat, tracer particles and pollutant in fluid. It is revealed that in the sub-diffusive process, the diffusion and dispersion is much slow and much less spread as compared to the same with the classical diffusion model. This is called the generalized porous medium flow phenomenon. And, thus, such a process is completely different from the classical diffusion-advection process, where the entire fluid pocket advects in the main flow direction, which at the same time also diffuses with spreading Gaussian profile. In contrast to the classical advection-diffusion of fluid where the tail of the initial substance distribution also advects in the downslope direction, for the fluid flow through porous media, the tail remains in its original position. Unlike the front of the classical diffusion-advection solution where the front is diffused, the front of the sub-diffusive and sub-advective fluid flow in porous media successively forms a downslope propagating strong bore [78].

As it was not possible to fully and analytically solve the model equation describing the sub-diffusive and sub-advective fluid flows in porous media, high resolution numerical solutions are presented for the full sub-diffusion and sub-advection model, which is then compared with the solution of the classical diffusion and advection model solution. Furthermore, the full sub-diffusion and sub-advection model solutions are presented both for the linear and quadratic drags, which reveal that the generalized drag plays important role in the form and propagation speed of the diffusion-advection waves. It is also demonstrated that the long time solution to sub-diffusive and sub-advective fluid flow through porous media is largely independent of the initial fluid profile [78].

Several exact analytical solutions to the sub-diffusion and sub-advection model equation are also presented. The complete solutions are derived for the reduced classical diffusion-advection fluid flows with linear fluxes, and the full sub-diffusive fluid flows [78]. Solutions for the classical linear diffusion and the new sub-diffusion with quadratic diffusive fluxes are compared. The similarities and differences in the solutions are discussed. Some exact solutions for the full sub-diffusion and sub-advection equation have been constructed, including the solutions for the reduced models in the form of the classical diffusion and advection equation, and with separation of variables leading to special ordinary differential equations in the form of Lienard and Abel canonical equations, and linearization of the model equation. Exact analytical solution are obtained for each of these special situations.

Analytical and exact solutions to simplified cases of nonlinear two-phase mass flow model equations are necessary to calibrate numerical simulations of flow depth and velocity pro-

files in the porous landscape and debris material. Of particular importance is the fluid flow through the immobile solid skeleton in the debris material and porous landscape. The reduced and problem-specific solutions provide important insights into the full behavior of the complex two-phase system, mainly the flow of fluid through the porous media. Such a solution, if one is able to compute it analytically and explicitly, is superior to all other possible solutions. Such special exact analytical solutions are important, because: they can in many cases predict phenomena that are observable in nature, they may help in comparing results with corresponding results obtained from other existing models, and they are crucial to test the efficiency and applicability of numerical solution techniques.

The exact solutions of the model equations reveal many essential physics of fluid flow in porous media and thus may find ample applications in modeling and simulation in environmental and industrial fluid flows through general porous media. These analytical solutions provide important insight in to the full behavior of the system. Analytical solutions allow for (in-depth) study of the physical feature of such processes. Broadly speaking, these results can further be applied to the problems related to the fluid flows in the reservoir embankment of the hydroelectric power plants, hydrogeology, the process of landslide initiation and deposition, environmental pollution remediation, and fluid flows through bone and skin in biomedical engineering [61].

Bibliography

[1] S. Abe and S. Thurner. Anomalous diffusion in view of Einstein's 1905 theory of Brownian motion. *Physica A*, 356:403–407, 2005.

[2] C. Ancey. Plasticity and geophysical flows: A review. *J. Non-Newtonian Fluid Mech.*, 142(1-3):4–35, 2007.

[3] C. Anteneodo and C. Tsallis. Multiplicative noise: A mechanism leading to nonextensive statistical mechanics. *J. Math. Phys.*, 44(11):5194–5203, 2003.

[4] R. A. Bagnold. Experiments on a gravity-free dispersion of large solid spheres in a Newtonian fluid under shear. *Proc. R. Soc. London., Ser. A*, 225:49–63, 1954.

[5] N. J. Balmforth and I. Frigaard. Viscoplastic fluids: From theory to application. *J. Non-Newtonian Fluid Mech.*, 142(1-3):1–3, 2007.

[6] G. I. Barenblatt. On some unsteady motions of a liquid or a gas in a porous medium. *Prikl. Mat. Mekh.*, 16(1):67–78, 1952. (in Russian).

[7] G. I. Barenblatt. On some class of solutions of the one-dimensional problem of nonsteady filtration of a gas in a porous medium. *Prikl. Mat. Mekh.*, 17:739–742, 1953. (in Russian).

[8] J. Bear. *Dynamics of Fluids in Porous Media*. Elsevier, Amsterdam, 1972.

[9] M. J. Blunt. Flow in porous media-pore-network models and multiphase flow. *Colloid and Interface Science*, 6(3):197–207, 2001.

[10] D. V. Boger. A highly elastic constant viscosity fluid. *J. Non-Newtonian Fluid Mech.*, 3:87–91, 1977/78.

[11] D. V. Boger and A. L. Halmos. *Non-Newtonian Flow I-Characterization of Fluid Behaviour, Module C* 2.1 *American Institute of Engineers*. ISSN 0270-7632/81/1123-0001, 1981.

[12] J. P. Boon and J. F. Lutsko. Generalized diffusion equation. *Physica A*, 368:55–62, 2006.

[13] J. P. Boon and S. Yip. *Molecular Hydrodynamics*. Dover, New York, 1991.

[14] L. Borland. Microscopic dynamics of the nonlinear Fokker-Planck equation. *Phys. Rev. E*, 57:6634–6642, 1998.

[15] J. Boussinesq. Recherches theoriques sur l'ecoulement des nappes d'eau infiltres dans le sol et sur le debit de sources. *Comptes Rendus Acad. Sci./J. Math. Pures Appl.*, 10:5–78, 1903 (1903/04).

[16] E. S. Bring. *Quart. J. Math.*, 6, 1864.

[17] T. A. Burton. The Nonlinear Wave Equation as a Lienard Equation. *Funkcialaj Ekvacioj*, 34:529–545, 1991.

[18] C. S. Campbell. Rapid granular flows. *Annu. Rev. Fluid Mech.*, 22:57–92, 1990.

[19] R. Courant, K. O. Friedrichs, and H. Levy. On the partial differential equations of mathematical physics. *IBM J.*, 11:215–234, 1967.

[20] P. Coussot and M. Meunier. Recognition, classification and mechanical description of debris flows. *Earth Science Reviews*, 40:209–227, 1996.

[21] E. M. F. Curado and F. D. Nobre. Derivation of nonlinear Fokker-Planck equations by means of approximations to the master equation. *Phys. Rev.*, E67, 021107, 2003.

[22] B. Cushman-Roisin. *Environmental Transport and Fate*. Thayer School of Engineering Dartmouth College, University Lecture, Chapter 2, Diffusion with advection, 2012.

[23] B. Cushman-Roisin and J. M. Becker. *Introduction to Geophysical Fluid Dynamics*. Academic Press, Amsterdam, 2011.

[24] H. P. G. Darcy. *Les fontaines publiques de la ville de Dijon*. Dalmont, Paris, 1856.

[25] B. Domnik and S. P. Pudasaini. Full two-dimensional rapid chute flows of simple viscosplastic granuular materials with a pressure-dependent dynamic slip-velocity and their numerical simulations. *J. Non-Newtonian Fluid Mech.*, 173-174:72–86, 2012.

[26] B. Domnik, S. P. Pudasaini, R. Katzenbach, and S. A. Miller. Coupling of full two-dimensional and depth-averaged models for granular flows. *J. Non-Newtonian Fluid Mech.*, 201:56–68, 2013.

[27] A. Einstein. Investigations on the Theory of Brownian Movement. *Ann. Phys. (Leipzig)*, 1905. 17, 549 English translation (Dover, New York, 1956).

[28] L. C. Evans. *Partial Differential Equations*. American Mathematical Society, 1998.

[29] E. D. Fernandez-Nieto, F. Bouchut, D. Bresch, M. J. Castro Diaz, and A. Mangeney. A new Savage-Hutter type model for submarine avalanches and generated tsunami. *J. Comput. Phys.*, 227(16):7720–7754, 2008.

[30] H. B. Fischer, E. G. List, R. C. Y. Koh, J. Imberger, and N. H. Brooks. Mixing in Inland and Coastal Waters. *Academic Press, New York*, 1979.

[31] Y. Forterre and O. Pouliquen. Flows of Dense Granular Media. *Annu. Rev. Fluid Mech.*, 40:1–24, 2008.

[32] R. W. Fox and A. McDonald. *Introduction to Fluid Mechanics*. Wiley, New York, 5th Edition, 2001.

[33] J. M. N. T. Gray, M. Wieland, and K. Hutter. Free surface flow of cohesionless granular avalanches over complex basal topography. *Proc. R. Soc. A*, 455:1841–1874, 1999.

[34] R. Greve and K. Hutter. Motion of a granular avalanche in a convex and concave curved chute: Experiments and theoretical predictions. *Phil. Trans. R. Soc. A*, 342:573–600, 1993.

[35] V. A. Hackley and C. F. Ferraris. Guide to Rheological Nomenclature: Measurements in Ceramic Particulate Systems. *NIST Special Publication*, 946:1–31, 2001.

[36] T. Harko, S. N. L. Franciso, and M. K. Mak. A class of exact solutions of the Lienard type ordinary non-linear differential equation. 2013. arXiv:1302.0836v2.

[37] A. Harten. High resolution schemes for hyperbolic conservation laws. *J. Comput. Phys. Appl. Math.*, 49:357–393, 1983.

[38] M. L. Hunt, R. Zenit, C. S. Campbell, and C. E. Brennen. Revisiting the 1954 suspension experiments of R. A. Bagnold. *J. Fluid Mech.*, 452:1–24, 2002.

[39] K. Hutter and K. Jöhnk. *Continuum Methods of Physical Modeling: Continuum Mechanics, Dimensional Analysis, Turbulence*. Springer, Berlin, New York, 2004.

[40] R. M. Iverson. The physics of debris flows. *Rev. Geophys.*, 35(3):245–296, 1997.

[41] R. M. Iverson and R. P. Denlinger. Flow of variably fluidized granular masses across three-dimensional terrain: 1. Coulomb mixture theory. *J. Geophys. Res.*, 106(B1):537–552, 2001.

[42] A. M. Johnson. *Physical Processes in Geology*. Freeman Cooper & Co., San Francisco, Calif, United States of America, 1970.

[43] P. Jop, Y. Forterre, and O. Pouliquen. A constitutive law for dense granular flows. *Nature*, 441(7094):727–730, 2006.

[44] J. Kafle, P. Kattel, P. R. Pokhrel, K. B. Khattri, D. B. Gurung, and S. P. Pudasaini. Dynamic interactions between a two-phase submarine landslide and a fluid reservoir. *Int. J. Lsld. Env.*, 1(1):35–36, 2013.

[45] J. Kafle, P. Kattel, P. R. Pokhrel, K. B. Khattri, D. B. Gurung, and S. P. Pudasaini. Dynamic interactions between a two-phase submarine landslide and a reservoir. 2014. (Submitted).

[46] P. Kattel. *Dynamics of Quasi-Three-Dimensional and Two-Phase Mass Flows*. M. Phil. Dissertation, Kathmandu University, Kavre, Dhulikhel, Nepal, 2014.

[47] P. Kattel, J. Kafle, P. R. Pokhrel, K. B. Khattri, D. B. Gurung, and S. P. Pudasaini. Dynamics of three-dimensional, two-phase landslides and debris flows. *Int. J. Lsld. Env.*, 1(1):39–40, 2013.

[48] P. Kattel, J. Kafle, P. R. Pokhrel, K. B. Khattri, D. B. Gurung, and S. P. Pudasaini. Dynamic simulations of three-dimensional, two-phase landslides and debris flows. 2014. (Submitted).

[49] K. B. Khattri, P. R. Pokhrel, P. Kattel, J. Kafle, D. B. Gurung, and S. P. Pudasaini. Some new insights into the fluid flows in debris material and porous landscape. *Int. J. Lsld. Env.*, 1(1):39–40, 2013.

[50] K. B. Khattri, P. R. Pokhrel, P. Kattel, J. Kafle, D. B. Gurung, and S. P. Pudasaini. Fluid flows in porous landscape and debris materials: Some new insights. 2014. (Submitted).

[51] T. Koch, R. Greve, and K. Hutter. Unconfined flow of granular avalanches along a partly curved chute.II: Experiments and numerical computations. *Proc. R. Soc. A*, 445:415–435, 1994.

[52] E. Kreyszig. *Advanced Engineering Mathematics.* John Wiley & Sons, Inc., 2010.

[53] P. Lax. Weak solutions of nonlinear hyperbolic equations and their numerical computation. *Comm. Pure Appl. Math.*, 7:159–193, 1954.

[54] L. S. Leibenzon. The motion of a gas in a porous medium. 1930. Complete works, vol 2, Acad. Sciences USSR, 1953 (Russian). First published in Neftance i slantsevoe khozyastvo, 10, 1929, and Neftanoe khozyastvo, 8-9, 1930 (Russian).

[55] L. S. Leibenzon. General problem of the movement of a compressible fluids in a porous medium. *Izv. Akad. Nauk USSR, Geography and Geophysics*, 9:7–10, 1945. (Russian).

[56] R. J. LeVeque. *Numerical Methods for Conservation laws.* Birkhäuser, Basel, 1990.

[57] A. Lienard. Etude des oscillations entretenues. *Revue gnrale de l'lectricit*, 23:901–912 and 946–954., 1928.

[58] J. F. Lutsko and J. P. Boon. Non-extensive diffusion as nonlinear response. *Euro. Phys. Lett.*, 71(6):906–911, 2005.

[59] J. F. Lutsko and J. P. Boon. Nonlinear diffusion from Einsteins master equation. *Euro. Phys. Lett.*, 80(6):60006, 2007.

[60] J. F. Lutsko and J. P. Boon. Generalized Diffusion. *Cond-Mat.Stat-Mech*, 1, 2008. arXiv/cond-mat.

[61] K. J. Maloy, J. Feder, F. Boger, and T. Jossang. Fractal structure of hydrodynamic dispersion in porous media. *Phys. Rev. Lett.*, 61(82):2925–2928, 1998.

[62] C. E. Martinez. *Eulerian-Lagrangian two-phase debris flow model.* Ph. D. Dissertation, Florida International University, Miami, Florida, 2009.

[63] GDR MiDi. On dense granular flows. *Eur. Phys. J. E*, 14(4):341–365, 2004.

[64] M. Muskat. *The flow of Homogenous Fluids Through Porous Media.* Mc Graw-Hill, New York, 1937.

[65] H. Nessyahu and E. Tadmor. Non-oscillatory central differencing for hyperbolic conservation laws. *J. Comput. Phys.*, 87:408–463, 1990.

[66] J. S. O'Brien and P. Y. Julien. Physical properties and mechanics of hyperconcentrated sediment flows. *ASCE Specialty Conference on the Delineation of Landslides, Floods and Debris Flows Hazards. ASCE, New York*, 260-279, 1985.

[67] E. B. Pitman and L. Le. A two-fluid model for avalanche and debris flows. *Phil. Trans. R. Soc. A*, 363:1573–1601, 2005.

[68] P. R. Pokhrel. *General Phase-Eigenvalues for Two-Phase Mass Flows: Supercritical and Subcritical States*. M. Phil. Dissertation, Kathmandu University, Kavre, Dhulikhel, Nepal, 2014.

[69] P. R. Pokhrel, K. B. Khattri, P. Kattel, J. Kafle, D. B. Gurung, and S. P. Pudasaini. Enhanced description of real two-phase landslides and debris flows. *Int. J. Lsld. Env.*, 1(1):75–76, 2013.

[70] P. R. Pokhrel, K. B. Khattri, P. Kattel, J. Kafle, D. B. Gurung, and S. P. Pudasaini. Real two-phase landslides and debris flows: Enhanced simulations. 2014. (Submitted).

[71] A. D. Polyanin, I. Z. Alexei, and A. V. Vyazmin. Generalized Separation of Variables in Nonlinear Heat and Mass Transfer Equations. *J. Non-Equilib. Thermodyn.*, 25:251–267, 2000.

[72] A. D. Polyanin and V. F. Zaitsev. *Handbook of Exact Solutions for Ordinary Differential Equations*. 2nd Edition, Chapman and Hall/CRC, Boca Raton, 2003.

[73] O. Pouliquen and Y. Forterre. Friction law for dense granular flows: Application to the motion of a mass down a rough inclined plane. *J. Fluid Mech*, 453:133–151, 2002.

[74] W. Prager and D.C. Drucker. Soil mechanics and plastic analysis or limit design. *Q. Appl. Math.*, 10(2):157–165, 1952.

[75] S. P. Pudasaini. *Dynamics of Geophysical Mass Movements, Vol. I, and Vol. II*. 2007. Department of Geodynamics and Geophysics, University of Bonn, Germany (Lecture Notes).

[76] S. P. Pudasaini. Some exact solutions for debris and avalanche flows. *Physics of Fluids*, 23(4):043301, 2011.

[77] S. P. Pudasaini. A General two-phase debris flow model. *Journal of Geophysical Research*, 117, F03010, doi:10.1029/2011JF002186, 2012.

[78] S. P. Pudasaini. Exact descriptions of fluid flow in porous and debris materials. 2014. (Submitted).

[79] S. P. Pudasaini and K. Hutter. Rapid shear flows of dry granular masses down curved and twisted channels. *J. Fluid Mech.*, 495:193–208, 2003.

[80] S. P. Pudasaini and K. Hutter. *Avalanche Dynamics: Dynamics of Rapid Flows of Dense Granular Avalanches*. Springer, Berlin, New York, 2007.

[81] S. P. Pudasaini and S. A. Miller. Buoyancy Induced Mobility in Two-phase Debris flow. *American Institute of Physics Proceedings*, 1479:149–152, 2012a.

[82] S. P. Pudasaini and S. A. Miller. A real two-phase submarine debris flow and tsunami. *American Institute of Physics Proceedings*, 1479:197–200, 2012b.

[83] S. P. Pudasaini, Y. Wang, and K. Hutter. Modelling debris flows down general channels. *Nat. Hazards Earth Syst. Sci.*, 5:799–819, 2005.

[84] S. P. Pudasaini, Y. Wang, and K. Hutter. Dynamics of avalanches along general mountain slopes. *Ann. Glacol.*, 38:357–362, 2005a.

[85] S. P. Pudasaini, Y. Wang, and K. Hutter. Rapid motions of free surface avalanches down curved and twisted channels and their numerical simulation. *Phil. Trans, R. Soc. A*, 363:1551–1571, 2005b.

[86] L. A. Richards. Capillary conduction of liquids through porous mediums. *Physics*, 5(1):318–333, 1931.

[87] J. F. Richardson and W. N. Zaki. Sedimentation and fluidization: Part 1. *Trans. Inst. Chem. Eng.*, 32:35–53, 1954.

[88] S. B. Savage and K. Hutter. The motion of a finite mass of granular material down a rough incline. *J. Fluid Mech.*, 199:177–215, 1989.

[89] S. B. Savage and K. Hutter. Dynamics of avalanches of granular materials from initiation to run-out Part I: Analysis. *Acta Mech.*, 86:201–223, 1991.

[90] L. E. Silbert, D. Ertas, G. S. Grest, T. C. Halsey, D. Levine, and S. J. Plimpton. Granular flow down an inclined plane: Bagnold scaling and rheology. *Phys. Rev. E*, 64(57):051302, 2001.

[91] A. H. P. Skelland. *Non-Newtonian Flow and Heat Transfer*. John Wiley and Sons Inc., 1967.

[92] N. F. Smyth and J. H. Hill. High-Order Nonlinear Diffusion. *IMA Journal of Applied Mathematics*, 40:73–86, 1998.

[93] T. Sochi. *Pore-Scale Modeling of Non-Newtonian Flow in Porous Media*. Ph. D. Dissertation, Imperial College London, 2007.

[94] S. A. Socolofsky and G. H. Jirka. Environmental Fluid Mechanics. *Mixing and Transport Processes in Environment.*, 2005. 5th Edition, Coastal and Ocean Engineering Division, Texas A and M University.

[95] J. Stewart. *Calculus Concepts and Contexts*. 4th Edition, Cenage Learning, 2001.

[96] P. K. Sweby. High resolution schemes using flux limiters for hyperbolic conservative laws. *SIAM J. Numer. Anal.*, 21(5):995–1101, 1984.

[97] Y. C. Tai. *Dynamics of Granular Avalanches and Their Simulations with Shock-capturing and Front-Tracking Numerical Schemes*. Ph. D. Dissertation, Darmstadt University of Technology, Darmstadt, Germany, 2000.

[98] Y. C. Tai, S. Noelle, J. M. N. T. Gray, and K. Hutter. Shock-capturing and front-tracking methods for granular avalanches. *J. Comput. Phys.*, 175(1):269–301, 2002.

[99] T. Takahashi. Debris flow. *Annu. Rev. Fluid Mech.*, 13:57–77, 1981.

[100] C. Tsallis and D. J. Bukman. Anomalous diffusion in the presence of external forces: Exact time-dependent solutions and their thermostatistical basis. *Phys. Rev. E*, 54(3):52–57, 1996.

[101] J. L. Vazquez. *Porous Media Equation: Mathematical Theory*. Oxford Univ. Press, 2007.

[102] J. L. Vazquez. Barenblatt solutions and asymptotic behavior for a non linear fractional heat equation of porous medium type. 2011. (arXiv:1205.6332v2).

[103] Y. Wang, K. Hutter, and S. P. Pudasaini. The Savage-Hutter Theory: a system of partial differential equations for avalanche flows of snow, debris and mud. *Journal of Applied Mathematics and Mechanics*, 84(8):507–527, 2004.

[104] S. Whitaker. Flow in porous media I: A theoretical derivation of Darcy's law. *Transport in Porous Media*, 1(1):3–25, 1986.

[105] M. Wieland, J. M. N. T. Gray, and K. Hutter. Channelized free surface flow of cohensionless granular avalanche in a chute with shallow lateral curvature. *J. Fluid. Mech.*, 392:73–100, 1999.